THE UNIVERSITY OF CHICAGO

DEVELOPING POLYMERIC MATERIALS FOR IMMUNOENGINEERING

A DISSERTATION SUBMITTED TO

THE FACULTY OF THE DIVISION OF THE PHYSICAL SCIENCES

IN CANDIDACY FOR THE DEGREE OF

DOCTOR OF PHILOSOPHY

DEPARTMENT OF CHEMISTRY

BY

RUYI WANG

CHICAGO, ILLINOIS

DECEMBER 2020

Table of Contents

List of Abbreviations

Ac	Acetate
ACN	Acetonitrile
ACS	American Chemical Society
AIBN	2,2'-Azobis(2-methylpropionitrile)
AMP	Anti-microbial peptides
ANOVA	Analysis of variance
ATCC	American Type Culture Collection
BMA	N-(2-butanoyloxyethyl) methacrylamide
BMDC	Bone marrow-derived dendritic cell
BOC	Tert-butyloxycarbonyl protecting group
BSA	Bovine serum albumin
But	Butyrate
CBD	Collagen binding domain
CD103	Cluster of Differentiation 103
CD206	Cluster of Differentiation 206
CD40	Cluster of Differentiation 40
CD80	Cluster of Differentiation 80
CLB001	ClostraBio polymer-001
CLB003	ClostraBio polymer-003
CMC	Critical micelle concentration
CryoEM	Cryogenic electron microscopy
CT	Cholera toxin

DC	Dendritic cell
DCC	N,N'-dicyclohecylcarbodiimide
DCM	Dichloromethane
DI	Deionized
DLS	Dynamic light scattering
DMAP	4-dimethylaminopyridine
DMEM	Dulbecco's modified Eagle's medium
DMF	Dimethylformaldehyde
DMSO	Dimethyl sulfoxide
EA	Ethyl acetate
EDC	1-Ethyl-3-(3-dimethylaminopropyl)carbodiimide
EDTA	Ethylenediaminetetraacetic acid
ELISA	Enzyme-linked immunosorbent assay
EMCH	(N-(ε-maleimidocaproic acid) hydrazide
EPR	Enhanced permeability and retention
ESI	Electrospray ionization
FBS	Fetal bovine serum
FDA	Food and Drug Administration
GI	Gastrointestinal
GPC	Gel permeation chromatography
GPCR	G-protein coupled receptor
HDAC	Histone deacetylases
HEMA	N-(2-hydroxyethyl) methacrylamide

HMA	N-hexyl methacrylamide
HPMA	N-(2-hydroxypropyl) methacrylamide
i.p.	Intraperitoneal
i.v.	Intravenous
IC50	Half maximal inhibitory concentration
IFNγ	Interferon gamma
IL-12	Interleukin 12
IL-4	Interleukin 4
IL-6	Interleukin 6
iLN	Inguinal lymph node
IVIS	In Vivo Imaging System
LC	Liquid chromatography
LEV	Levulinic acid
LN	Lymph node
LPS	Lipopolysaccharide
MAA	Methacrylic acid
mAb	Monoclonal antibody
MAL	Maleimide
MALDI	Matrix-assisted laser desorption/ionization
Man	Mannose
MeOH	Methanol
MFI	Mean fluorescent intensity
mLN	Mesenteric lymph node

MRM	Multiple reaction monitoring
MS	Mass spectrometry
MSA	Mouse serum albumin
MTT	3-(4,5-dimethylthiazol-2-yl)-2,5-diphenyltetrazolium bromide
Mw	Molecular weight
NMR	Nuclear magnetic resonance
NPH	3-nitrophenylhydrazine
OIT	Oral immunotherapy
PB2	Peanut butter powder
PBS	Phosphate-buffered saline
PBS-T	Phosphate-buffered saline with Tween 20
PE	Petroleum ether
PEG	poly(ethylene glycol)
PhBut	Phenol butyrate
pLN	Popliteal lymph node
PN	Peanut extract
PPS	poly(propylene sulfide)
PTX	Paclitaxel
RAFT	Reversible addition-fragmentation chain-transfer
Rf	Retention factor
RNA	Ribonucleic acid
RNA-Seq	RNA sequencing
RORγt	RAR-related orphan receptor gamma two

s.c.	Subcutaneous
s.e.m.	Standard error of the mean
SAXS	Small angel x-ray scattering
SCFA	Short chain fatty acid
SDS-PAGE	Sodium dodecyl sulfate polyacrylamide gel electrophoresis
SLD	Scattering length densities
SPF	Specific pathogen free
TEA	Triethylamine
TFA	Trifluoroacetic acid
TLC	Thin-layer chromatography
TLR	Toll like receptor
TNFα	Tumour Necrosis Factor alpha
TOF	Time of flight
Treg	Regulatory T cell
UHPLC	Ultra high performance liquid chromatography
UV	Ultraviolet

List of Figures

List of Schemes

Acknowledgements

First of all, I would like to express my great thanks to Prof. Jeffrey A. Hubbell for accepting me to do interesting and meaningful projects. Jeff is such a great mentor that he allows me freedom in research and always provides insightful advice when I need.

I would like to thank Prof. Cathryn Nagler for starting the collaboration and providing support in the animal study. Her enthusiasm for science inspires me a lot. I am also grateful for the support and advice from my committee members: Prof. Wenbin Lin, Prof. Stuart Rowan.

I would like to thank Dr. Scott Wilson for his guidance in synthesis and answering all my questions thoroughly. After he showed me how to do RAFT polymerization properly, I never had any issue with polymer synthesis.

I would like to thank Dr. Shijie Cao for his help on the flow cytometry and animal study. He is always clear about what to do next and what we should add to the experiment.

I also want to thank Dr. Jun Ishihara for his help on my project. His hard work and humor are both inspiration to me.

I would like to thank Michal Raczy for being energetic and critical on the projects we worked on together. We supported each other whenever there was issue in the experiment. I also want to thank my collaborator Sung Min Choi Hong for his hard work in the animal models. I enjoyed sharing background knowledge with Sung.

I want to show my special thanks to members of Hubbell lab for always being supportive and helpful to me. I would like to thank Dr. Michael White for introducing me to the wound healing project, Dr. Carrie Brubacker for showing me anionic polymerization of PPS, Levi Bennish for insightful discussion in organic synthesis, Koichi Sasaki for showing me protein conjugation, Dr. Priscilla Briquez for training me on microscope, Aaron Alpar for solving the

problem I had when using chemistry analyzer, Andrew Tremain for explaining immune response and tolerance to me, Suzana Gomes for always helping me in the lab and bringing me candies and donuts, and the whole group: Jialu Liu, Jennifer Antane, Aslan Mansurov, Tiffany Marchell, Erica Budina, Chitavi Maulloo, Dr. Nick Mitrousis, Mindy Nguyen, Talyor Gray, Joe Reda, Dr. Jieun Han, Dr. Lisa Volpatti, Rachel Wallace, Dr. Ako Ishihara, Elyse Watkins, Dr. Marcin Kwissa, Dr. Kym Brunggel, Dr. Kiyomitsu Katsumata, Dr. Martina Damo, Dr. Sarah MacEwan, Kazuto Fukunaga, Dr. John-Michael Williford, Dr. Alizee Grimm, Wendan Hou for being a supportive family. Especially in this difficult time of COVID-19, the whole "Swabbellians" group are working together to develop vaccines.

I would like to acknowledge my best collaborators from Nagler lab: Andrew Thompson for establishing HPLC method to quantify butyrate, Elliot Culleen and Mohamed Bashir for hard work on peanut sensitization model, Ande Hesser for intelectin stain and help on sac day. I also want to thank John Colson and Mathew Martin for organizing and coordinating experiments.

In addition, I would like to thank Ani Solanki for his help in injections, Dr. Hao Wu for introducing me to SAXS and running SAXS samples, Dr. Phil Griffin for always helping me solve problems related with GPC, Dr. Tera Lavoie for showing me beautiful CryoEM images, Dr. Yunus Tuncil for introducing me to GC and butyrate quantification.

Lastly, I would like to thank my friends and family. My friends at the University of Chicago are amazing people and I can learn a lot from them. I must thank my parents for always supporting me through the journey. And this journey would not complete without the encouragement from my wife, Ning Wang.

Thesis Abstract

In this thesis, we developed three polymer-based drug delivery platforms to address three health problems: oral immunotherapy for food allergy, tolerance against protein-based therapeutics, and tumor target therapy. As a major commensal bacterial metabolite, butyrate showed protective effect to the gut immunity and suppressed the activation of antigen presenting cells. However, there is an unmet need of developing an efficient formulation to deliver butyrate to either gastrointestinal (GI) tract or draining lymph nodes.

In order to delivery butyrate to the GI tract, we developed two polymeric micelle platforms with butyrate ester in the core, and either neutral or negatively charged shell. We characterized the size and structure of the micelles. We validated both micelles released butyrate in the GI tract. Importantly, our formulations showed enhanced performance in the treatment of peanut allergy when combined with oral immunotherapy. Furthermore, we demonstrated the butyrate formulation up-regulated the expression of anti-microbial peptides and induced GATA3+ and RORγt^{+} regulatory T cells.

To investigate the butyrate effect on inducing tolerogenic dendritic cells in the lymph node, we developed a statistical copolymer containing butyrate ester and mannose that targeted dendritic cells. We validated the release profile and the biodistribution of the polymer. The copolymer suppressed the activation of bone marrow-derived dendritic cells *in vitro* and induced tolerogenic dendritic cells *in vivo*.

In a third project, we investigated tumor target delivery of paclitaxel, a famous chemotherapeutic drug, to address its problems in low solubility and adverse events. Collagen binding peptide has shown capability of targeting tumor environment. To explore extracellular matrix affinity-based cancer target therapy, we developed a water-soluble conjugate between

collagen binding peptide and paclitaxel. We characterized the protein-drug conjugate and demonstrated the efficacy of the conjugate on cancer cells *in vitro*. Furthermore, we studied the protein-paclitaxel conjugate on mouse tumor model.

Keywords

polymer synthesis, micelles, drug delivery, food allergy, tolerance, dendritic cells, protein-drug conjugate, cancer, paclitaxel

Chapter 1

Motivations, Background, and Aims

1.1 Motivations and Background

Our laboratory has focused on developing platforms to regulate the immune system either in an activation way, which leads to humoral or cellular responses against antigens, or in a tolerogenic way, which suppresses the activation of the immune system and protects the body from over-reaction against antigens. The approaches we used include chemical synthesis of functional polymers, formulation of nanoparticles for delivery of immunomodulatory molecules, and engineered protein for target immunotherapy. In this thesis, we sought to develop polymeric materials to solve three health problems: treatment of food allergy, tolerance against protein-based therapeutics, and cancer target therapy.

1.1.1 Food allergy

Food allergy is a prevalent health problem that affecting over 32 million Americans[1]. Currently, most patients manage their food allergy by maintaining strict avoidance of specific allergens in their diet. Recently, FDA has approved Palforzia as an oral immunotherapy (OIT) for peanut allergies[2]. The goal of the therapy is to establish a desensitization state by exposing patients to gradually increasing doses of peanut protein. However, OIT may cause severe adverse events like anaphylaxis because it is difficult to maintain the dose of peanut protein below the allergic level to patients. In addition, OIT cannot achieve long-lasting tolerance against peanut antigen after peanut antigen exposure is stopped. One possible supportive treatment for OIT is the supply of butyrate. Recently, researchers have demonstrated the effects of butyrate to gut immunity[3,4]. Butyrate induced the differentiation of colonic regulatory T cells[5-7] and protected

the barrier functions of the small intestine[8]. However, sodium butyrate itself is not suitable for oral administration because it has foul odor and taste and as a small molecule, butyrate is absorbed or metabolized very quickly in the upper gastrointestinal tract.

To address the problem of food allergy and the delivery of butyrate, we sought to use the nano-scale polymeric micelles to deliver butyrate to the gastrointestinal tract. Previously, our laboratory has developed different nanocarriers for vaccines or cancer immunotherapy. The nanocarriers were formulated from block copolymer poly(ethylene glycol)-b-poly(propylene sulfide) (PEG-PPS)[9-11]. Depending on different ratio between hydrophilic PEG and hydrophobic PPS, the polymer formulated into either micelles that encapsulated hydrophobic drug in the core, or polymersomes that encapsulated both hydrophilic antigens inside and hydrophobic drug in the membrane. Based on the similar design, we could synthesize monomer of butyrate ester as the hydrophobic block of the copolymer that formulated into water-soluble micelles. Additionally, our collaborator Prof. Nagler's lab has developed a peanut sensitization model[12]. We could use such model to test the efficacy our formulations.

1.1.2 Immunogenicity of protein-based therapeutics

Protein-based drugs have been growing rapidly in sales. However, the immunogenicity of protein-based drugs is a major issue affecting both safety and efficacy of the therapy[13,14]. The generation of anti-drug antibodies is prevalent among licensed protein-based therapeutics. Thus, it would be important to induce the tolerance to protein-based drugs. Recently, butyrate, as an inhibitor of histone deacetylases and an agonist of G-protein coupled receptor[15], has shown its capability of modulating the immune system towards a tolerogenic way[16,17]. It would be

interesting to investigate whether target delivery of butyrate to the draining lymph nodes can induce tolerogenic dendritic cells *in vivo*.

Our laboratory has developed a glycopolymer-antigen conjugate platform that targets antigen presenting cells with polysaccharide[18,19]. The statistical copolymer of mannose and an adjuvant like toll like receptor agonist induced both humoral and cellular response as a vaccine[18]. Moreover, the antigen conjugated to glycopolymer without adjuvants induced antigen-specific tolerance[19]. Given the potential of butyrate in inducing tolerogenic dendritic cells, we could synthesize glycopolymer containing butyrate ester to target delivery of butyrate to antigen presenting cells and investigate the potential of inducing tolerogenic effects.

1.1.3 Cancer target therapy

Cancer is a major health problem worldwide. Paclitaxel, as one of the most effective chemotherapeutic drugs, has been used in the treatment of many cancers[20]. However, paclitaxel has limitations of low solubility and strong adverse events[21]. To improve the safety and efficacy of the paclitaxel treatment, one method is to conjugate it with a tumor target protein. With the help of soluble protein, the conjugate can enhance the solubility of paclitaxel and increase the circulation time of the drug in the blood. Moreover, the target effect to tumor or tumor environment can reduce the toxicity of the paclitaxel by reducing the concentration of the drug in other organs.

To address the tumor-targeting problem, our lab has developed a platform of fused protein between collagen-binding peptide and mouse serum albumin[22-27]. The collagen-binding domain of A3 can bind actively to the collagens over-expressed in the tumor environment. In addition, serum albumin can increase the passive uptake of tumor cells by enhanced permeability

and retention effect. The platform has proven successful in cancer immunotherapy when A3 domain is conjugated checkpoint blockade inhibitors[24], chemokines[26], cytokines[27], or chemotherapeutics like doxorubicin[25]. Given the capability of targeting tumor, we could conjugate paclitaxel to A3 domain and investigate the performance of the conjugate in tumor models.

1.2 Aims

On the basis of previous studies, we started the research by developing novel polymer-based drug carriers and investigating their efficacy in both cell and animal models. For the first project, we developed polymeric micelles for delivery of butyrate and characterized the nano-carrier. Then we validated the efficacy of the butyrate-containing micelles and investigated the mechanism of how butyrate affects the gut immunity (1). For the second project, we further explored a statistical copolymer system that delivers butyrate to dendritic cells or macrophages and investigated the capability of such material in inducing tolerogenic dendritic cells both *in vitro* and *in vivo* (2). For the third project, we conjugated paclitaxel to collagen binding proteins to obtain a soluble formulation of paclitaxel that targets tumor environment (3). Overall, the thesis aims at developing polymeric materials to deliver pharmacological active ingredients for immunoengineering purpose.

1.3 Scope of the thesis

The second chapter focuses on the development of butyrate-containing micelles made from block copolymers. After synthesizing the polymers with butyrate ester, we successfully formulated the polymer into nano-scale micelles. Then, we characterized the size, surface charge,

and critical micelle concentration of the micelles. In addition, the biodistribution and butyrate release profile were investigated. Importantly, the formulation showed efficacy in enhancing the performance of oral immunotherapy in the peanut sensitized mice. Furthermore, we investigated the mechanism of how butyrate-containing micelles interact with the gut immunity and found they up-regulated gene expression of anti-microbial peptides and induced regulatory T cells in the mesenteric lymph nodes.

The third chapter extended the research on butyrate delivery to target dendritic cells in the lymph node. We developed statistical copolymers with mannose and butyrate ester based on previous research. Then, we proved the release of butyrate and the efficacy of the polymer in suppressing the cytokine IL12p70 production in bone marrow-derived dendritic cells. More importantly, the polymer showed capability of inducing tolerogenic dendritic cells *in vivo*.

The fourth chapter opened a new study on the tumor target therapy based on the conjugate between paclitaxel and collagen binding protein. We developed the soluble paclitaxel conjugate and validated the drug release at acidic pH. The protein drug conjugate showed efficacy *in vitro* and a potential for tumor treatment *in vivo*.

The fifth chapter summarized the key results of the thesis. We also discussed the future direction and applications of the materials we developed.

1.4 References

1. Gupta, R.S.*, et al.* Prevalence and Severity of Food Allergies Among US Adults. *JAMA Netw Open* **2**, e185630 (2019).

2. Patrawala, M., Shih, J., Lee, G. & Vickery, B. Peanut Oral Immunotherapy: a Current Perspective. *Curr Allergy Asthma Rep* **20**, 14 (2020).

3. Tan, J.*, et al.* Dietary Fiber and Bacterial SCFA Enhance Oral Tolerance and Protect against Food Allergy through Diverse Cellular Pathways. *Cell Rep* **15**, 2809-2824 (2016).

4. Mathewson, N.D.*, et al.* Gut microbiome-derived metabolites modulate intestinal epithelial cell damage and mitigate graft-versus-host disease. *Nat Immunol* **17**, 505-513 (2016).

5. Furusawa, Y.*, et al.* Commensal microbe-derived butyrate induces the differentiation of colonic regulatory T cells. *Nature* **504**, 446-450 (2013).

6. Smith, P.M.*, et al.* The microbial metabolites, short-chain fatty acids, regulate colonic Treg cell homeostasis. *Science* **341**, 569-573 (2013).

7. Arpaia, N.*, et al.* Metabolites produced by commensal bacteria promote peripheral regulatory T-cell generation. *Nature* **504**, 451-455 (2013).

8. Fachi, J.L.*, et al.* Butyrate Protects Mice from Clostridium difficile-Induced Colitis through an HIF-1-Dependent Mechanism. *Cell Rep* **27**, 750-761.e757 (2019).

9. Dane, K.Y.*, et al.* Nano-sized drug-loaded micelles deliver payload to lymph node immune cells and prolong allograft survival. *J Control Release* **156**, 154-160 (2011).

10. van der Vlies, A.J., Hasegawa, U. & Hubbell, J.A. Reduction-sensitive tioguanine prodrug micelles. *Mol Pharm* **9**, 2812-2818 (2012).

11. Jeanbart, L., Kourtis, I.C., van der Vlies, A.J., Swartz, M.A. & Hubbell, J.A. 6-Thioguanine-loaded polymeric micelles deplete myeloid-derived suppressor cells and enhance the efficacy of T cell immunotherapy in tumor-bearing mice. *Cancer Immunol Immunother* **64**, 1033-1046 (2015).

12. Stefka, A.T.*, et al.* Commensal bacteria protect against food allergen sensitization. *Proc Natl Acad Sci U S A* **111**, 13145-13150 (2014).

13. Baker, M.P., Reynolds, H.M., Lumicisi, B. & Bryson, C.J. Immunogenicity of protein therapeutics: The key causes, consequences and challenges. *Self Nonself* **1**, 314-322 (2010).

14. Fu, K.*, et al.* Immunogenicity of Protein Therapeutics: A Lymph Node Perspective. *Front Immunol* **11**, 791 (2020).

15. Kaisar, M.M.M., Pelgrom, L.R., van der Ham, A.J., Yazdanbakhsh, M. & Everts, B. Butyrate Conditions Human Dendritic Cells to Prime Type 1 Regulatory T Cells. *Front Immunol* **8**, 1429 (2017).

16. Chang, P.V., Hao, L., Offermanns, S. & Medzhitov, R. The microbial metabolite butyrate regulates intestinal macrophage function via histone deacetylase inhibition. *Proc Natl Acad Sci U S A* **111**, 2247-2252 (2014).

17. Singh, N.*, et al.* Blockade of dendritic cell development by bacterial fermentation products butyrate and propionate through a transporter (Slc5a8)-dependent inhibition of histone deacetylases. *J Biol Chem* **285**, 27601-27608 (2010).

18. Wilson, D.S.*, et al.* Antigens reversibly conjugated to a polymeric glyco-adjuvant induce protective humoral and cellular immunity. *Nat Mater* **18**, 175-185 (2019).

19. Wilson, D.S.*, et al.* Synthetically glycosylated antigens induce antigen-specific tolerance and prevent the onset of diabetes. *Nat Biomed Eng* **3**, 817-829 (2019).

20. Zhu, L. & Chen, L. Progress in research on paclitaxel and tumor immunotherapy. *Cell Mol Biol Lett* **24**, 40 (2019).

21. Frederiks, C.N., Lam, S.W., Guchelaar, H.J. & Boven, E. Genetic polymorphisms and paclitaxel- or docetaxel-induced toxicities: A systematic review. *Cancer Treat Rev* **41**, 935-950 (2015).

22. Ishihara, J.*, et al.* Matrix-binding checkpoint immunotherapies enhance antitumor efficacy and reduce adverse events. *Sci Transl Med* **9**(2017).

23. Ishihara, J.*, et al.* Improving Efficacy and Safety of Agonistic Anti-CD40 Antibody Through Extracellular Matrix Affinity. *Mol Cancer Ther* **17**, 2399-2411 (2018).

24. Ishihara, J.*, et al.* Targeted antibody and cytokine cancer immunotherapies through collagen affinity. *Sci Transl Med* **11**(2019).

25. Sasaki, K.*, et al.* Engineered collagen-binding serum albumin as a drug conjugate carrier for cancer therapy. *Sci Adv* **5**, eaaw6081 (2019).

26. Williford, J.M.*, et al.* Recruitment of CD103. *Sci Adv* **5**, eaay1357 (2019).

27. Mansurov, A.*, et al.* Collagen-binding IL-12 enhances tumour inflammation and drives the complete remission of established immunologically cold mouse tumours. *Nat Biomed Eng* **4**, 531-543 (2020).

Chapter 2

Butyrate-containing Polymeric Micelles Improve the Efficacy of Oral Immunotherapy

2.1 Abstract

Butyrate as a HDAC inhibitor plays an important role in regulating gut immunity and promoting epithelial barrier function. However, current formulations of butyrate have limitations in high dosage or low efficiency in delivering butyrate. Here, we developed two polymeric micelle systems to deliver butyrate to the gastrointestinal (GI) tract. The water-soluble micelles have nano-scale spherical structures with butyrate ester as the core and either neutral hydrophilic polymer (CLB001) or negatively charged polymer (CLB003) as the shell. In addition, both polymeric micelles were proven to release butyrate in the GI tract of mouse and enhance the butyrate level of GI content. Importantly, the treatment of butyrate containing micelles CLB001 and CLB003 enhanced the performance of oral immunotherapy in mice that developed peanut allergy. Furthermore, we showed CLB001 can up-regulate genes expressing anti-microbial peptides in the ileum epithelial cells. And CLB003 promoted $GATA3^+$ or $ROR\gamma t^+$ regulatory T cells in the ileal mesenteric lymph nodes. The butyrate containing polymeric micelles CLB001 and CLB003 may provide a potential approach in the treatment of food allergy.

2.2 Introduction

Food allergy is a prevalent and severe health problem that affects over 32 million Americans[1]. Among the adults with food allergy in the US, 38% reported at lease 1 emergency department visit related to food allergy in their lifetime[1]. Peanut is the most prevalent allergens

to patients with food allergy[2]. Most patients manage their food allergy by avoiding specific allergens in their diet, despite the difficulty of complying with strict avoidance. Recently, Palforzia was approved by FDA as an oral immunotherapy (OIT) for peanut allergies[3-5]. The goal of the therapy is to establish a desensitization state by exposing patients to gradually increasing doses of peanut protein. Although OIT shows efficacy in inducing desensitization of peanut antigen, the OIT treatment often induces adverse events including anaphylaxis. Moreover, OIT cannot achieve long-lasting tolerance against peanut antigen after peanut antigen exposure is stopped. Apart from OIT, anti-IgE (Omalizumab) and anti-IL-4 receptor (Dupilumab) are in clinical trials as solutions for food allergy[6-8]. Due to adverse effects and limited efficacy of OIT, there is an urgent need to develop new therapies for food allergy, either as an individual therapy or in combination with oral immunotherapy.

The gut microbiome plays an important role in gut health[9-11]. Studies show the dysbiosis caused by antibiotic treatment breaks the gut barrier function, resulting in increased exposure to food antigens[12]. Additionally, gut bacteria affect the gut immunity via their metabolites: short chain fatty acids, especially butyrate[13,14]. Butyrate, produced by commensal bacteria via metabolizing dietary fiber, is known to be an agonist to G-protein coupled receptor and an inhibitor to histone deacetylase (HDAC)[15]. Butyrate is the preferred substrate for intestinal epithelial cells[16]. In addition, butyrate strengthens the gut barrier function by stabilizing hypoxia-inducible factor and increasing tight junctions[17]. More importantly, butyrate has been demonstrated to induce the colonic regulatory T cells[18-20]. Given the important role butyrate plays in gut immunity, it would be a potential drug to protect the gut immunity and to induce oral tolerance.

However, butyrate itself is not suitable for oral administration because of the foul odor and taste. Moreover, as a small molecule, butyrate gets absorbed and metabolized quickly after oral administration[21]. In previous studies, butyrate was delivered either dissolved in drinking water at a very high concentration[19,20], or mixed in mouse chow as butyrylated starch[18]. Neither method was a controlled and quantitative way of administering butyrate. Other routes of administrations of butyrate, including intrarectal delivery (enema)[22] or continuous intravenous infusion[23], are complicated and unacceptable to all patients. There is an unmet need for developing a straightforward and controllable oral delivery of butyrate.

Polymeric micelles have been well studied as a carrier of hydrophobic drugs[24-26]. Polymeric micelles have a hydrophobic core that can encapsulate hydrophobic drugs via physical interaction or chemical bonding[27]. The hydrophilic shell of the micelle makes it water soluble, which is essential for oral delivery as the most popular route of drug administration. Previously in the lab, micelles formulated from block copolymer poly(ethylene glycol)-b-poly(propylene sulfide), PEG-PPS, were used as a platform to encapsulate immunomodulatory drugs and showed enhanced efficacy of immunotherapy[28-32].

Here, we present a formulation strategy to incorporate butyrate into water soluble polymeric micelles. We synthesized and formulated two types of butyrate-containing micelles: neutral CLB001 and negatively charged CLB003. The structures of the micelles were characterized to be sub-hundred nanometer in size. Both micelles released butyrate in the ileum and cecum of the mice based on the pharmacokinetics study. Importantly, the combination of CLB001/CLB003 and oral immunotherapy significantly reduced the

allergic response on peanut sensitized mice compared to OIT only group. In addition, RNA sequencing showed CLB001 up-regulate genes related to antibacterial peptides in the ileal epithelial cells. Finally, we validated the regulatory T cell induction in mesenteric lymph nodes after the treatment of CLB001 and CLB003 micelles.

2.3 Results

2.3.1 Block copolymer pHPMA-*b*-pBMA (CLB001) and pMAA-*b*-pBMA (CLB003) are synthesized by RAFT polymerization

To deliver butyrate into the gastrointestinal tract, we designed block copolymers that can form water-soluble micelles carrying butyrate in their core. Block copolymer pHPMA-*b*-pBMA (CLB001) was synthesized through two steps of reversible addition-fragmentation chain-transfer (RAFT) polymerization in order to achieve controllable polydispersity and degree of polymerization (Figure 2.1.A). The hydrophilic block was made of N-(2-hydroxypropyl) methacrylamide (HPMA), while the hydrophobic block was made of N-(2-butanoyloxyethyl) methacrylamide (BMA) with an ester bond connecting to butyrate. Given the block copolymer consisted of both hydrophilic block and hydrophobic block, it could self-assemble into micelles with hydrophilic block on the outside shell and hydrophobic in the core. The design of ester bonding in the polymer allowed the release of butyrate at acidic pH or catalyzed by esterase in the gastrointestinal tract. NMR analysis confirmed the degrees of polymerization of HPMA or BMA were around 100 and 133, respectively. Thus, the ratio between HPMA and BMA was around 0.75. Polymers with different HPMA/BMA ratios were also synthesized and tested for micelle formulation. However, a ratio of 0.75 was picked for further studies because of the simplicity of synthesis and the acceptable size of formulated micelles.

In addition to CLB001, pMAA-*b*-pBMA (CLB003) was also synthesized through RAFT polymerization, with the first block made of hydrophilic methacrylic acid (MAA) and the second block made of hydrophobic BMA. NMR analysis confirmed the degrees of polymerization of MAA or BMA to be 100 and 77, respectively. The ratio between MAA and BMA was around 1.3. The butyrate content by mass was around 28% for both CLB001 and CLB003.

2.3.2 Both CLB001 and CLB003 formulate into micelles with diameters of sub-hundred nanometer

Given thst the polymers were synthesized through RAFT polymerization, we tested the abilities of the polymers to form nanoscale micelles. Block copolymer CLB001 was able to formulate into micelles through the cosolvent evaporation method, using ethanol as good solvent to dissolve the polymer (Figure 2.1.B). Then 1 × PBS was added and the solution was allowed to evaporate and polymers self-assembled into micellar structures. The hydrophilic HPMA block formed the shell and hydrophobic BMA block formed the core of the micelles. On the contrary, CLB003 could not formulate into micelles through the cosolvent evaporation method. The reason was pMAA formed intramolecular hydrogen bonding, making the whole block hydrophobic[33]. Such bonding was broken when strong base like sodium hydroxide was titrated into the mixture of CLB003 polymer to change methacrylic acid into ionized methacrylate[34-36]. After base titration, CLB003 polymer self-assembled into micellar structures (Figure 2.1.B).

Given we formulated CLB001 and CLB003 into micelles, we used dynamic light scattering (DLS) to characterize the hydrodynamic size of micelles. The hydrodynamic diameter of CLB001 was around 44.7 ± 0.8 nm, which was similar to CLB003 with a diameter of 39.9 ± 1.6 nm. Moreover, the polydispersity of CLB001 and CLB003 were 0.07 ± 0.02 and 0.09 ± 0.02,

respectively (Figure 2.1.C, G). Small polydispersity suggested the formulations were uniform. In addition, cryogenic electron microscopy (CryoEM) revealed the detailed structure of micelles, especially the core structure as the cores were made of pBMA, which were more condensed with higher contrast. CryoEM images indicated the diameter of the core of CLB001 micelle was 30 nm, while CLB003 had a smaller core diameter of 15 nm. Both CLB001 and CLB003 micelles had spherical core structures (Figure 2.1.E, F).

In order to further understand the structures of CLB001 and CLB003, especially the aggregation number, we did small angel x-ray scattering (SAXS) analysis on both micelles (Figure 2.1.D). SAXS data of CLB001 and CLB003 were acquired in PBS at a low concentration of 2 mg/mL. As indicated from Guinier plots, radii of gyration for CLB001 and CLB003 were 14.2 nm and 13.5 nm, respectively (Figure 2.1.G). In addition, the structures of micelles were confirmed to be spheres from Kratky plots of SAXS data. More importantly, we fitted the SAXS data with polydispersity core-shell sphere model[37]. The model assumes the micelle has a spherical core with a higher scattering length densities (SLD) and a shell with a lower SLD. The model gave us volume fraction of micelles, radius of core, and thickness of shell. Those were used to calculate aggregation number and mean distance between micelles. According to the fitting results, aggregation numbers for CLB001 and CLB003 were 119 and 92, respectively (Figure 2.1.G).

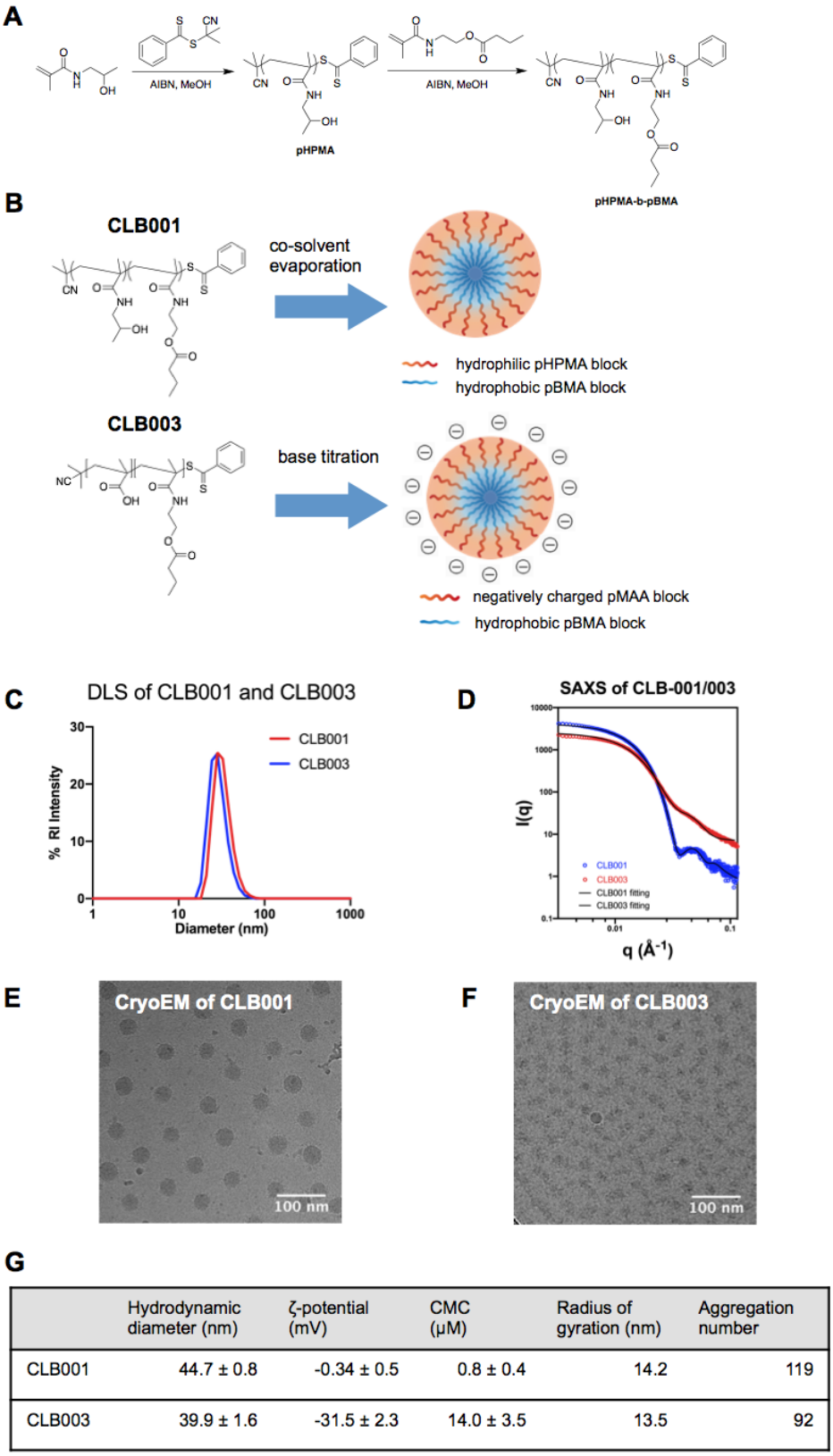

G

	Hydrodynamic diameter (nm)	ζ-potential (mV)	CMC (μM)	Radius of gyration (nm)	Aggregation number
CLB001	44.7 ± 0.8	-0.34 ± 0.5	0.8 ± 0.4	14.2	119
CLB003	39.9 ± 1.6	-31.5 ± 2.3	14.0 ± 3.5	13.5	92

Figure 2.1 Chemical description and structural characterization of butyrate-releasing polymers.

(**Figure 2.1, continued**) (**A**) Representative synthetic route of pHPMA-b-pBMA (CLB001). (**B**) (**upper**) The block copolymer CLB-001 contains a hydrophilic (HPMA) block as corona of the micelle, while a hydrophobic (BMA) block forms the core of the micelle and is capable of releasing butyrate. (**lower**) The block copolymer CLB003 contains a hydrophilic (MAA) block that forms negatively charged corona of the micelle, while the hydrophobic (BMA) block is the same as CLB001. (**C**) Dynamic light scattering (DLS) shows the micelles formed by CLB001 or CLB003 have similar hydrodynamic diameters at sub-hundred nanometer. (**D**) SAXS data of CLB001 and CLB003. Data are fitted with polydisperse core-shell model. (**E, F**) Cryogenic electron microscopy (CryoEM) images show the spherical structures of micelles formed by CLB001 (**E**) or CLB003 (**F**). (**G**) Table summarizing the characterizations of micelle CLB001 and CLB003, including hydrodynamic diameter and zeta-potential from DLS, critical micelle concentration, radius of gyration and aggregation number from SAXS. The critical micelle concentration of CLB003 is significantly higher than CLB001.

2.3.3 CLB003 micelles have negative surface charge and high critical micelle concentration

To study the surface charge of micelles, we used DLS to measure the ζ-potential of CLB001 and CLB003. As we expected, CLB001 micelle had a neutral surface charge (-0.4 ± 0.5 mV), while CLB003 had a negative surface charge (-31.5 ± 2.3 mV) due to the ionization of methacrylic acid (Figure 2.1.G). It was reported that negatively charged nanoparticles could stay in the gastrointestinal tract for longer time and had adherent effect to the gut mucosa[33,38,39]. The negative surface charge of CLB003 micelle also extended its usage to a subcutaneous injection route because negatively charged particles were reported to be drained to the lymph nodes more efficiently[40]. In order to understand the of critical micelle concentration (CMC) of CLB001 and CLB003, pyrene was added during the formulation and the fluorescence intensity ratio between the first and third vibronic bands of pyrene was plotted to calculate CMC[41,42]. Results showed CLB003 had a higher CMC of 14.0 ± 3.5 μM while the CMC of CLB001 was 0.8 ± 0.3 μM (Figure 2.1.G). Higher CMC indicated CLB003 micelle was easier to dissociate in solution, possibly because the surface charge made the micellar structure unstable compared to neutral micelle CLB001.

2.3.5 Polymeric micelles release butyrate in complete serum and simulated gastric/intestinal fluids

Given the second block of polymers have butyrate ester and micelles have a dissociation equilibrium with polymer in the solution, we wanted to validate the release of butyrate in an *ex vivo* environment. The released butyrate from CLB001 or CLB003 was quantified by LC-UV or LC-MS/MS. In order to detect small molecule butyrate in UV detector or Mass Spectrometry, butyrate was derivatized with 3-nitrophenylhydrazine[43,44]. We added polymeric micelles to fetal bovine serum to evaluate the butyrate release from the formulations catalyzed by esterase in serum[45]. CLB003 showed a faster release rate and reached 100% after 12 hours, while at the same time point CLB001 only got 10% of release (Figure 2.2.A). The reason might be that CLB003 had a higher critical micelle concentration, resulting in higher concentration of dissociated polymer in the solution. Then, the dissociated polymer was hydrolyzed by the esterase in the serum at a rapid rate. A similar release study was done in simulated gastric fluid and simulated intestinal fluid (Figure 2.16.C, D). In simulated gastric fluid, CLB003 had a slower release rate than CLB001 probably due to the interaction of CLB003 surface with low pH resulting in resistance to the hydrolysis of BMA core. However, in simulated intestinal fluid, both micelles released all butyrate within minutes because of high concentration of pancreatin. These results validated the formulation CLB001 and CLB003 could release butyrate in serum and simulated gastric/intestinal fluids.

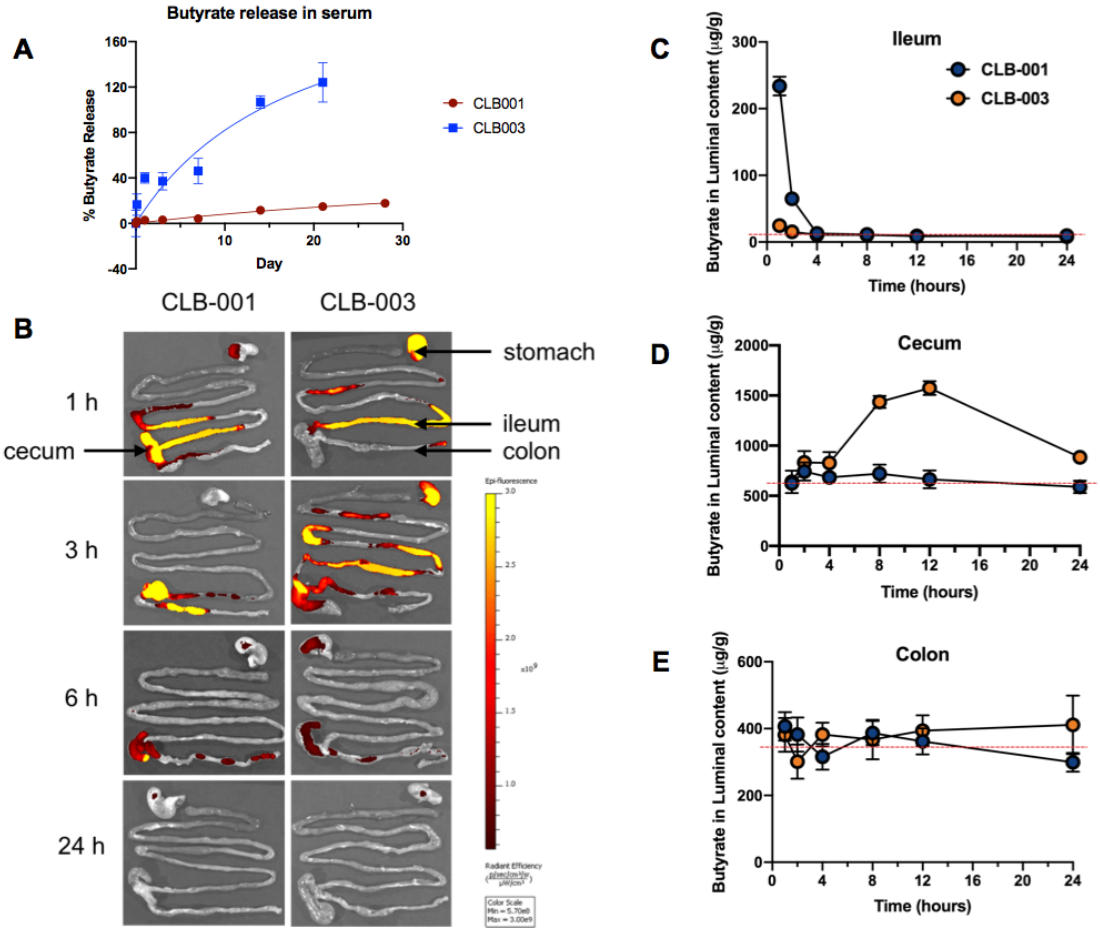

Figure 2.2 Biodistribution and pharmacokinetic study of CLB001 and CLB003. (**A**) *ex vivo* release of butyrate in fetal bovine serum. CLB003 releases faster than CLB-001. (**B**) The distribution of CLB001 or CLB003 in the gastrointestinal tract (GI) reviewed by in vivo imaging system (IVIS). Both polymers were chemically modified with azide and labeled with dye IR750. IVIS showed CLB003 adhered to stomach for more than 6 hours while CLB001 moved to cecum directly after the gavage. Both polymers got cleared from the body after 24 hours. (**C-E**) Butyrate concentrations of ileum, cecum, or colon contents after one single gavage of CLB001 or CLB003. Butyrate was derivatized with 3-nitrophenylhydrazine and quantified with LC-MS/MS. Results indicated CLB001 raised the butyrate concentration of ileum for up to 2 hours after gavage. CLB003 increased the butyrate concentration in cecum after 4 hour and maintained high concentration for more than 8 hours.

2.3.4 CLB003 has longer retention time in stomach and small intestine

Given the structures of micelles were characterized by several instruments, we further studied the biodistribution of CLB001 and CLB003 via In Vivo Imaging System (IVIS) (Figure 2.2.B). Azide function group was incorporated into the hydrophilic blocks of both polymers through copolymerization of azide monomer with either HPMA or MAA. The azide containing polymers were labeled with near infrared dye IR750-DBCO through copper-free azide alkyne cycloaddition. IVIS results validated the polymeric micelles stayed in the mouse GI tract for more than 6 hours after gavage. Neutral micelle CLB001 passed through stomach and small intestine within 2 hours and accumulated in the cecum. However, negative charged CLB003 accumulated in the stomach first and then gradually traveled through small intestine to the cecum. Overall, CLB003 had a longer retention time in the stomach and small intestine due to the adherence to mucosa caused by surface charge. Both micelles were cleared from the GI tract 24 hours after gavage.

2.3.6 Polymeric micelles increase the butyrate levels in the mouse GI tract

Given both CLB001 and CLB003 release butyrate in *ex vivo* conditions, we validated the butyrate levels in the mouse GI tract affected by polymeric micelles. Both LC-UV and LC-MS/MS methods were used to measure the butyrate concentrations in the fecal contents of ileum, cecum, or colon of mice gavaged with either CLB001 or CLB003[43,46]. LC-MS/MS method was mainly used to measure the butyrate concentration in ileum because the base concentration in ileum was too low for UV detector. The results showed CLB001 raised the butyrate level in ileum for up to 2 hours after gavage (Figure 2.2.C). But CLB001 did not have any effect on butyrate levels in cecum or colon (Figure 2.2.D, E). Interestingly, CLB003 raised butyrate

concentrations in the cecum starting from 4 hours after gavage and lasting for more than 8 hours (Figure 2.2.D). However, CLB003 did not increase butyrate concentrations in ileum or colon (Figure 2.2.C, E). The butyrate release of CLB001 in ileum was also validated by gel permeation chromatography (GPC). GPC monitored the molecular weight change of polymers extracted from the fecal contents of mouse GI tract. The release of butyrate could be derived from molecular weight difference and polymer mass. Due to the different butyrate release behavior, we believed the combine dosage of CLB001 and CLB003 could cover the most section of GI tract and last for longer time when we studied the efficacy of polymeric micelles in the animal model.

2.3.7 Butyrate-containing polymers enhance the performance of oral immunotherapy

To evaluate the efficacy of butyrate-containing polymers, we performed the treatment of oral immunotherapy to peanut sensitized mice with or without the combination of CLB001 and CLB003. To establish peanut sensitization model, starting at weaning, SPF C3H/FeJ mice were sensitized weekly for four weeks with 6 mg per mouse of peanut extract (PN) plus 10 μg of the mucosal adjuvant cholera toxin (CT) (Figure 2.3.A) as previously described[12]. Following sensitization, mice were challenged with 5 mg PN per mouse and the change in core body temperature was measured over 60-120 minutes as a marker of the allergic response. Mice that exhibited an allergic response were then treated twice daily for two weeks with either low dose PB2 (peanut butter powder, 200 μg) as OIT alone or PB2 OIT plus the combined polymer formulations CLB001 and CLB003 at 0.4 mg per g of body weight each.

Upon a secondary i.p. challenge with 5 mg PN, the mice treated with OIT alone exhibited no improvement and had a drop in core body temperature as severe as that observed in the initial

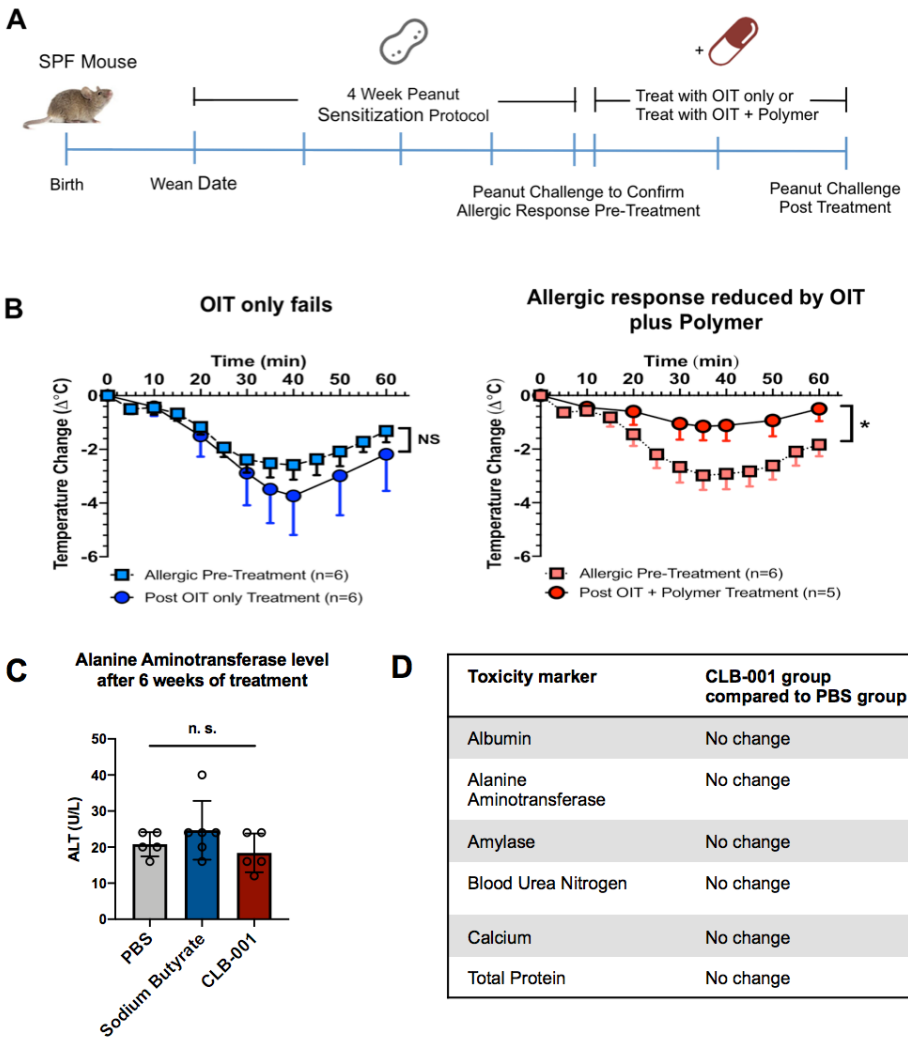

Toxicity marker	CLB-001 group compared to PBS group
Albumin	No change
Alanine Aminotransferase	No change
Amylase	No change
Blood Urea Nitrogen	No change
Calcium	No change
Total Protein	No change

Figure 2.3. Core body temperature decrease after enteral PN challenge of C3H/FeJ sensitized with PN plus CT. Co-administration of polymer (CLB001+CLB003) twice daily enhances therapeutic efficacy of peanut oral immunotherapy (OIT) and in tolerance restoration during desensitization. (**A**) Experiment design and the animal model for OIT and polymer treatment. C3H/FeJ mice were sensitized with peanut antigen and cholera toxin for four weeks after weaning. Then mice were challenged to confirm their allergic response. Mice were treated with OIT with or without CLB001 and CLB003 co-treatment for two weeks before final challenge. (**B**) OIT treatment only failed to rescue the body temperature after challenge, while CLB001/CLB003 plus OIT successfully reduced the temperature drop. Pre-treatment (filled square) and post-treatment (filled circle). Values are presented as means and SEMs. (**C, D**) CLB001 showed no toxic effect to mice. SPF C3H/HeJ mice were treated with PBS, sodium butyrate, or CLB001 every day for 6 weeks. Mouse serum samples were measured on chemistry analyzer for 6 toxicity markers every week. None of the markers showed significant difference between CLB001 group and PBS group. (Results of alanine aminotransferase level on week 6 were showed as an example (**C**)

challenge (Figure 2.3.B, left). However, mice treated with OIT plus the polymer drugs exhibited a significantly reduced change in core body temperature, evidence that they experienced a less extreme allergic response (Figure 2.3.B, right). This preliminary data shows that polymer-encapsulated butyrate can improve the efficacy of OIT and reduce the allergic response to peanut upon secondary challenge.

2.3.8 CLB001 shows no toxicity

In order to investigate the toxicity of materials, we gavaged C3H/FeJ mice with CLB001 at 0.8 mg/g of body weight everyday for 6 weeks. We bled mice every week to test the toxicity markers using blood chemistry analyzer. The results indicated that CLB001 had no toxic effect to mice because none of the toxicity markers, including albumin, alanine aminotransferase, amylase, blood urea nitrogen, calcium, or total protein, changed significantly between CLB001 dosage group and control groups, either PBS or sodium butyrate treated group, through out six weeks (Figure 2.3.C, D).

2.3.9 CLB001 polymer upregulates the genes encoding anti-microbial peptides in ileum

Given that the combination treatment of CLB001/CLB003 and oral immunotherapy showed enhanced performance over oral immunotherapy alone, we moved forward to RNA sequencing to investigate the mechanism of how polymeric micelles affect the GI tract (Figure 2.4.A). Gem-free C3H/FeJ mice were treated with CLB001 for two weeks and then ileal epithelial cells were collected for RNA isolation. The RNA samples were sequenced to reveal the gene expression levels. The results showed significant differences between CLB001 treated mice and mice treated with PBS or control polymers that did not contain butyrate. Such

differences showed no dependence on gender or experiment. Interestingly, the majority of genes upregulated by CLB001 were related to anti-microbial peptides, including angiogenin 4 (*Ang4*), lysozyme C-1 (*Lyz1*), and several defensins (*Defa3*, *Defa22*, *Defa24* etc.). Anti-microbial peptides expressed by Paneth cells in the ileum are essential for maintaining the balance of ileal microbiome[47,48]. Previously in the pharmacokinetics study, we demonstrated CLB001 increased the butyrate level in ileum. Thus, we believe the butyrate released by CLB001 might affect the gene expression levels of Paneth cells and that such effect could rescue the gut dysbiosis to help alleviate food allergic response.

2.3.10 Intelectin stain validates one of the anti-microbial peptide identified by RNA-Seq at the protein level

Given that CLB001 up-regulates the expression of anti-microbial peptides (AMPs) in the epithelial cells of the ileum, we further validated the translation of one of these AMPs. We chose intelectin as a sample AMP for study (Figure 2.4.B, C). Intelectin can recognize the carbohydrate chains of bacterial cell wall and is known to be expressed by Paneth cells in the small intestine[49]. C3H/FeJ mice were gavaged with CLB001 at 0.8 mg/g of body weight everyday for one week. Then the mice were sacrificed and ileum tissues were fixed on microscope slides. The tissue was stained with fluorescent labeled anti-intelectin antibody and imaged under microscope. The images showed that the CLB001 treated group expressed large amount of intelectin in the crypts of ileal tissue, while as a control, PBS group showed limited amount of intelectin signal (Figure 2.4.C). The statistics also showed CLB001 group has significantly high expression of intelectin, with a *P* value smaller than 0.0001 compared to PBS control (Figure 2.4.B). Intelectin stain further supported the pharmacodynamic effects of CLB001. The up-regulation of genes induced

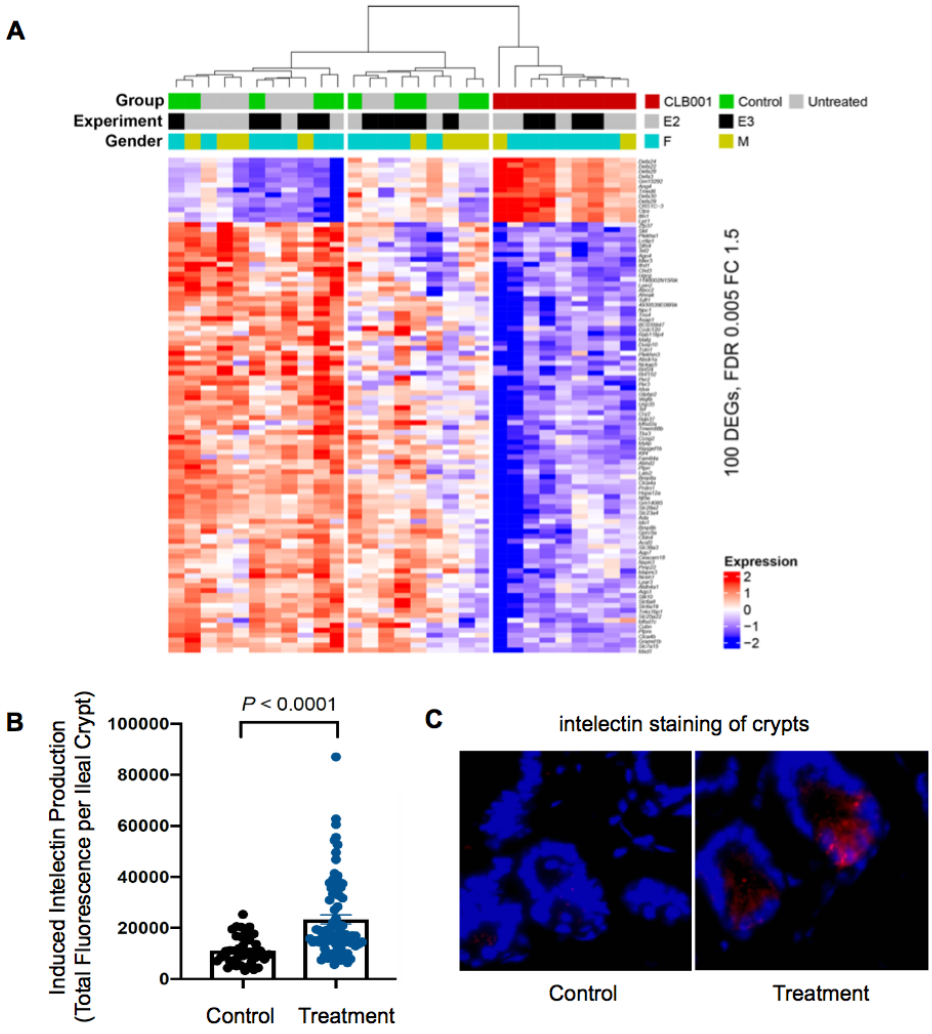

Figure 2.4. CLB001 induced an ileal gene expression signature that was almost entirely Anti-Microbial Peptides (AMP). (**A**) One week of daily dosing of CLB001 induced a unique gene expression signature in the ileum of germ-free mice compared to untreated and "inactive" polymer controls as measured by RNA sequencing of isolated intestinal epithelial cells. (**B**) Intelectin staining validated the gene expression can translate to anti-microbial peptide production. (**C**) Representative images of Intelectin staining of crypts of ileum imaged by fluorescence microscopy. Treatment group was dosed with CLB001 everyday for two weeks before imaging. Control group was dosed with PBS only for two weeks.

by CLB001 was not only demonstrated in the transcription level by RNA-Seq, but also validated in the translational level.

2.3.11 CLB003 induces the proliferation of GATA3$^+$ and RORγt$^+$ regulatory T cells

After we validated CLB001 could induce the expression of AMPs in the ileum, we also investigated other possible mechanisms to explain the enhanced effect of butyrate micelles on oral immunotherapy. It was known that butyrate induced the proliferation of regulatory T cells (Treg) in the gut lamina propria and mesenteric lymph nodes[18-20]. In addition, GATA3 was known to play an important role in maintaining Treg function in immune tolerance[50]. Moreover, Treg expressing RORγt represented a stable regulatory T cell effector lineage with enhanced suppressive capacity[51]. Given that both CLB001 and CLB003 released butyrate in the GI tract, we also studied the regulatory T cell population after the treatment of CLB001 or CLB003. After weaning, C57BL/6 Foxp3^{GFP+} mice were gavaged everyday for three weeks with either CLB001 or CLB003 at a dosage of 0.8 mg/g of body weight (Figure 2.5.A). Cells from spleen, mesenteric lymph nodes, and gut lamina propria were stained and sorted for cell markers including CD25, Foxp3, GATA3, and RORγt. Among all the tissues, we did not see differences in the Foxp3$^+$CD25$^+$ cell population between CLB001, CLB003 or control groups, suggesting the number of Tregs was not increased by the treatment. However, we observed a significant increase of Foxp3$^+$GATA3$^+$ cells and Foxp3$^+$RORγt$^+$ cells in the ileal mesenteric lymph nodes of CLB003 treated group (Figure 2.5.B, C, D). Since GATA3 and RORγt were both found playing an important role for regulatory T cell function, we believe butyrate released by CLB003 could increase of expression of GATA3 and RORγt, providing suppressive immunity to the ileum. However, such increased expression of GATA3 or RORγt was limited to ileal mesenteric lymph

nodes and was not observed in colon mesenteric lymph nodes. CLB001 treated groups did not show such effect either.

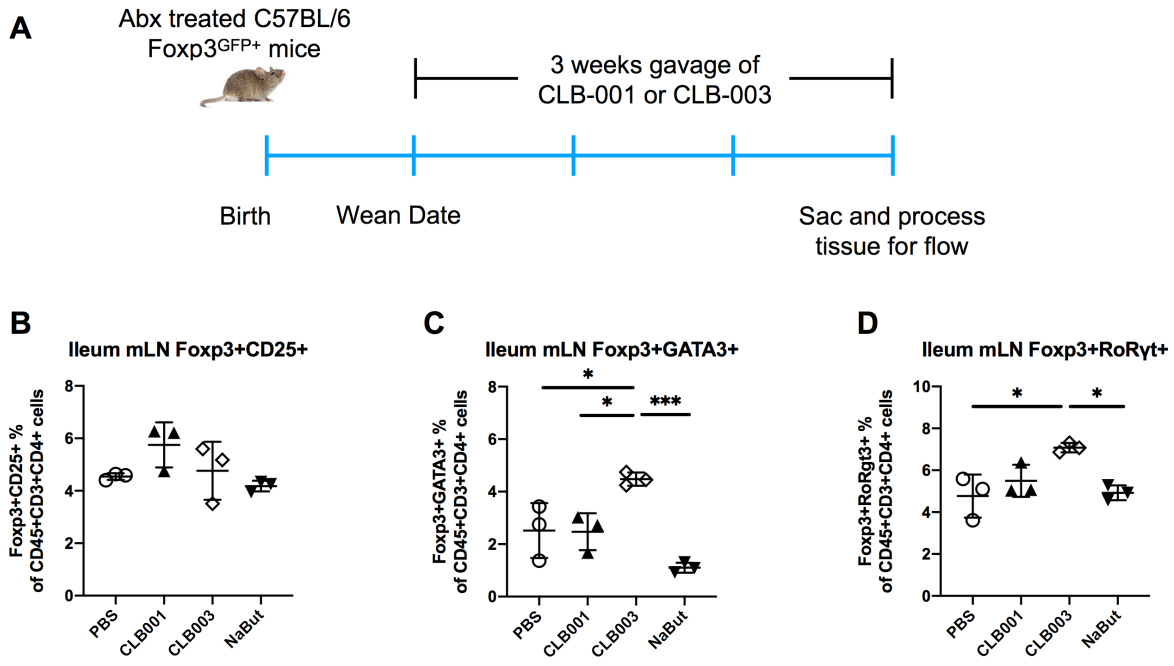

Figure 2.5. CLB003 induced the reproduction of GATA3$^+$ and RORγt$^+$ regulatory T cells in the ileum mesentery lymph nodes. (**A**) Experiment design. C3H/FeJ mice were treated with antibiotics to induce dysbiosis. After the wean date, mice were gavaged with either CLB001 or CLB003 twice per day for 3 weeks before sacrifice and tissue process for flow cytometry. (**B. C. D**) Flow cytometry results of Foxp3$^+$, GATA3$^+$, or RORγt$^+$ T cells in mesentery lymph nodes of ileum. Results indicated in ileum mesentery lymph nodes, CLB003 induced the production of GATA3$^+$ and RORγt$^+$ regulatory T cells while didn't induced more Foxp3$^+$ T cells in general. However, such effect was not seen in colon mesentery lymph nodes.

2.4 Discussion

In this study, we developed a polymeric nano-scale delivery system for butyrate to the gastrointestinal tract. The system was based on polymeric micelles formed by block copolymers. The hydrophobic block contained butyrate esters that can release butyrate at acidic pH or be catalyzed by esterase in the GI tract. For the hydrophilic block, we designed two platforms:

pHPMA with neutral surface charge as CLB001, or pMAA with negative surface charge due to ionization as CLB003. The reason for using pMAA as hydrophilic block of CLB003 was to take advantage of the adhesion effect between negative charge and gut mucosa in order to extend the retention time of CLB003 in the GI tract. Unlike CLB001, which could formulate into micelles through cosolvent evaporation, CLB003 could not formulate into micelles using the same method. However, if base was added to ionize methacrylic acid, the pMAA block became hydrophilic again and the polymer CLB003 self-assembled into micelles.

Given the micelles formulated from block copolymer CLB001 or CLB003, we characterized the size, surface charge, morphology, and critical micelle concentration of both micelles. DLS revealed the hydrodynamic diameter of the micelles and proved the negative surface charge of CLB003. In addition, cryo-EM images showed the shape of micelles, especially the core structure. Furthermore, SAXS analysis revealed not only the radius of gyrations, but also the aggregation numbers of CLB001 and CLB003. The critical micelle concentration of CLB003 was higher than CLB001 as shown by the measurement of fluorescence of pyrene.

Given the detailed characterizations of micellar structures, we studied the drug release of micelles *ex vivo* in fetal bovine serum or simulated gastric/intestinal fluids. As shown by the quantification of derivatized butyrate using LC-MS/MS, both CLB001 and CLB003 released butyrate catalyzed by esterase in all conditions including complete serum, simulated gastric or intestinal fluid. After proving the release of butyrate in *ex vivo* condition, we investigated the biodistribution of micelles in the GI tract using fluorescent dye labeled CLB001 or CLB003. Then, we studied the pharmacokinetics of CLB001 and CLB003 by measuring the butyrate level of GI content of mice gavaged by polymeric micelles. To our surprise, CLB001 and CLB003

showed very different profiles of release in the gut. CLB001 could elevate butyrate levels in ileum within 2 hours after gavage, while CLB003 raised the butyrate level in cecum between 4 and 8 hours after gavage. The different release profiles were the results of different biodistribution of two polymeric micelles. After gavage, CLB001 bypassed stomach and moved to the small intestine quickly. The esterase in the small intestine catalyzed the hydrolysis of butyrate ester of pBMA block as demonstrated in the *ex vivo* hydrolysis study. Thus the butyrate level of ileum content was raised right after the treatment of CLB001 and then dropped within two hours. However, as shown in the IVIS images, CLB003 stayed in the stomach for much longer, probably due to the acidic pH in the stomach protonized the pMAA block and caused aggregation. Another reason was that the adhesive effect between the micelles and mucosa in the stomach extended the retention time. Then, CLB003 gradually moved into the small intestine or cecum and released butyrate there. Importantly, the LC-MS/MS method only measured the local butyrate level of GI content and it could not reveal the total released butyrate because as a short chain fatty acid, butyrate could be consumed or digested quickly after release. However, the increase of local butyrate level in ileum or cecum did prove that CLB001 and CLB003 micelle systems could deliver butyrate to the GI tract.

Given the promising results from biodistribution and pharmacokinetics studies of CLB001 and CLB003, we decided to combine CLB001 and CLB003 together and used the mixture as treatment in the peanut sensitization and oral immunotherapy model. The combination of CLB001 and CLB003 could cover both ileum and cecum and provide a long term of increase of butyrate level. After 5 weeks of treatment of antibiotics cocktail peanut sensitization, C3H/FeJ mice that developed allergic response were divided into two groups. One group was treated with oral immunotherapy, which was desensitization therapy via daily dosage

of a small amount of peanut antigens. The other group was treated with both oral immunotherapy and butyrate containing micelles. After two weeks of treatment, the allergy symptoms of butyrate treated group were alleviated significantly as shown from the reduced temperature drop after peanut antigen challenge. On the contrary, the oral immunotherapy only group did not show any reduction of temperature drop. In addition to the peanut allergy model, we also investigated the safety of the butyrate micelles. After gavage of CLB001 everyday for six weeks, the blood samples from mice were tested on several toxicity markers via chemistry analyzer. The results showed no differences between polymer treated group and control. These results proved the butyrate treatment enhanced the performance of oral immunotherapy in alleviating the allergy symptoms. The safety of the materials also provided potential of translating the combination of butyrate treatment and oral immunotherapy into clinic.

To investigate the mechanism of how butyrate-containing polymers affect the GI tract, we did RNA sequencing of ileum epithelial cells after treatment with CLB001 micelles. The RNA-seq results indicated significant differences between CLB001 group and the control group. Genes related with anti-microbial peptides were expressed in a higher level in the CLB001 group. To validate the up-regulated genes, we made tissue sections and stained one of the anti-microbial peptide: interlectin-1. The stained tissue sections indicated that CLB001 treatment enhanced the expression of interlectin-1 in the crypt of the ileum. The interlectin-1 stain demonstrated the pharmacodynamic effect of CLB001 in up-regulating the expression of genes related to anti-microbial peptides. In addition to RNA-Seq, we also investigated the regulatory T cells induction by butyrate treatment. After treating mice with CLB001 or CLB003 for 3 weeks, we prepared cells from the mice mesenteric lymph nodes, spleen, and lamina propria for flow cytometry. Although the flow data did not show an increase of Treg population in the butyrate

polymer treated group, the $Foxp3^{+}GATA3^{+}$ or $Foxp3^{+}ROR\gamma t^{+}$ cell populations were increased in the CLB003 treated group in the ileum mesenteric lymph nodes. GATA3 and RORγt expressions in regulatory T cells contributed to suppressive effect in the GI tract immune response. Thus, the role of genes regulating the induction of $Foxp3^{+}GATA3^{+}$ or $Foxp3^{+}ROR\gamma t^{+}$ cells in the gut could contribute to the enhanced performance of oral immunotherapy in peanut allergy model.

2.5 Materials and Methods:

2.5.1 Mice

C3H/FeJ mice were used for peanut sensitization study, biodistribution study, and pharmacokinetics study. C57BL/6 $Foxp3^{GFP+}$ were used for regulatory T cell study. Mice were breed in the lab and treatment started at weaning. All experiments were littermate controlled. For RNAseq or intelectin stain, gem-free C3H/FeJ or C57BL/6 mice were used. All animal experiments performed in this study were approved by the Institutional Animal Care and Use Committee of the University of Chicago.

2.5.2 Synthesis of polymers

N-(2-hydroxyethyl) methacrylamide (HPMA) monomer was obtained from Sigma-Aldrich or Polysciences Inc. Solvents like dichloromethane, methanol, hexanes, and ethanol were ACS reagent grade and were obtained from Fisher Scientific. All other chemicals were obtained from Sigma-Aldrich. Chemicals were used in the synthesis without further purifications.

2.5.2.1 Synthesis of N-(2-hydroxyethyl) methacrylamide (2)

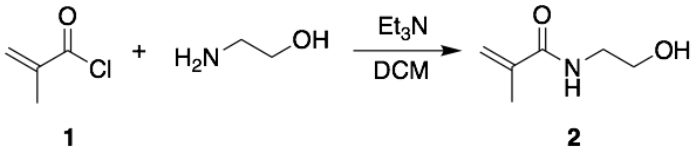

Scheme 2.1 Synthesis of N-(2-hydroxyethyl) methacrylamide (HEMA, **2**)

To synthesize N-(2-hydroxyethyl) methacrylamide (HEMA, **2**), ethanolamine (3.70 mL, 61.4 mmol, 2.0 eq), triethylamine (4.72 mL, 33.8 mmol, 1.1 eq) and 50 mL DCM were added into a 250 mL flask. After the system was cooled down by an ice bath, methacryloyl chloride (**1**, 3.00 mL, 30.7 mmol, 1.0 eq) was added dropwise under the protection of nitrogen. The reaction was allowed to warm up to room temperature and reacted overnight. Then the reaction mixture was concentrated by rotary evaporation and purified on a silica column using DCM/MeOH (MeOH fraction v/v from 0% to 5%). The product was obtained as colorless oil (3.42 g, 86.3%). MS (ESI). $C_6H_{11}NO_2$, m/z calculated for $[M+H]^+$: 129.08, found: 129.0. ^{1}H-NMR (500 MHz, $CDCl_3$) δ 1.93 (s, 3H), 3.43 (m, 2H), 3.71 (m, 2H), 5.32 (s, 1H), 5.70 (s, 1H), 6.44 (br s, 1H)

2.5.2.2 Synthesis of N-(2-butanoyloxyethyl) methacrylamide (3)

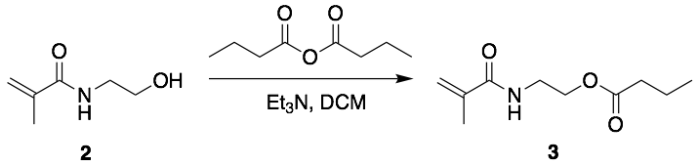

Scheme 2.2 Synthesis of N-(2-butanoyloxyethyl) methacrylamide (BMA, **3**)

To synthesize N-(2-butanoyloxyethyl) methacrylamide (BMA, **3**), N-(2-hydroxyethyl) methacrylamide (3.30 mL, 25.6 mmol, 1.0 eq), triethylamine (7.15 mL,

51.2 mmol, 2.0 eq) and 50 mL DCM were added into a 250 mL flask. After the reaction system was cooled down by an ice bath, butyric anhydride (5.00 mL, 30.7 mmol, 1.2 eq) was added dropwise under the protection of nitrogen. The system was allowed to react overnight. The reaction mixture was filtered and washed by NH_4Cl solution, $NaHCO_3$ solution, and water. After dried by anhydrous $MgSO_4$, the organic layer was concentrated by rotary evaporation and purified on a silica column using DCM/MeOH (MeOH fraction v/v from 0% to 5%). The product was obtained as pale yellow oil (4.56 g, 89.6%). MS (ESI). $C_{10}H_{17}NO_3$, m/z calculated for $[M+H]^+$: 199.12, found: 199.1. ^{1}H-NMR (500 MHz, $CDCl_3$) δ 0.95 (t, 3H), 1.66 (m, 2H), 1.97 (s, 3H), 2.32 (t, 2H), 3.59 (dt, 2H), 4.23 (t, 2H), 5.35 (s, 1H), 5.71 (s, 1H), 6.19 (br s, 1H)

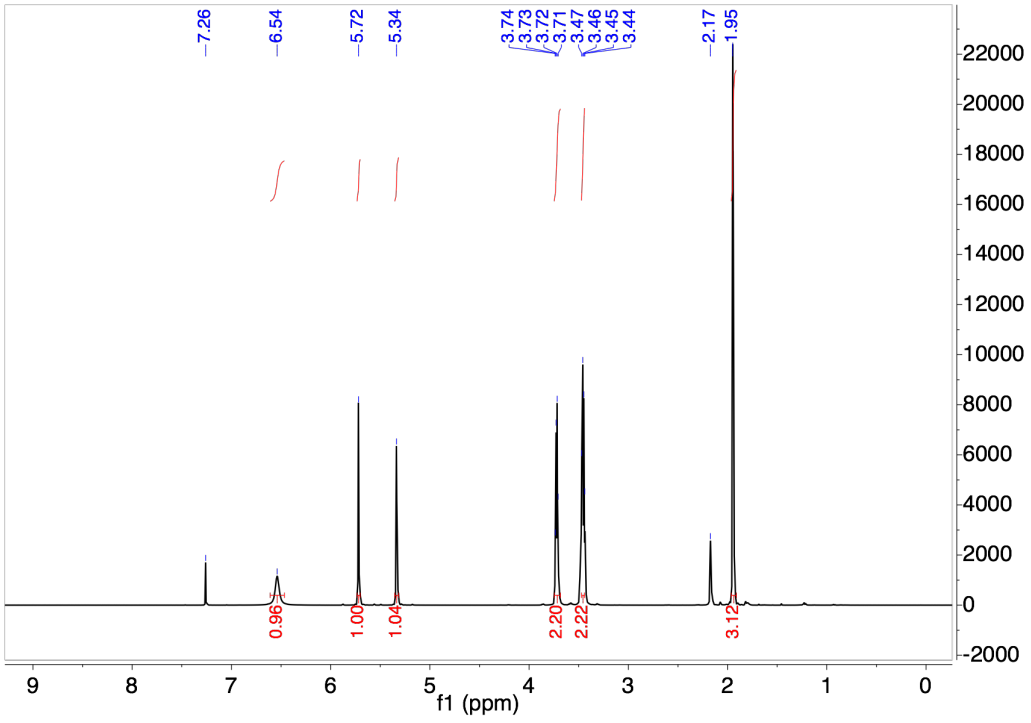

Figure 2.6 ^{1}H-NMR (500 MHz, $CDCl_3$) of HEMA (**2**)

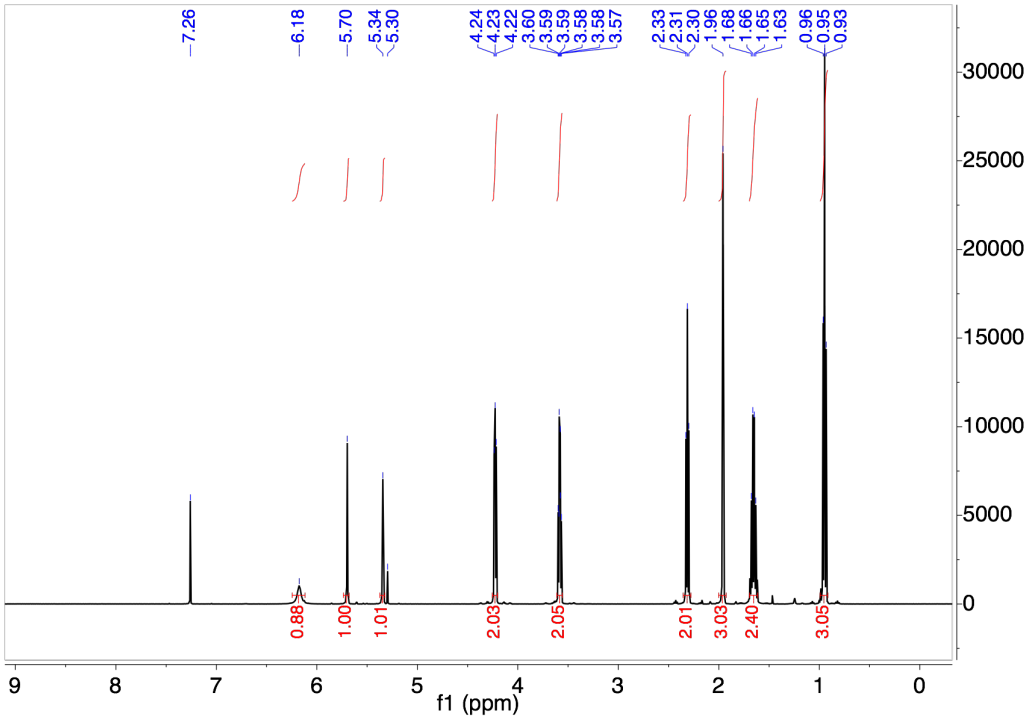

Figure 2.7 ^{1}H-NMR (500 MHz, $CDCl_3$) of BMA (**3**)

2.5.2.3 Synthesis of poly(2-hydroxypropyl methacrylamide) (pHPMA, 5)

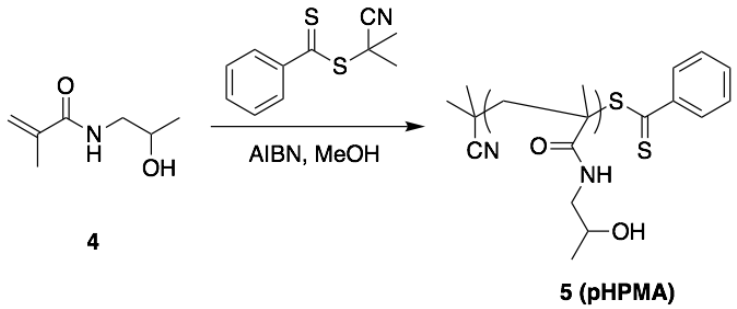

Scheme 2.3 Synthesis of poly(2-hydroxypropyl methacrylamide) (pHPMA, **5**)

pHPMA was prepared using 2-cyano-2-propyl benzodithioate as the RAFT chain transfer agent and 2,2'-Azobis(2-methylpropionitrile) (AIBN) as the initiator. Briefly, HPMA (**4**, 3.0 g, 20.9 mmol, 1.0 eq), 2-cyano-2-propyl benzodithioate (28.3 mg, 0.128 mmol, 1/164 eq), and AIBN (5.25 mg, 0.032 mmol, 1/656 eq) were dissolved in 10 mL

MeOH in a 25 mL Schlenk tube. The reaction mixture was subjected to four freeze-pump-thaw cycles. The polymerization was conducted at 70 °C for 30 h. The polymer was precipitated in a large volume of petroleum ether and dried in the vacuum chamber overnight. The product was obtained as light pink solid (1.8 g, 60 %). ^{1}H-NMR (500 MHz, DMSO-d6) δ 0.8-1.2 (m, 6H, CH(OH)-CH_3 and backbone CH_3), 1.5-1.8 (m, 2H, backbone CH_2), 2.91 (m, 2H, NH-CH_2), 3.68 (m, 1H, C(OH)-H), 4.70 (m, 1H, CH-OH), 7.18 (m, 1H, NH)

2.5.2.4 Synthesis of pHPMA-*b*-pBMA (CLB001, 6)

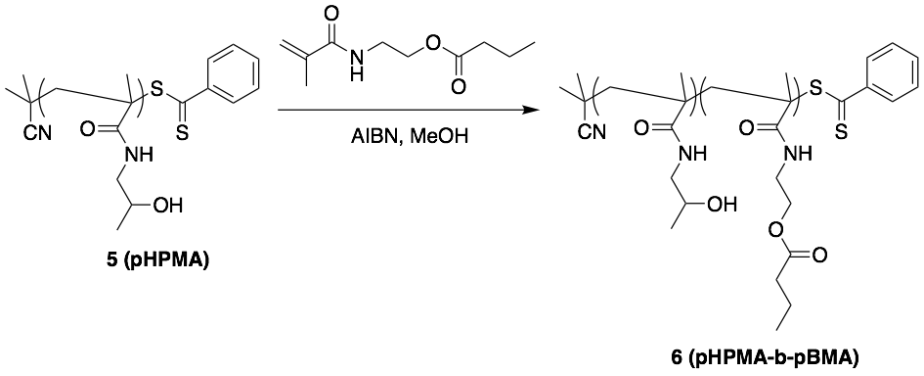

Scheme 2.4 Synthesis of pHPMA-*b*-pBMA, or CLB001 polymer (**6**)

The block copolymer CLB001 was prepared using pHPMA (**5**) as the macro-RAFT chain transfer agent and N-(2-butanoyloxyethyl) methacrylamide (**3**) as the monomer of the second RAFT polymerization. Briefly, pHPMA (1.50 g, 0.105 mmol, 1.0 eq), N-(2-butanoyloxyethyl) methacrylamide (4.18 g, 21.0 mmol, 200 eq), and AIBN (8.3 mg, 0.050 mmol, 0.50 eq) were dissolved in 10 mL MeOH in a 50 mL Schlenk tube. The reaction mixture was subjected to four freeze-pump-thaw cycles. The polymerization was conducted at 70 °C for 20 h. The polymer was precipitated in petroleum ether and dried

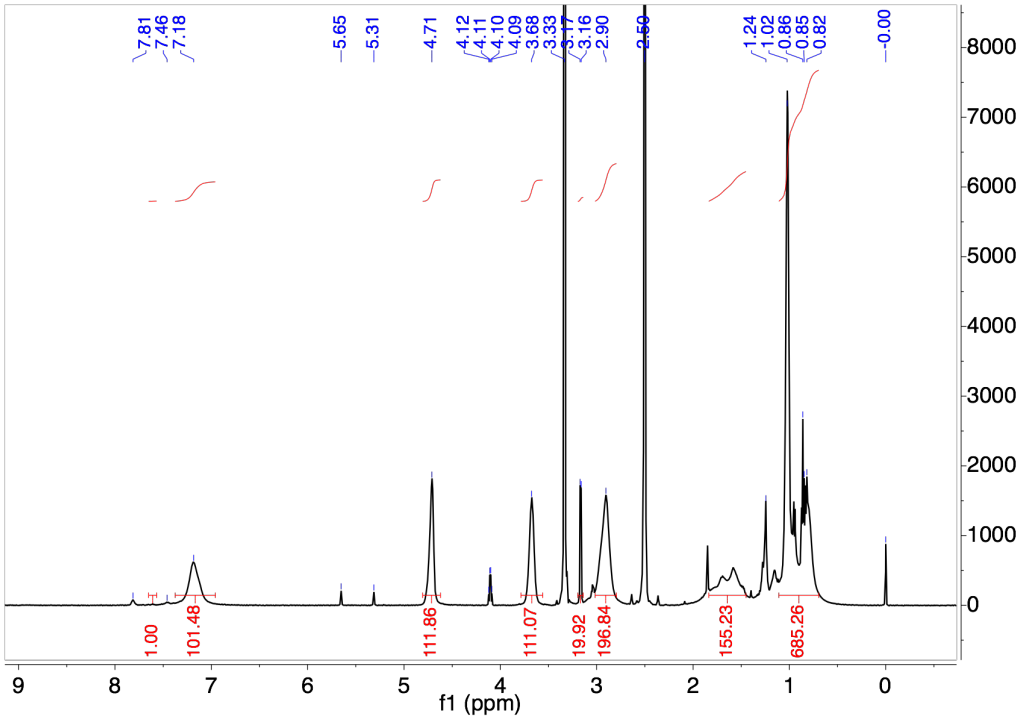

Figure 2.8 [1]H-NMR (500 MHz, DMSO-d6) of pHPMA (**5**)

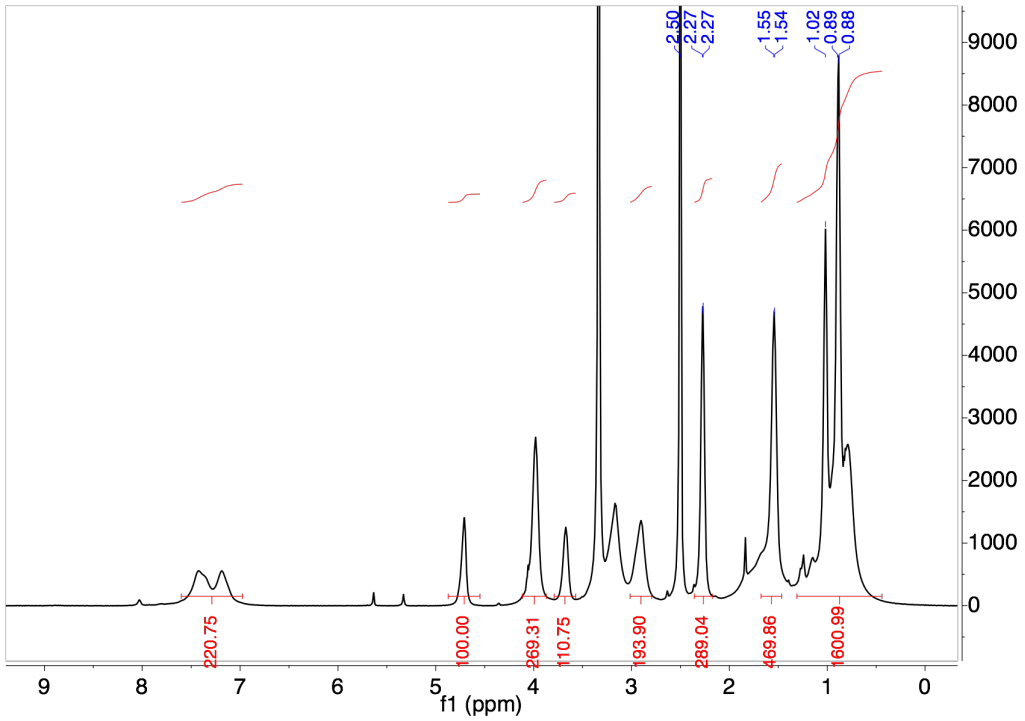

Figure 2.9 [1]H-NMR (500 MHz, DMSO-d6) of pHPMA-*b*-pBMA (**6**)

in the vacuum chamber overnight. The product was obtained as light pink solid (4.22 g, 74%). ^{1}H-NMR (500 MHz, DMSO-d6) δ 0.80-1.1 (m, 9H, CH(OH)-CH_3 (HPMA), CH_2-CH_3 (BMA), and backbone CH_3), 1.55 (m, 4H, CH_2-CH_2 (BMA) and backbone CH_2), 2.28 (m, 2H, CO-CH_2 (BMA)), 2.91 (m, 2H, NH-CH_2 (HPMA)), 3.16 (m, 2H, NH-CH_2 (BMA)), 3.67 (m, 1H, CH(OH)-H), 3.98 (m, 2H, O-CH_2 (BMA)), 4.71 (m, 1H, CH-OH (HPMA)), 7.19 (m, 1H, NH), 7.44 (m, 1H, NH)

2.5.2.5 Synthesis of pMAA (7) and pMAA-*b*-pBMA (8)

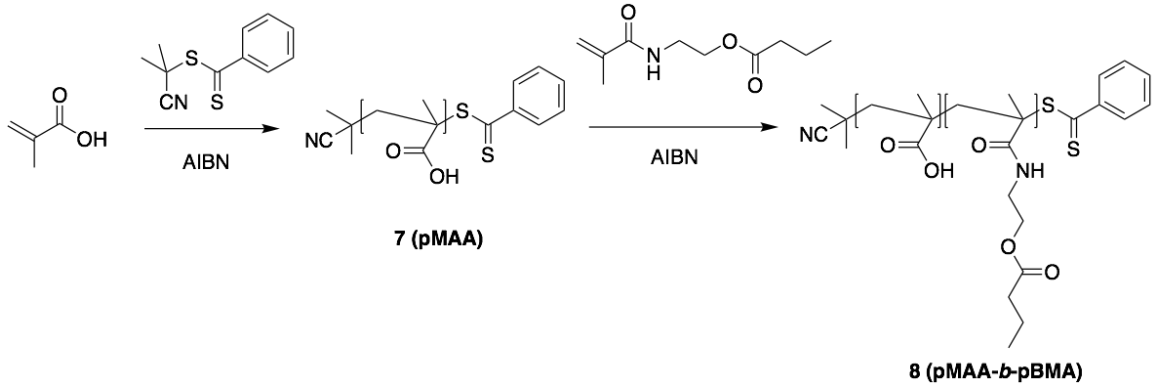

Scheme 2.5 Synthetic route of pMAA-*b*-pBMA, or CLB003 polymer (**8**)

pMAA (**7**) was prepared using 2-cyano-2-propyl benzodithioate as the RAFT chain transfer agent and 2,2'-Azobis(2-methylpropionitrile) (AIBN) as the initiator. Briefly, methacrylic acid (MAA) (4.0 mL, 47.2 mmol, 1.0 eq), 2-cyano-2-propyl benzodithioate (104.4 mg, 0.472 mmol, 1/100 eq), and AIBN (19.4 mg, 0.118 mmol, 1/400 eq) were dissolved in 20 mL MeOH in a 50 mL Schlenk tube. The reaction mixture was subjected to four freeze-pump-thaw cycles. The polymerization was conducted at 70 °C for 24 h. The polymer was precipitated in hexanes and dried in the vacuum oven overnight. The product was obtained as light pink solid (4.0 g, 100 %). ^{1}H-NMR (500 MHz, DMSO-d6) δ 0.8-1.2 (m, 3H, backbone CH_3), 1.5-1.8 (m, 2H, backbone CH_2), 7.4-7.8 (three peaks, 5H, aromatic H), 12.3 (m, 1H, CO-OH)

The block copolymer pMAA-*b*-pBMA (CLB003, **8**) was prepared using (**7**) pMAA as the macro-RAFT chain transfer agent and (**3**) N-(2-butanoyloxyethyl) methacrylamide (BMA) as the monomer of the second RAFT polymerization. Briefly, pMAA (0.50 g, 0.058 mmol, 1.0 eq), N-(2-butanoyloxyethyl) methacrylamide (1.47 g, 7.38 mmol, 127 eq), and AIBN (2.4 mg, 0.015 mmol, 0.25 eq) were dissolved in 10 mL MeOH in a 25 mL Schlenk tube. The reaction mixture was subjected to four freeze-pump-thaw cycles. The polymerization was conducted at 70 °C for 24 h. The polymer was precipitated in hexanes and dried in the vacuum oven overnight. The product was obtained as light pink solid (1.5 g, 70%). ^{1}H-NMR (500 MHz, DMSO-d6) δ 0.8-1.1 (m, 6H, CH_2-CH_3 (BMA), and backbone CH_3), 1.5-1.7 (m, 4H, CH_2-CH_2 (BMA) and backbone CH_2), 2.3 (m, 2H, CO-CH_2 (BMA)), 3.2 (m, 2H, NH-CH_2 (BMA)), 4.0 (m, 2H, O-CH_2 (BMA)), 7.4 (m, 1H, NH), 12.3 (m, 1H, CO-OH)

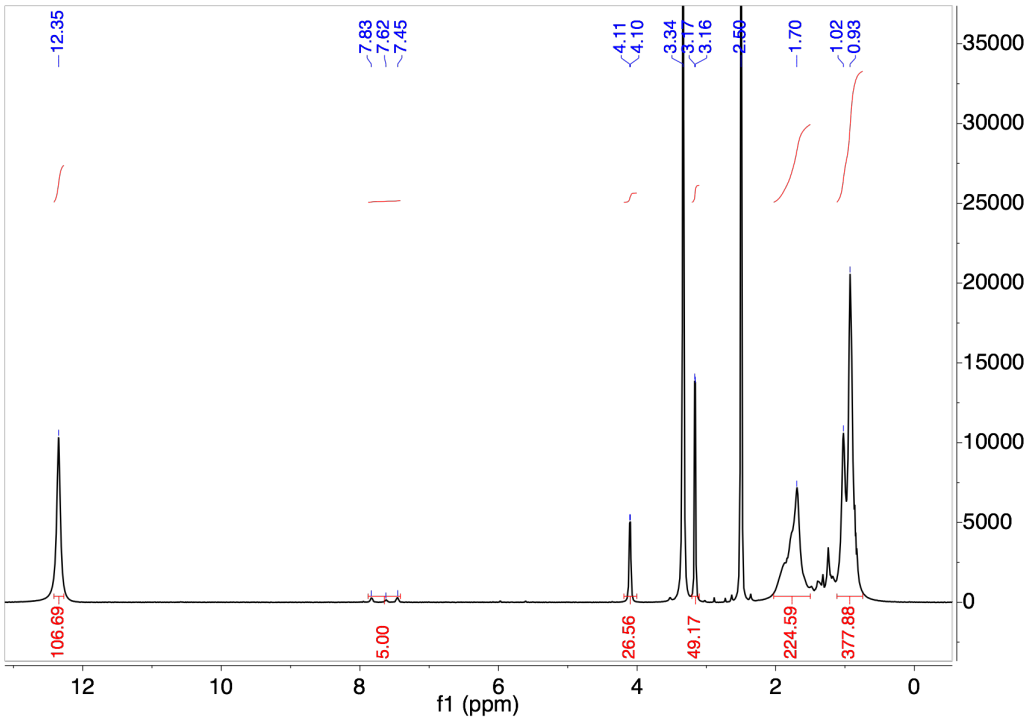

Figure 2.10 ^{1}H-NMR (500 MHz, DMSO-d6) of pMAA (**7**)

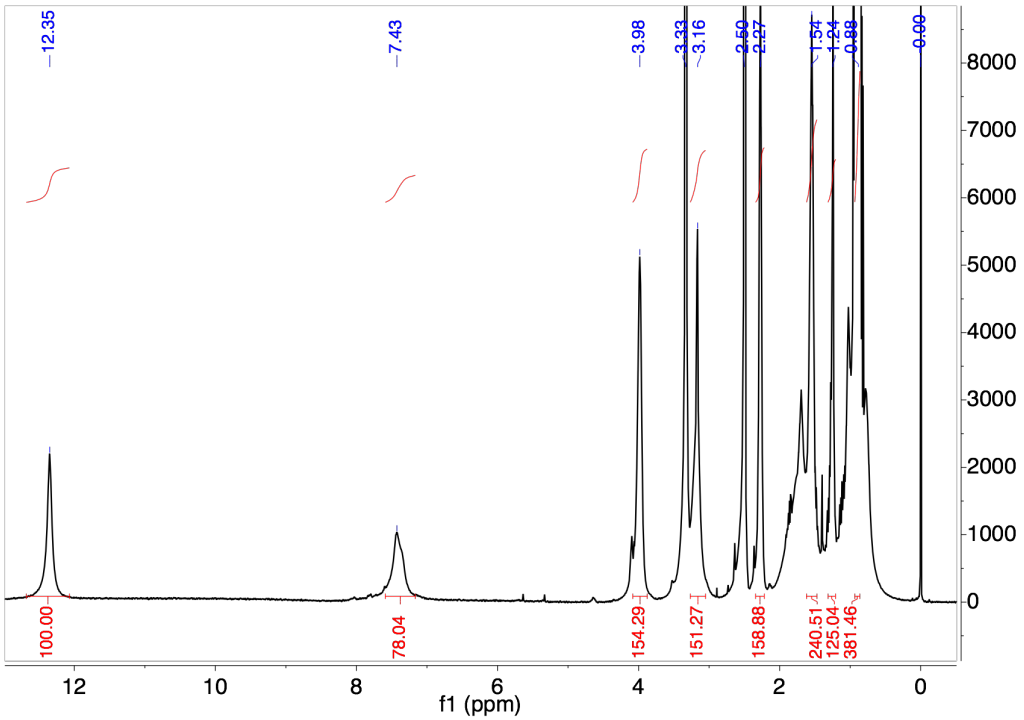

Figure 2.11 [1]H-NMR (500 MHz, DMSO-d6) of pMAA-*b*-pBMA (**8**)

2.5.2.6 Synthesis of N_3-PEG_4-MA (9) and azide-PEG polymer

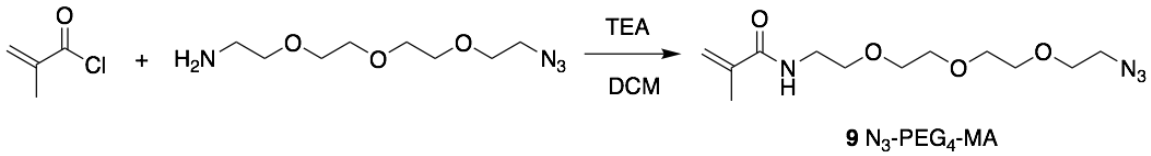

Scheme 2.6 Synthesis of hydrophilic azide monomer N_3-PEG_4-MA (**9**)

In order to include an azide group into CLB001 or CLB003 polymers, monomer N-(2-(2-(2-(2-azidoethoxy)ethoxy)ethoxy)ethyl) methacrylamide (**9**) was synthesized and used in the copolymerization with HPMA or MAA to obtain the hydrophilic block with azide function.

Briefly, N_3-PEG_4-NH_2 (0.5 g, 2.14 mmol, 1.0 eq) and triethylamine (0.60 mL, 4.3 mmol, 2.0 eq) was dissolved in dry DCM. After the reaction system was cooled down by an ice bath, methacrylic chloride (0.42 mL, 2.6 mmol, 1.2 eq) was added dropwise under the protection of

nitrogen. The system was allowed to react overnight. The reaction mixture was filtered and washed by NH_4Cl solution, $NaHCO_3$ solution, and water. After dried by anhydrous $MgSO_4$, the organic layer was concentrated by rotary evaporation and purified on a silica column using DCM/MeOH (MeOH fraction v/v from 0% to 5%). The product was obtained as pale yellow oil (0.47 g, 73 %). MS (ESI). $C_{12}H_{22}N_4O_4$, m/z calculated for $[M+H]^+$: 287.16, found: 287.2. ^{1}H-NMR (500 MHz, $CDCl_3$) δ 6.35 (br, 1H), 5.70 (s, 1H), 5.32 (s, 1H), 3.55-3.67 (m, 12H), 3.52 (m, 2H), 3.38 (t, 2H), 1.97 (s, 3H)

Monomer N_3-PEG_4-MA was mixed with HPMA or MAA in a 2:98 wt:wt ratio during the RAFT polymerization to obtain N_3-pHPMA or N_3-pMAA. Then, the second block of BMA was added to the macro initiator to obtain N_3-pHPMA-*b*-pBMA or N_3-pMAA-*b*-pBMA, respectively. The synthesis procedures were the same as previous description.

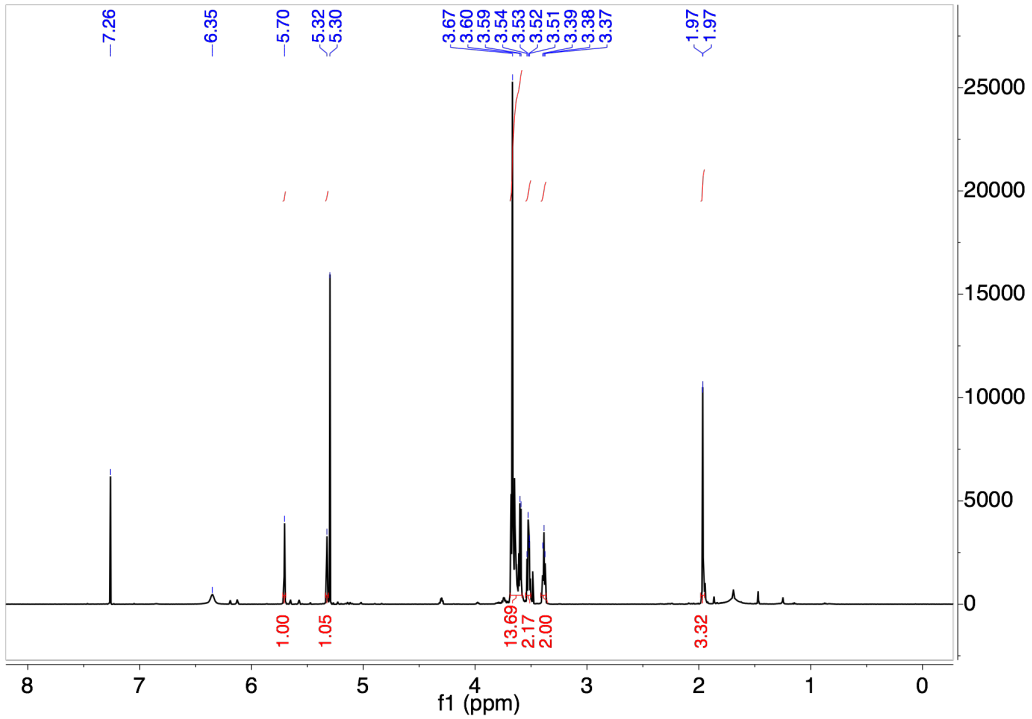

Figure 2.12 ^{1}H-NMR (500 MHz, $CDCl_3$) of N_3-PEG_4-MA (**9**)

2.5.2.7 Synthesis of N-hexyl methacrylamide (10) and control polymer

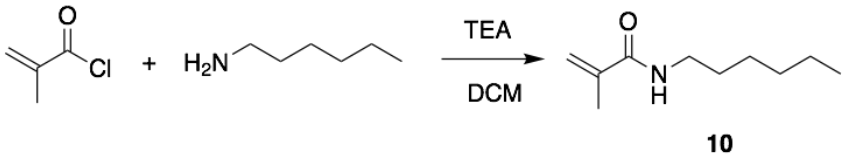

10

Scheme 2.7 Synthesis of hydrophobic control monomer N-hexyl methacrylamide (**10**)

In order to synthesize control polymer that does not contain butyrate ether, monomer N-hexyl methacrylamide (**11**) was synthesized and used in the polymerization of hydrophobic block. Briefly, hexanamine (5.8 mL, 46.0 mmol, 1.5 eq), triethylamine (4.7 mL, 33.8 mmol, 1.1 eq) and 50 mL DCM were added into a 250 mL flask. After the system was cooled down by an ice bath, methacryloyl chloride (3.0 mL, 30.7 mmol, 1.0 eq) was added dropwise under the protection of nitrogen. The reaction was allowed to warm up to room temperature and reacted overnight. Then the reaction mixture was concentrated by rotary evaporation and purified on a silica column using DCM/MeOH (MeOH fraction v/v from 0% to 5%). The product was obtained as colorless oil (4.6 g, 88%). MS (ESI). $C_{11}H_{21}NO$, m/z calculated for $[M+H]^+$: 184.16, found: 184.2. ^{1}H-NMR (500 MHz, $CDCl_3$) δ 5.75 (br, 1H), 5.66 (s, 1H), 5.30 (s, 1H), 3.31 (t, 2H), 1.96 (s, 3H), 1.54 (m, 2H), 1.28-1.32 (m, 8H), 0.88 (t, 3H)

After the synthesis of pHPMA or pMAA, monomer N-hexyl methacrylamide (**11**) was used in the polymerization of second block instead of N-(2-butanoyloxyethyl) methacrylamide to obtain control polymers as pHPMA-*b*-pHMA or pMAA-*b*-pHMA, respectively. The synthesis procedures were the same as previous description.

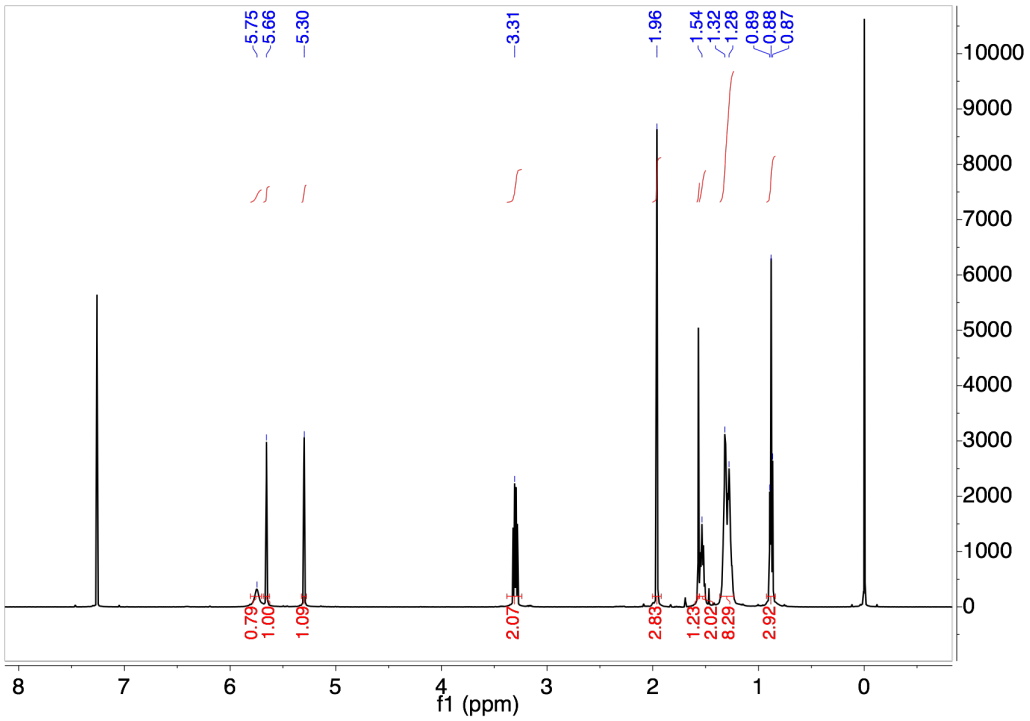

Figure 2.13 ^{1}H-NMR (500 MHz, $CDCl_3$) of N-hexyl methacrylamide (**10**)

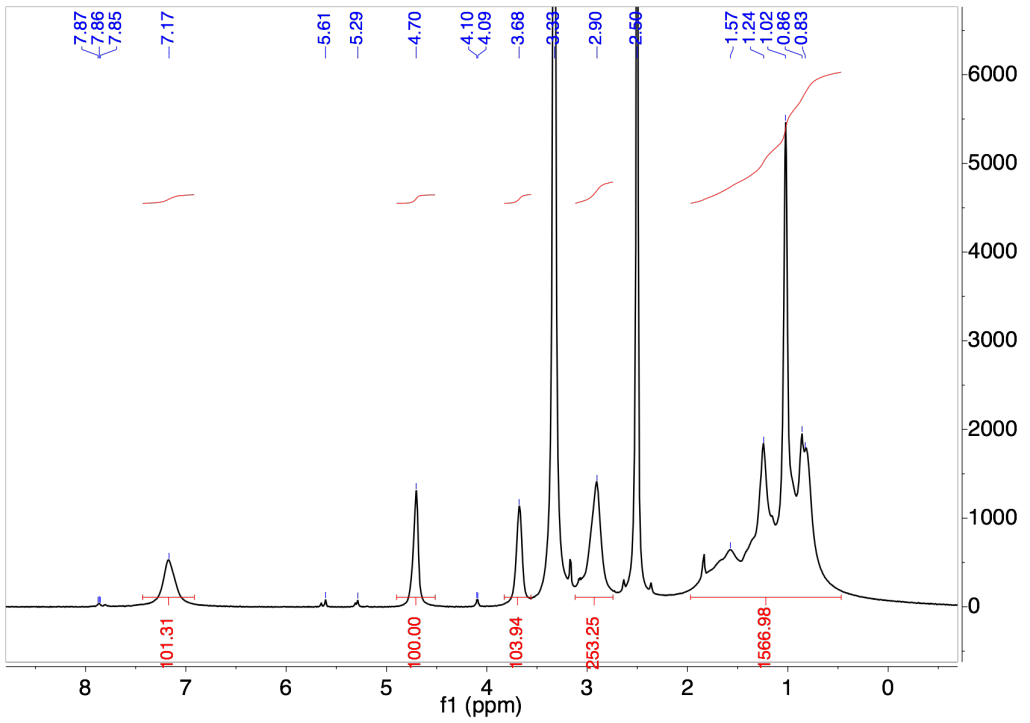

Figure 2.14 ^{1}H-NMR (500 MHz, DMSO-d6) of control polymer pHPMA-*b*-pHMA

2.5.3 Gel permeation chromatography

GPC analyses of pHPMA, CLB001, or CLB003 were performed on Tosoh EcoSEC size exclusion chromatography System using Tosoh SuperAW3000 column. Samples were dissolved in eluent DMF with 0.01 M LiBr at 1 mg/mL. Refreactive index (RI) detector was used to detect polymers. Polymethyl methacrylate (PMMA) was used as calibration standards to determine the molecular weight. GPC analysis of pMAA was performed on Wyatt/Waters size exclusion chromatography System using Agilent PL aquagel-OH columns. Samples were dissolved in aqueous eluent at 1 mg/mL. Refreactive index (RI) detector was used to detect polymers and PEO was used as calibration standards.

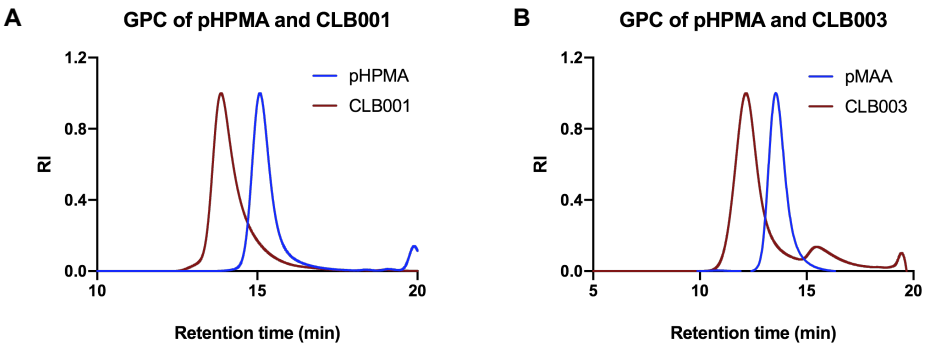

C

	Mn (kDa) by NMR	Mn (kDa) by GPC	Mw (kDa) by GPC	PDI
pHPMA	14.87	17.38	18.97	1.09
CLB001	40.94	36.77	42.69	1.16
pMAA	8.53	34.30	37.56	1.10
CLB003	23.45	136.3	181.3	1.33

Figure 2.15 Gel permeation chromatography analysis of polymers. (**A**) GPC chromatography of pHPMA and CLB001. Samples were run in DMF eluent. (**B**) GPC chromatography of pMAA and CLB003. pMAA was analyzed by aqueous eluent. CLB003 was analyzed by DMF eluent. (**C**) Table of number averaged molecular weight, weight averaged molecular weight, and polydisperse index. Polymethyl methacrylate (PMMA) was used as calibration standards for samples run in DMF. PEO was used as calibration standards for samples run in aqueous eluent.

2.5.4 Formulation of polymeric micelles

CLB001 micelle was formulated by cosolvent evaporation method. 80 mg of CLB001 polymer was dissolved in 10 mL of ethanol under stirring. After polymer was completely dissolved, same volume of 1 × PBS was added slowly to the solution. The solution was allowed evaporating at room temperature for 6 h. After the evaporation, the CLB001 solution was filtered through 0.22 μm filter and stored at 4 °C. The size of the micelle was measured by DLS.

CLB003 micelle was prepared by base titration[34,35]. 60 mg of CLB003 polymer was added to 8 mL of 1 × PBS under vigorous stirring. Sodium hydroxide solution in equivalent to methacrylic acid was added to the polymer solution in three portions during 2 h. After adding base solution, the polymer solution was allowed stirring at room temperature overnight. After that time, 1 × PBS was added to reach the target volume and the solution was filtered through 0.22 μm filter and the pH of the solution was checked to make sure it was neutral. The size of the micelle was measured by DLS.

2.5.5 Dynamic light scattering (DLS) characterizations of micelles

DLS data were obtained from Malvern Nano Zetasizer instrument. Zetasizer software was used to process the data. Samples were diluted 400 times in 1×PBS and 300 μL was transferred to DLS cuvette for data acquisition. Samples were scanned for 16 times at 20 °C and pure water was selected as solvent. The intensity distributions of DLS were used to determine the hydrodynamic diameter of micelles. For zeta-potential data, micelles were diluted in DI water and transferred to disposable folded capillary zeta cells for data acquisition.

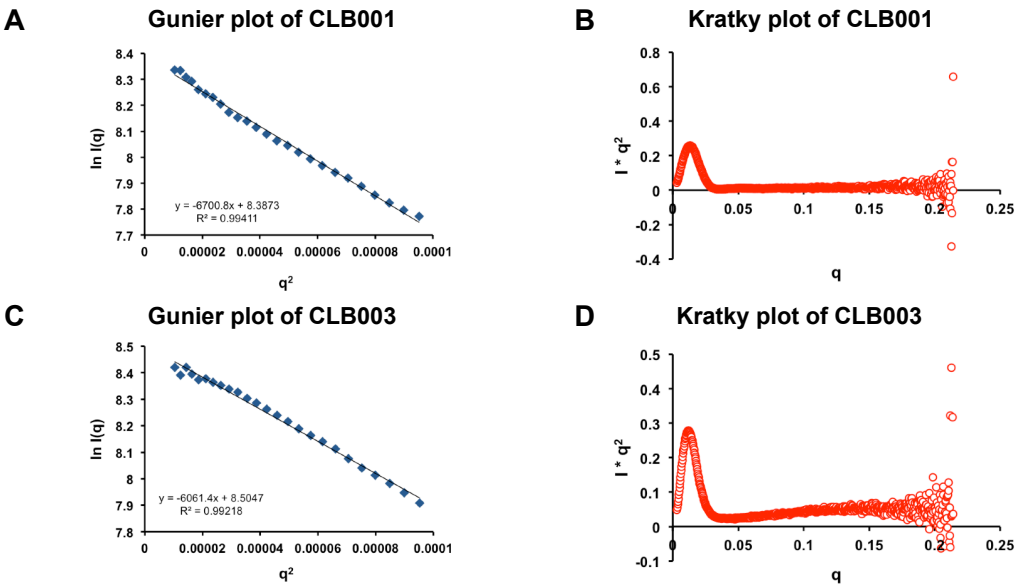

E

	c (mg mL^{-1})	radius$_{core}$ (Å)	thickness$_{shell}$ (Å)	SLD$_{core}$ (10^{-6} Å^{-2})	SLD$_{shell}$ (10^{-6} Å^{-2})	volume fraction
CLB001	2.0	119.31 ± 0.16	72.63 ± 0.31	16.1821 ± 0.0016	10.5338 ± 0.0003	0.007381
CLB003	2.0	83.84 ± 0.34	98.97 ± 0.22	16.9295 ± 0.0023	10.8700 ± 0.0004	0.01393

F

	c (mg mL^{-1})	d (nm)	N (×10^{14} mL^{-1})	Mw (×10^{6} g mol^{-1})	N_{agg}
CLB001	2.0	158.9	2.492	4.831	**119**
CLB003	2.0	122.5	5.441	2.213	**92**

Figure 2.16 SAXS characterizations of CLB001 and CLB003 micelles. (**A**) Gunier plot (ln(q) vs. q^2) of CLB001 revealed the radius of gyration of the micelle. (**B**) Kratky plot ($I\,q^2$ vs. q) of CLB001 revealed the spherical structure if the micelle. (**C**) Gunier plot of CLB003 micelle. (**D**) Kratky plot of CLB003 micelle. (**E**) Table of fitting parameters of CLB001 and CLB003 using polydispersed core-shell sphere model. (**F**) Table of the mean distance between micelles d, number of micelles per unit volume N, molecular weight of the micelle Mw, and the aggregation number N_{agg}, calculated from the fitting parameters of polydispersed core-shell sphere model.

2.5.6 Cryogenic electron microscope imaging of micelles

CryoEM image was acquired on a FEI Talos 200kV FEG electron microscope. Polymeric nanoparticle samples were prepared in 1XPBS and diluted to 2 mg/mL with MilliQ water. 2 µL sample solution was applied to electron microscopy grid (Agar Scientific) with holey carbon film. Sample grids were blotted and flash vitrified in liquid ethane using an automatic plunge

freezing apparatus (Vitrbot) to control humidity (100%) and temperature (20 °C). Analysis was performed at -170 °C on a FEI Talos 200kV FEG electron microscope, using the Gatan 626 cry-specimen holder (120,000 × magnification; -5 μm defocus). Digital images were recorded on in-line Eagle CCD camera, and processed by ImageJ.

2.5.7 Small angle x-ray scattering analysis of micelles

SAXS samples were made in 1 × PBS and filtered through 0.2 μm filters. All samples were acquired at Stanford Synchrotron Radiation Lightsource, SLAC National Accelerator Laboratory. SAXS data were analyzed by Igor Pro 8 software (Figure 2.15). To acquire radius of gyration (R_g), data were plotted as ln(intensity) vs. q^2 at low q range. Then R_g were calculated from the slope of the linear fitting as shown in the equation:

$$ln(I(q)) = ln(I(0)) - \frac{q^2 R_g^2}{3} \quad (1)$$

Kratky plot of the data were plotted from I q^2 vs. q to show the structure of the particles. Moreover, the data were fitted using polydispersed core-shell sphere model (Figure 2.15.E,F)[37]. From the fitting, radius of core, thickness of shell, and volume fraction of micelle were derived and used to calculate the molecular weight of micelle and the mean distance between micelles using flowing equations:

$$N = \frac{\phi_{micelle}}{v_{micelle}} \quad (2)$$

$$M_w = \frac{cN_A}{N} \quad (3)$$

$$d = N^{-1/3} \times 10^7 \quad (4)$$

where N is the number of micelles per unit volume. $\phi_{micelle}$ is the volume fraction of micelles derived from fitting. $v_{micelle}$ is the volume of a single micelle, which is calculated from $4/3\ \pi R^3$, where R is the sum of radius of core and thickness of shell. M_w is the molecular weight

of micelle. c is the polymer concentration. N_A is Avogadro constant. d is the mean distance between the micelles in the unit of nm. The aggregation number of micelles were calculated from dividing the molecular weight of micelle by the molecular weight of polymer.

2.5.8 Measurement of critical micelle concentration

The critical micelle concentrations of CLB001 and CLB003 were determined by a fluorescence spectroscopic method using pyrene as a hydrophobic fluorescent probe[41,42]. A series of polymer solutions with concentration ranging from 1.0×10^{-4} to 2.0 mg mL^{-1} were mixed with pyrene solution with a concentration of 1.2×10^{-3} mg mL^{-1}. The emission spectra of samples were recorded on a fluorescence spectrophotometer (HORIBA Fluorolog-3) at 20 °C using 335 nm as excitation wavelength. The ratio between the first (372 nm) and the third (383 nm) vibronic band of pyrene was used to plot against the concentration of polymer. The data were processed on Prism software and fitted using Sigmoidal model (Figure 2.16).

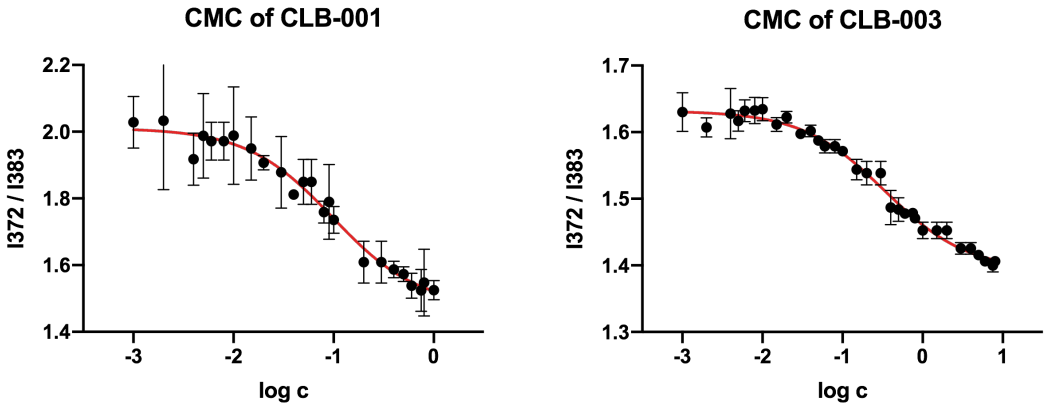

Figure 2.17 Critical micelle concentrations (CMC) of CLB001 (**left**) and CLB003 (**right**) measured by pyrene fluorescent intensity of peak 1 over peak 3. The CMC was determined by the IC50 fitted by Sigmoidal curve.

2.5.9 Biodistribution study using in vivo imaging system (IVIS)

C3H/FeJ mice were used for biodistribution study. CLB001 or CLB003 polymer with azide function was labeled with IR 750-DBCO (Thermo Fisher) and purified by hexane precipitation. After formulation into micelles, the solution was injected to the mice GI tract by gavage. After 1 h, 3 h, 6 h, or 24 h, major organs were collected from the mice and whole-organ fluorescence were measured via an IVIS Spectrum in vivo imaging system (Perkin Elmer). Images were processed and analyzed by Living Imaging 4.5.5 (Perkin Elmer).

2.5.10 Butyrate derivatization and quantification using LC-UV or LC-MS/MS

Sample preparation: Simulated gastric fluid and simulated intestinal fluid were as described before[52,53]. For *ex vivo* hydrolysis study, CLB001 or CLB003 was added to fetal bovine serum, simulated gastric fluid, or simulated intestinal fluid at a final concentration of 2 mg/mL at 37 °C. At pre-determined time points, 20 μL of the solution was transferred into 500 μL of water:acetonitrile 1:1 v/v. The sample was centrifuged using Amicon Ultra (Merck, 3 kDa molecular mass cutoff) at 13,000 × g for 15 min, to remove polymers. The filtrate was stored at -80 °C before derivatization. For *in vivo* pharmacokinetics study, CLB001 or CLB003 micelle solution was gavaged to C3H/HeJ mice at 0.8 mg per g of body weight. Mice were euthanized at 1 h, 2 h, 4 h, 8 h, and 24 h after the gavage. GI tract content from different small intestinal portions, cecum, or colon were collected in EP tube. After adding 500 μL of 1 × PBS, the mixture was vortex and sonicated for 10 min and then centrifuged at 13,000 × g for 10 min. The supernatant was transferred and filtered through 0.45 m filter. The filtered solution was stored at -80 °C before derivatization.

Sample derivatization (Figure 2.17 A): Samples were prepared and derivatized as describe in the literature[43,46]. 3-nitrophenylhydrazine (NPH) stock solution was prepared at 0.02 M in water:acetonitrile 1:1 v/v. EDC stock solution was prepared at 0.25 M in water:acetonitrile 1:1 v/v. 4-methylvaleric acid was added as internal standard. Samples were mixed with NPH stock and EDC stock at 1:1:1 ratio by volume. The mixture was heated by heating block at 60 °C for 30 min. Samples were transferred into HPLC vials and stored at 4 °C before analysis.

LC conditions: The instrument used for quantification of butyrate was Agilent 1290 UHPLC. Column: ThermoScientific C18 4.6 × 50 mm, 1.8 m particle size, at room temperature. Mobile phase A: water with 0.1% v/v formic acid. Mobile phase B: acetonitrile with 0.1% v/v formic acid. Injection volume: 5.0 μL. Flow rate: 0.5 mL/min. Gradient of solvent: 15% mobile phase B at 0.0 min; 100% mobile phase B at 3.5 min; 100% mobile phase B at 6.0 min; 15% mobile phase B at 6.5 min.

ESI-MS/MS method (Figure 2.17 B): The instrument used to detect butyrate was Agilent 6460 Triple Quad MS-MS. Both derivatized butyrate-NPH and 4-methylvaleric-NPH were detected in negative mode. The MS conditions were optimized on pure butyrate-NPH or 4-methylvaleric-NPH at 1 mM. The fragment voltage was 135 V and collision energy was set to 18 V. Multiple reaction monitoring (MRM) of 222 → 137 was assigned to butyrate, and MRM of 250 → 137 was assigned to 4-methylvaleric acid as internal standard. The ratio between MRM of butyrate and 4-methylvaleric acid was used to quantify the concentration of butyrate.

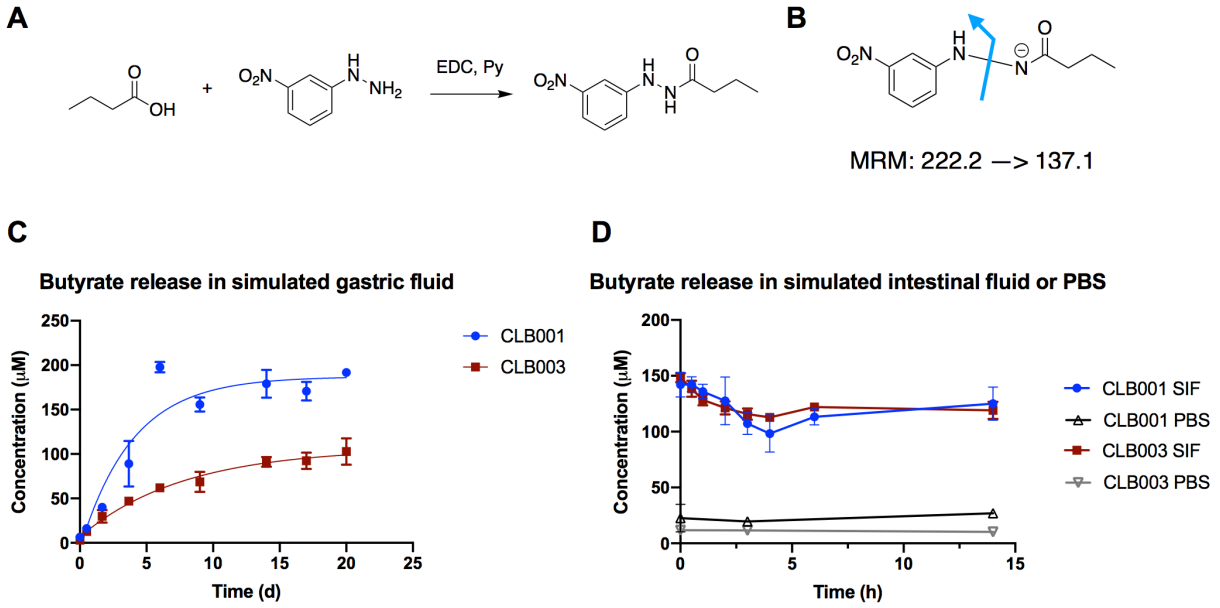

Figure 2.18 Derivatization of butyrate for LC-MS/MS analysis and the release of butyrate from CLB001/003 in simulated gastric/intestinal fluids. (**A**) Derivatization reaction of butyrate with 3-nitrophenylhydrazine (NPH) to generate UV active butyrate-NPH. (**B**) The multiple reaction monitoring (MRM) of 222 → 137 was used to quantify butyrate-NPH in LC-MS/MS. (**C**) CLB001 released butyrate at a faster rate in the simulated gastric fluid compared to CLB003. (**D**) Both CLB001 and CLB003 released complete butyrate load within minutes in simulated intestinal fluid. Neither polymer released butyrate in PBS only.

2.5.11 Butyrate release determined by GPC

In addition to LC-MS/MS measurement of butyrate concentration, butyrate release from CLB001 was also confirmed by determining the molecular weight change of polymer using GPC. First, the method was validated *ex vivo* by adding 50 mM NaOH to CLB001 formulation. The aliquot of polymer solution was obtained and dried in vaccum oven. Then polymer was dissolved in DMF with 0.01 M LiBr. The samples were analyzed by GPC to determine the molecular weight using PMMA as calibration standards. However, the GPC method was not applicable for CLB003 because the dn/dc of CLB003 polymer was too low, resulting in low RI signal for CLB003. To investigate the release of butyrate in mouse GI tract, C3H/FeJ mice were

gavaged with CLB001 and the GI content was obtained at different time points. The GI content was extracted with PBS by vortexing and sonication. The mixture was centrifuged and supernatant was transferred to an Amicon ultracentrifuge tube to concentrate the polymer. Then the concentrated polymer solution was dried in vacuum chamber and then resuspended in DMF with 0.01 M LiBr. After filtration through 0.22 μm filter, samples were analyzed by GPC to determine the molecular weight using PMMA as calibration standards. The number averaged molecular weight of the polymer was used to calculate the percentage release of butyrate by assuming the molecular weight decrease resulted from the release of butyrate. The mass of polymer was also obtained from the RI signal from GPC.

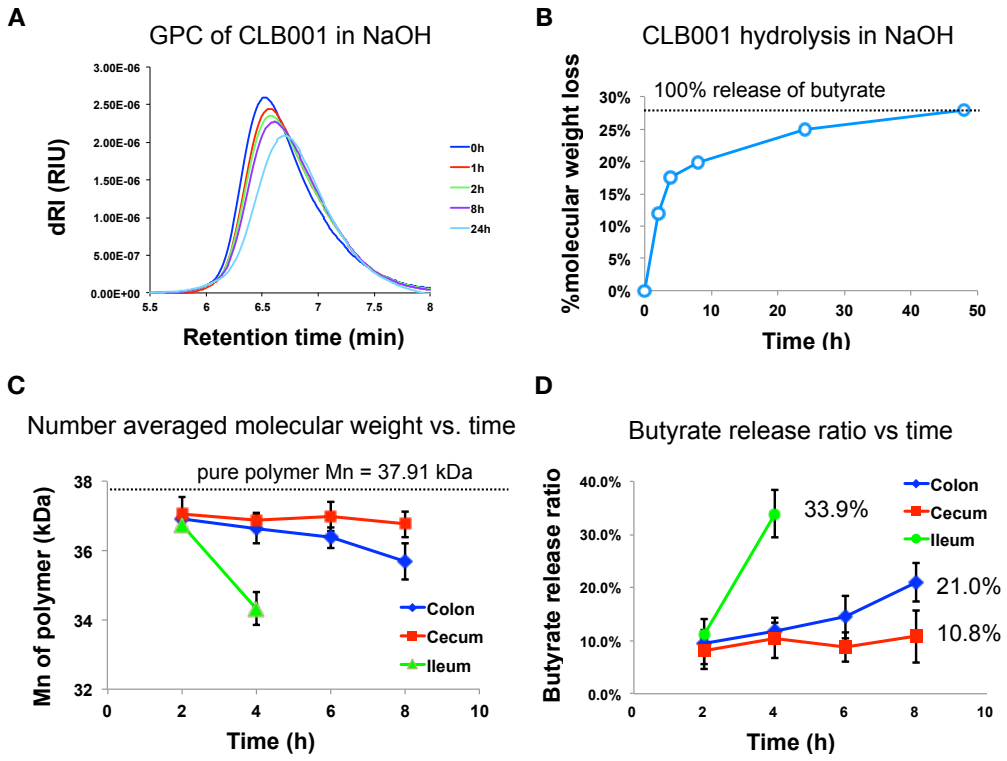

Figure 2.19 Determine the butyrate release via GPC analysis of the molecular weight change of CLB001. (**A**, **B**) Validation of GPC method of CLB001 treated with NaOH. The GPC chromatograph showed the peak of CLB001 moved towards low molecular weight range (**A**) and the molecular weight loss was related to butyrate release (**B**). (**C**, **D**) The butyrate of CLB001 was released in mouse GI tract. GPC showed the molecular weight of CLB001 decreased (**C**) and the butyrate release ratio was calculated based on the decrease of Mn (**D**).

2.5.12 Peanut sensitization model and oral immunotherapy

C3H/FeJ mice were used in the peanut sensitization model and oral immunotherapy as previously described[12]. Specific pathogen free C3H/FeJ mice were treated with antibiotics cocktail to induce dysbiosis for the model starting at wean day. Then, mice were sensitized weekly with 6 mg of peanut antigen and 10 μg of cholera toxin (CT) for 5 weeks to induce peanut allergy. After that time, mice were challenged with i. p. administration of 5 mg peanut antigen in 500 μL of PBS. The change in core body temperature of each mouse after challenge was measured over 60 - 120 min as a marker of allergic response. Allergic mice were randomly assigned into two groups. One group of mice was treated twice daily for two weeks with low dose of peanut butter powder (PB2, 200 μg) as oral immunotherapy only group. The other group of mice was co-administrated twice daily with oral immunotherapy (PB2, 200 μg) and CLB001/CLB003 at 0.4 mg of polymer each per gram of mouse body weight every day for two weeks. After the treatments, mice were challenged again with i.p. administration of 5 mg peanut antigen. The temperature drop was measured after the challenge. The blood samples of mice were collected and the peanut specific IgG or IgE, and mMCP-1 were measured by ELISA.

2.5.13 ELISA of peanut specific antibodies

The ELISA assays of peanut specific antibodies or mMCP-1 were performed according to the protocol provided by manufacturer (Thermo Fisher). The standard peanut antigen was purified from peanut extract in the lab. A 96 well plate was coated with capture antibodies overnight at 4 °C, followed by blocking with 2% BSA in PBS with 0.05% Tween 20 (PBS-T) for 1 hour at room temperature. After washing with PBS-T, the plate was incubated with samples for 2 hours at room temperature. After three washes with PBS-T, the plate was incubated with

biotinylated detection antibodies. After washes, streptavidin-horse radish peroxidase was added and the level of cytokine was detected with tetramethylbenzidine substrate by measuring the absorbance at 450 nm subtracting the absorbance at 570 nm. The data were plotted and analyzed by Prism software.

2.5.14 Toxicity study

The toxicity effect of CLB001 on C3H/FeJ mice was measured by hematological analysis on Vet Axcel Chemistry Analyzer. Mice were treated with CLB001 at 0.8 mg/g of body weight daily by gavage for 6 weeks. Every week, blood sample of each mouse was obtained and analyzed by the chemistry analyzer according to manufacturer's instruction.

2.5.15 RNA sequencing and data process

Starting at the wean time, gem-free C3H/FeJ mice were treated with PBS, CLB001, or control polymer at 0.8 mg/g of body weight for two weeks. After that time, mice were euthanized and the ileum tissue were collected and washed thoroughly. The RNA samples were extracted from the ileal epithelial cells using RNA isolation kit (Thermo Fisher Scientific) according to manufacturer's instruction. RNA samples were submitted to Argonne National Lab for sequencing and the data were analyzed by Illumina software.

2.5.16 Intelectin stain and microscope imaging

Gem-free C57BL/6 mice were treated with CLB001 at 0.8 mg/g of body weight everyday for 2 weeks. After that time, the mice were euthanized and small intestine tissue was obtained and prepared into tissue section slides. The tissue section slides were fixed and stained with

fluorescent anti-intelectin antibody. The slides were imaged using Leica fluorescence microscope. Images were processed by ImageJ software and data were plotted and analyzed by Prism software.

2.5.17 Regulatory T cell induction study and flow cytometry

Antibiotics treated C57BL/6 Foxp3^{GFP+} mice were gavaged with CLB001 or CLB003 at 0.8 mg/g of body weight for 3 weeks starting from the wean date. After the treatment, mice were euthanized and spleen, mesenteric lymph nodes, and lamina propria of small intestine and colon were obtained and processed for flow cytometry analysis.

Flow cytometry analysis were performed as described in previous paper[54]. Briefly, the measurements were performed using a LSRII flow cytometer (BD) and the data were analyzed by FlowJo software. For staining, cells were washed with PBS and stained for 15 min on ice with eFluor 780 fixable live/dead dye (eBioscience). Then, cells were washed with PBS three times, and stained with an antibody cocktail and PBS + 2% FBS for 30 min. The antibody cocktail included antibodies against CD3, CD4, CD45, and CD25. Free antibodies were washed from the cells three times with PBS + 2% FBS. Cells were then fixed for 15 min in PBS + 2% paraformaldehyde. Then intracellular markers were stained with antibodies against Foxp3, GATA3, and RORγt. Samples were washed three times and resuspended in PBS + 2% FBS before analysis by flow cytometry instrument.

2.6 Conclusions

In this study, we developed a polymeric micelle platform to deliver butyrate to the GI tract to enhance the performance of oral immunotherapy in peanut allergy mice. The polymeric

micelles consisted of butyrate ester as hydrophobic core and either neutral or negatively charged hydrophilic shell, namely CLB001 and CLB003, respectively. After structural characterizations of micelles, we validated the butyrate release profiles of polymeric micelles both *ex vivo* and *in vivo*. More importantly, the treatment of CLB001 and CLB003 combined with oral immunotherapy significantly lower the temperature drop of peanut allergic mice after challenge, while mice in the oral immunotherapy only group did not show reduced temperature drop. Furthermore, the effect of butyrate polymers to mice GI tract may result from up-regulated anti-microbial peptide expression in the ileum as indicated from RNA-Seq data. The stain of interlectin-1 further proved the pharmacodynamic effect of CLB001. In addition, CLB003 showed the increase of $GATA3^+$ or $ROR\gamma t^+$ regulatory T cells in the ileal mesenteric lymph nodes. Thus, the polymeric micelles CLB001 and CLB003 had the potential to alleviate food allergy symptoms if combined with oral immunotherapy.

2.7 References

1. Gupta, R.S.*, et al.* Prevalence and Severity of Food Allergies Among US Adults. *JAMA Netw Open* **2**, e185630 (2019).

2. Fisher, H.R., Keet, C.A., Lack, G. & du Toit, G. Preventing Peanut Allergy: Where Are We Now? *J Allergy Clin Immunol Pract* **7**, 367-373 (2019).

3. Dunlop, J.H. Oral immunotherapy for treatment of peanut allergy. *J Investig Med* **68**, 1152-1155 (2020).

4. Dougherty, J.A., Wagner, J.D. & Stanton, M.C. Peanut Allergen Powder-dnfp: A Novel Oral Immunotherapy to Mitigate Peanut Allergy. *Ann Pharmacother*, 1060028020944370 (2020).

5. Patrawala, M., Shih, J., Lee, G. & Vickery, B. Peanut Oral Immunotherapy: a Current Perspective. *Curr Allergy Asthma Rep* **20**, 14 (2020).

6. Labrosse, R., Graham, F., Des Roches, A. & Bégin, P. The Use of Omalizumab in Food Oral Immunotherapy. *Arch Immunol Ther Exp (Warsz)* **65**, 189-199 (2017).

7. Albuhairi, S. & Rachid, R. Novel Therapies for Treatment of Food Allergy. *Immunol Allergy Clin North Am* **40**, 175-186 (2020).

8. Long, A., Borro, M., Sampath, V. & Chinthrajah, R.S. New Developments in Non-allergen-specific Therapy for the Treatment of Food Allergy. *Curr Allergy Asthma Rep* **20**, 3 (2020).

9. Iweala, O.I. & Nagler, C.R. The Microbiome and Food Allergy. *Annu Rev Immunol* **37**, 377-403 (2019).

10. Berni Canani, R.*, et al.* Gut Microbiome as Target for Innovative Strategies Against Food Allergy. *Front Immunol* **10**, 191 (2019).

11. Plunkett, C.H. & Nagler, C.R. The Influence of the Microbiome on Allergic Sensitization to Food. *J Immunol* **198**, 581-589 (2017).

12. Stefka, A.T.*, et al.* Commensal bacteria protect against food allergen sensitization. *Proc Natl Acad Sci U S A* **111**, 13145-13150 (2014).

13. Tan, J.*, et al.* The role of short-chain fatty acids in health and disease. *Adv Immunol* **121**, 91-119 (2014).

14. Tan, J.*, et al.* Dietary Fiber and Bacterial SCFA Enhance Oral Tolerance and Protect against Food Allergy through Diverse Cellular Pathways. *Cell Rep* **15**, 2809-2824 (2016).

15. Chang, P.V., Hao, L., Offermanns, S. & Medzhitov, R. The microbial metabolite butyrate regulates intestinal macrophage function via histone deacetylase inhibition. *Proc Natl Acad Sci U S A* **111**, 2247-2252 (2014).

16. Mathewson, N.D.*, et al.* Gut microbiome-derived metabolites modulate intestinal epithelial cell damage and mitigate graft-versus-host disease. *Nat Immunol* **17**, 505-513 (2016).

17. Fachi, J.L.*, et al.* Butyrate Protects Mice from Clostridium difficile-Induced Colitis through an HIF-1-Dependent Mechanism. *Cell Rep* **27**, 750-761.e757 (2019).

18. Furusawa, Y.*, et al.* Commensal microbe-derived butyrate induces the differentiation of colonic regulatory T cells. *Nature* **504**, 446-450 (2013).

19. Arpaia, N.*, et al.* Metabolites produced by commensal bacteria promote peripheral regulatory T-cell generation. *Nature* **504**, 451-455 (2013).

20. Smith, P.M.*, et al.* The microbial metabolites, short-chain fatty acids, regulate colonic Treg cell homeostasis. *Science* **341**, 569-573 (2013).

21. Liu, H.*, et al.* Butyrate: A Double-Edged Sword for Health? *Adv Nutr* **9**, 21-29 (2018).

22. Butzner, J.D., Parmar, R., Bell, C.J. & Dalal, V. Butyrate enema therapy stimulates mucosal repair in experimental colitis in the rat. *Gut* **38**, 568-573 (1996).

23. Chen, X., Xu, J., Su, Y. & Zhu, W. Effects of Intravenous Infusion With Sodium Butyrate on Colonic Microbiota, Intestinal Development- and Mucosal Immune-Related Gene Expression in Normal Growing Pigs. *Front Microbiol* **9**, 1652 (2018).

24. Gaucher, G.*, et al.* Block copolymer micelles: preparation, characterization and application in drug delivery. *J Control Release* **109**, 169-188 (2005).

25. Yokoyama, M. Polymeric micelles as drug carriers: their lights and shadows. *J Drug Target* **22**, 576-583 (2014).

26. Cagel, M.*, et al.* Polymeric mixed micelles as nanomedicines: Achievements and perspectives. *Eur J Pharm Biopharm* **113**, 211-228 (2017).

27. Sze, L.P.*, et al.* Oral delivery of paclitaxel by polymeric micelles: A comparison of different block length on uptake, permeability and oral bioavailability. *Colloids Surf B Biointerfaces* **184**, 110554 (2019).

28. Jeanbart, L., Kourtis, I.C., van der Vlies, A.J., Swartz, M.A. & Hubbell, J.A. 6-Thioguanine-loaded polymeric micelles deplete myeloid-derived suppressor cells and enhance the efficacy of T cell immunotherapy in tumor-bearing mice. *Cancer Immunol Immunother* **64**, 1033-1046 (2015).

29. Hasegawa, U., van der Vlies, A.J., Simeoni, E., Wandrey, C. & Hubbell, J.A. Carbon monoxide-releasing micelles for immunotherapy. *J Am Chem Soc* **132**, 18273-18280 (2010).

30. O'Neil, C.P.*, et al.* Extracellular matrix binding mixed micelles for drug delivery applications. *J Control Release* **137**, 146-151 (2009).

31. Dane, K.Y.*, et al.* Nano-sized drug-loaded micelles deliver payload to lymph node immune cells and prolong allograft survival. *J Control Release* **156**, 154-160 (2011).

32. van der Vlies, A.J., Hasegawa, U. & Hubbell, J.A. Reduction-sensitive tioguanine prodrug micelles. *Mol Pharm* **9**, 2812-2818 (2012).

33. Xu, F., Xu, J.W. & Luo, Y.L. Impact of hydrogenation on physicochemical and biomedical properties of pH-sensitive PMAA-b-HTPB-b-PMAA triblock copolymer drug carriers. *J Biomater Appl* **30**, 1473-1484 (2016).

34. Colombani, O.*, et al.* Synthesis of poly(n-butyl acrylate)-block-poly(acrylic acid) diblock copolymers by ATRP and their micellization in water. *Macromolecules* **40**, 4338-4350 (2007).

35. Colombani, O.*, et al.* Structure of micelles of poly(n-butyl acrylate)-block-poly (acrylic acid) diblock copolymers in aqueous solution. *Macromolecules* **40**, 4351-4362 (2007).

36. Felber, A.E., Dufresne, M.H. & Leroux, J.C. pH-sensitive vesicles, polymeric micelles, and nanospheres prepared with polycarboxylates. *Adv Drug Deliv Rev* **64**, 979-992 (2012).

37. Wu, H., Ting, J., Weiss, T. & Tirrell, M. Interparticle Interactions in Dilute Solutions of Polyelectrolyte Complex Micelles. *Acs Macro Letters* **8**, 819-825 (2019).

38. Lele, B.S. & Hoffman, A.S. Mucoadhesive drug carriers based on complexes of poly(acrylic acid) and PEGylated drugs having hydrolysable PEG-anhydride-drug linkages. *J Control Release* **69**, 237-248 (2000).

39. Serra, L., Doménech, J. & Peppas, N.A. Engineering design and molecular dynamics of mucoadhesive drug delivery systems as targeting agents. *Eur J Pharm Biopharm* **71**, 519-528 (2009).

40. Jiang, H., Wang, Q. & Sun, X. Lymph node targeting strategies to improve vaccination efficacy. *J Control Release* **267**, 47-56 (2017).

41. Aguiar, J., Carpena, P., Molina-Bolivar, J. & Ruiz, C. On the determination of the critical micelle concentration by the pyrene 1 : 3 ratio method. *Journal of Colloid and Interface Science* **258**, 116-122 (2003).

42. Cai, R., Li, R., Qian, J., Xie, A. & Nie, K. The morphology and fabrication of nanostructured micelle by a novel block copolymer with linear-dendritic structure. *Mater Sci Eng C Mater Biol Appl* **33**, 2070-2077 (2013).

43. Torii, T.*, et al.* Measurement of short-chain fatty acids in human faeces using high-performance liquid chromatography: specimen stability. *Ann Clin Biochem* **47**, 447-452 (2010).

44. Tyagi, A.M.*, et al.* The Microbial Metabolite Butyrate Stimulates Bone Formation via T Regulatory Cell-Mediated Regulation of WNT10B Expression. *Immunity* **49**, 1116-1131.e1117 (2018).

45. Goncharov, N.V.*, et al.* Serum Albumin Binding and Esterase Activity: Mechanistic Interactions with Organophosphates. *Molecules* **22**(2017).

46. Tyagi, A.*, et al.* The Microbial Metabolite Butyrate Stimulates Bone Formation via T Regulatory Cell-Mediated Regulation of WNT10B Expression. *Immunity* **49**, 1116-+ (2018).

47. Gallo, R.L. & Hooper, L.V. Epithelial antimicrobial defence of the skin and intestine. *Nat Rev Immunol* **12**, 503-516 (2012).

48. Ganz, T. Defensins: antimicrobial peptides of innate immunity. *Nat Rev Immunol* **3**, 710-720 (2003).

49. Tsuji, S.*, et al.* Human intelectin is a novel soluble lectin that recognizes galactofuranose in carbohydrate chains of bacterial cell wall. *Journal of Biological Chemistry* **276**, 23456-23463 (2001).

50. Wang, Y., Su, M.A. & Wan, Y.Y. An essential role of the transcription factor GATA-3 for the function of regulatory T cells. *Immunity* **35**, 337-348 (2011).

51. Yang, B.H.*, et al.* Foxp3(+) T cells expressing RORγt represent a stable regulatory T-cell effector lineage with enhanced suppressive capacity during intestinal inflammation. *Mucosal Immunol* **9**, 444-457 (2016).

52. Megias, C.*, et al.* Stability of sunflower protein hydrolysates in simulated gastric and intestinal fluids and Caco-2 cell extracts. *Lwt-Food Science and Technology* **42**, 1496-1500 (2009).

53. Fu, T.J., Abbott, U.R. & Hatzos, C. Digestibility of food allergens and nonallergenic proteins in simulated gastric fluid and simulated intestinal fluid-a comparative study. *J Agric Food Chem* **50**, 7154-7160 (2002).

54. Wilson, D.S.*, et al.* Antigens reversibly conjugated to a polymeric glyco-adjuvant induce protective humoral and cellular immunity. *Nat Mater* **18**, 175-185 (2019).

Chapter 3

Mannosylated and Butyrate Statistical Copolymer Induces Tolerogenic Dendritic Cells

3.1 Abstract

Butyrate suppresses the activation of dendritic cells (DCs) and can be used to induce tolerance against antigens. Dendritic cells express a high level of C-type lectin mannose receptor CD206. Here, we present a statistical copolymer platform of butyrate and mannose with the capabilities of inducing tolerogenic dendritic cells. The copolymer is composed of mannose monomer, which targets DCs via mannose-binding receptor CD206, and butyrate monomer in the form of aliphatic butyrate ester (pMan-But) or phenol butyrate ester (pMan-PhBut), which release butyrate in cell culture media via ester hydrolysis. Both pMan-But and pMan-PhBut suppress the production of cytokine IL12p70 from bone marrow-derived dendritic cells activated by LPS. Moreover, pMan-PhBut induces tolerogenic DCs in the draining lymph nodes *in vivo* by suppressing the production of inflammatory cytokines activated by LPS. The pMan-But or pMan-PhBut platforms offer a strategy to induce tolerogenic dendritic cells or T cell tolerance in potential.

3.2 Introduction

Protein-based therapeutics has been growing rapidly in sales. Among the best selling pharmaceuticals of 2017-2018, seven out of ten are protein-based drugs, including the largest selling drug named Humira developed by AbbVie[1]. However, the immunogenicity of protein-based drugs is a major issue affecting both safety and efficacy of the therapy[2,3]. According to a

study of anti-TNFα antibodies, patients treated with human mAb adalimumab developed antibodies against the therapeutic with a range from <1% to up to 87%[4]. The generation of anti-drug antibodies is also prevalence among other licensed protein-based therapeutics[3]. Thus, it is very essential to induce the tolerance to proteins when applying protein therapies.

Short chain fatty acids, especially butyrate, have shown anti-inflammatory effects[5-8]. Butyrate is known as inhibitor of histone deacetylase (HDAC) and ligand for G protein-coupled receptor 109A[9]. It is reported that butyrate can promote regulatory T cells via the induction of tolerogenic dendritic cells (DCs) in murine studies[5,6,10]. In addition, butyrate also regulates macrophage functions via HDAC inhibition[11]. Since both dendritic cells and macrophages have important roles in antigen presenting, it would be interesting to deliver butyrate targeting dendritic cells or macrophages to induce tolerogenic functions against protein-based therapeutics.

Mannose receptor (CD206) is a C-type lectin expressed on immature dendritic cells and macrophages[12,13]. The receptor recognizes terminal mannose and promotes the uptake of glycoproteins. Previously in the lab, Dr. Scott Wilson developed a polymeric glyco-adjuvant named p(Man-TLR7) composed of mannose and TLR7 adjuvant[14]. The copolymer targeted DCs via mannose-binding receptors and activated DCs via Toll-like receptor 7 (TLR7). The copolymer conjugated to antigens induced protective humoral and cellular immunity. Antigens conjugated to glycopolymers without adjuvant were also developed in the lab and showed efficacy in inducing T-cell tolerance[15].

Given the ability of butyrate in inducing tolerogenic DCs, it is important to develop a butyrate delivery system to the draining lymph nodes. Small molecule sodium butyrate is used directly in previous *in vitro* studies. However, it is difficult to administer free butyrate to mouse

because it will only have local effect at the injection site but not in the draining lymph nodes. To solve this, one straightforward way is to form butyrate ester as ester formation is widely used in the formulation of drug with carboxylic acid structure[16,17]. Additionally, compared to aliphatic ester, phenol ester has a faster hydrolysis rate and can provide fast release kinetics for the study[18,19].

Here, we present a platform that targets DCs through mannose-binding receptors and releases butyrate to DCs to induce tolerogenic effects. The statistical copolymers composed of either aliphatic butyrate ester (pMan-But) or phenol butyrate ester (pMan-PhBut) show different hydrolysis kinetics. Both polymers suppress the production of IL12p70 in bone marrow-derived dendritic cells (BMDCs) activated by LPS. Furthermore, pMan-PhBut suppresses the activation of DCs *in vivo*, providing potentials to induce immune tolerance.

3.3 Results

3.3.1 Mannosylated and butyrate polymers pMan-But and pMan-PhBut are synthesized by RAFT polymerization

Statistical copolymer pMan-But and pMan-PhBut were synthesized through reversible addition-fragmentation chain-transfer (RAFT) polymerization using an azide modified chain transfer agent (Figure 3.1.A, B). Mannose monomer N-[2-(α-D-mannose)ethyl] methacrylamide was incorporated into the polymer to provide targeting effect. A biologically inert monomer hydroxyethyl methacrylamide (HEMA) was added to increase the solubility and to act as a spacer for mannose. Butyrate containing monomer for pMan-But was the same as previously described N-(2-butanoyloxyethyl) methacrylamide (BMA). However, as an aliphatic butyrate ester, BMA had a relatively slow hydrolysis rate in solution catalyzed by either acid or esterase.

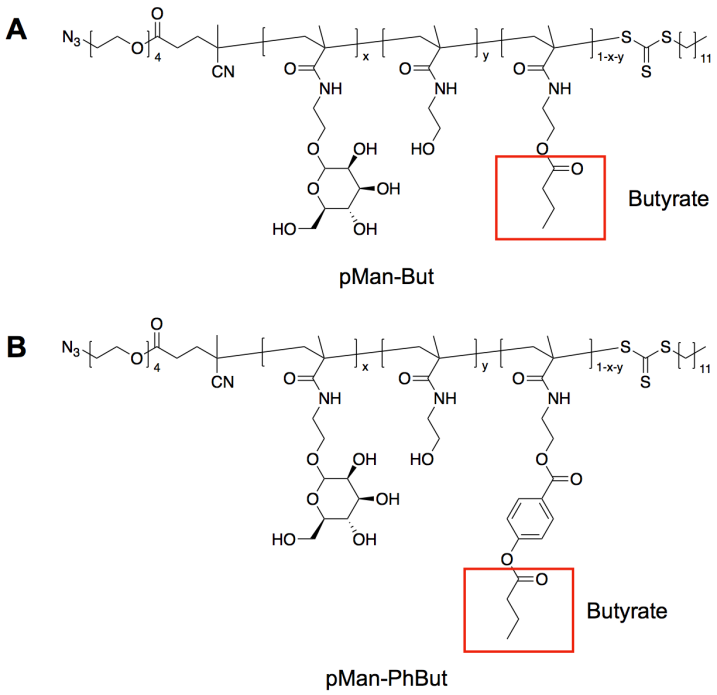

Figure 3.1 Chemical structures of statistical copolymer pMan-But (**A**) with aliphatic butyrate and pMan-PhBut (**B**) with phenol butyrate.

To improve the release rate of butyrate, we also developed a butyrate-containing monomer with a structure of phenol ester, N-[2-(4-butanoyloxybenzoyloxy)ethyl] methacrylamide (PhBMA)[18,19]. Thus, we synthesized two forms of polymers, pMan-But and pMan-PhBut, with different butyrate release rates. The number average molecular weight of both polymers were 11 kDa determined by gel permeation chromatography (GPC) with DMF as eluent and PMMA as calibration standards (Figure 3.13). The mass ratio for Mannose monomer, HEMA, and BMA (or PhBMA) were 30:50:20 in order to balance good water-solubility and high butyrate payload. The actual butyrate content of the polymer was determined by LC-MS/MS.

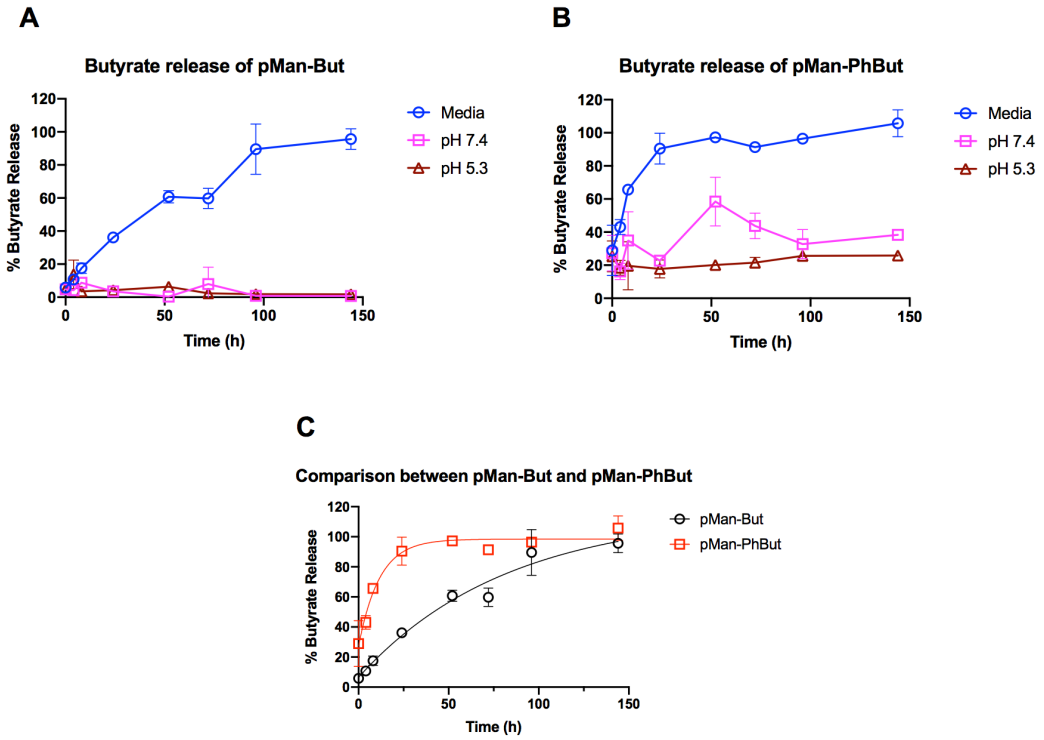

Figure 3.2 Butyrate was released from pMan-But or pMan-PhBut in complete cell culture media, pH 7.3 buffer or pH 5.3 buffer. (**A**) pMan-But reached 100% release of butyrate at day 5 in the complete cell culture media. (**B**) pMan-PhBut reached 100% release of butyrate at day 2 in the complete cell culture media. (**C**) The butyrate release of pMan-But or pMan-PhBut in complete cell culture media was fitted assuming first order reaction of ester hydrolysis. Data were presented as mean ± s.e.m.

3.3.2 Phenol ester has a higher release rate of butyrate than aliphatic ester in the complete cell culture media

Given we synthesized the polymer containing butyrate as pharmacological active ingredient, we would like to determine the butyrate content in the polymer. In order to quantify the concentration of butyrate, we derivatized butyrate with 3-nitrophenylhydrazine to generate a yellow butyrate hydrazide that could be analyzed by LC-MS/MS[20]. The analysis of complete released samples showed pMan-But and pMan-PhBut had a butyrate mass ratio of around 5%.

Given we established the LC-MS/MS method to quantify butyrate concentration, we studied the butyrate release of both polymers in pH = 7.4 PBS buffer, pH = 5.3 acetic acid buffer, or complete cell culture media (Figure 3.2.A, B). Both polymers show butyrate release in the cell culture media. As we expected, pMan-PhBut had a faster release rate than pMan-But. If we fitted the curve using the first order reaction kinetics, the k_1 for pMan-But was 0.012 h^{-1} and k_1 for pMan-PhBut was 0.086 h^{-1}. Furthermore, the half lives for pMan-But and pMan-PhBut were 56.9 h and 8.0 h, respectively (Figure 3.2.C). However, such release of butyrate was not observed in pH = 5.3 buffer or pH = 7.4 buffer (Figure 3.2.A, B). So we concluded the hydrolysis of butyrate ester was catalyzed by esterase enzyme in the serum of the media and was not caused by pH. The butyrate release measured by LC-MS/MS not only validated our polymer could release butyrate in the cell culture media, but also demonstrated the design of phenol ester performed better than aliphatic ester in terms of hydrolysis rate.

3.3.3 Both pMan-But and pMan-PhBut suppress the expression of IL12p70 from BMDCs

After validating the release of butyrate in cell culture media, we further investigated if pMan-But or pMan-PhBut could suppress the activation of mouse bone marrow-derived dendritic cells (BMDC) cause by a common adjuvant, lipopolysaccharide (LPS). The activation marker of BMDCs was IL12p70, an interleukin produced by dendritic cells in response to antigen stimulation[21,22]. First, we treated BMDCs with different concentrations of LPS and found 100 ng/mL was a good concentration to use (Figure 3.3.A). Then, we treated cells with both sodium butyrate and LPS together for 48 h. ELISA of IL12p70 levels revealed sodium butyrate successfully suppressed the activation of BMDCs at both 0.5 mM and 2.0 mM (Figure 3.3.B). Furthermore, we treated BMDCs with pMan-But and LPS together for 24 h. However, this time

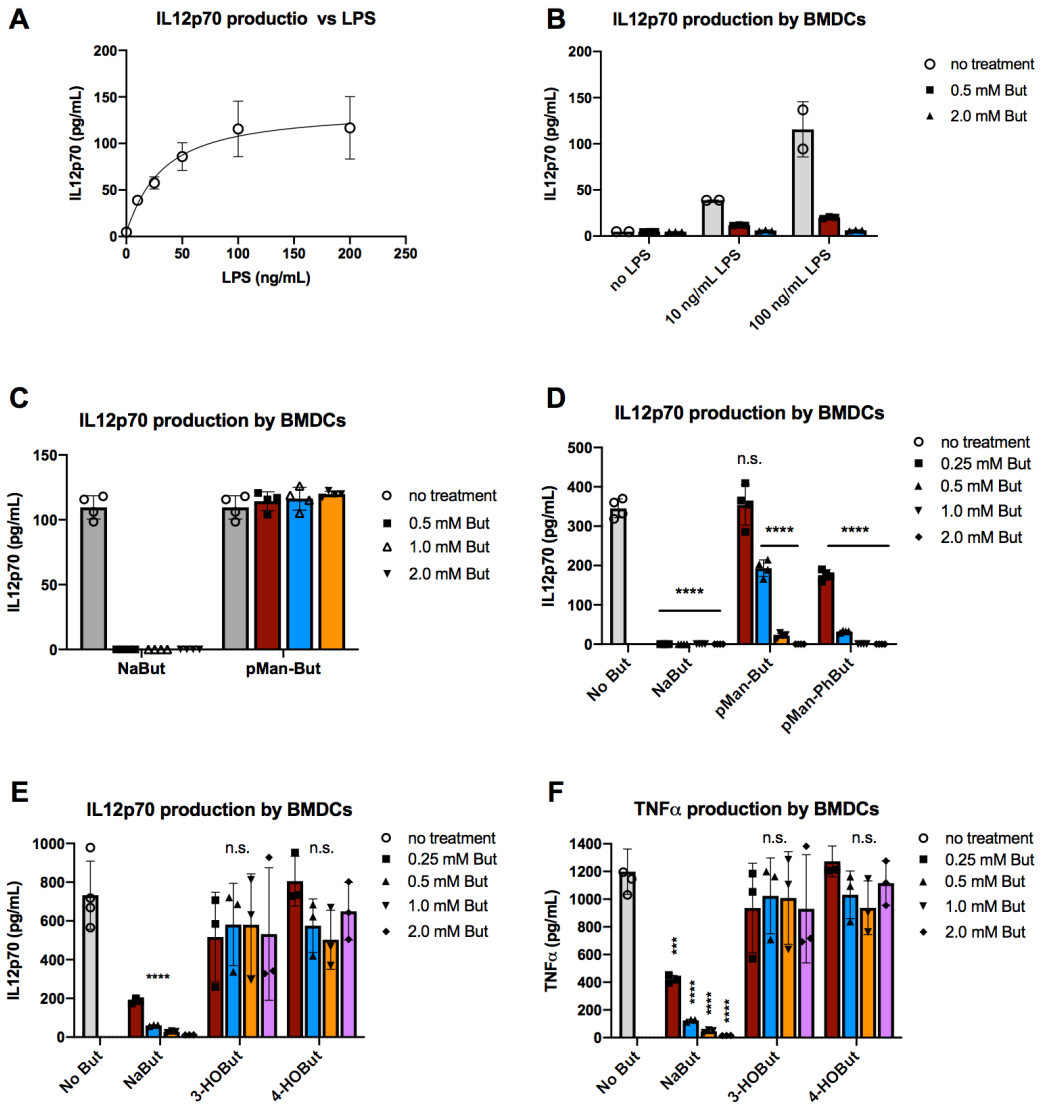

Figure 3.3 pMan-But or pMan-PhBut suppressed IL12p70 production in mouse bone marrow-derived dendritic cells (BMDCs) activated by LPS. (**A**) Test of IL12p70 production from BMDCs at different LPS concentration. (**B**) Sodium butyrate (NaBut) suppressed the activation of BMDCs if it was co-treated with LPS at the same time. (**C**) BMDCs were treated with NaBut or pMan-But and LPS together for 24 h. Only NaBut and pMan-PhBut showed suppression effect of IL12p70 production. pMan-But did not show suppression effect at 0.5 mM. (**D**) BMDCs were treated with butyrate polymer or NaBut for 24 h before the addition of LPS. After another 24 h both pMan-But and pMan-PhBut showed suppression effect of IL12p70 production. (**E**, **F**) 3-hydroxybutyrate or 4-hydroxybutyrate did not suppress the IL12p70 (**E**) or TNFα (**F**) production in BMDCs activated by LPS. All data were presented as mean ± s.e.m. Statistical differences were determined by two-way ANOVA using Turkey's multiple comparisons test. (**D**, **E**, **F**) Significances were compared with no treatment or no group. (* $p < 0.05$, ** $p < 0.01$, *** $p < 0.001$, **** $p < 0.0001$)

the IL12p70 levels of pMan-But group did not decrease compared to control group (Figure 3.3.C). The reason could be the hydrolysis of pMan-But was slow and it needed more time to release butyrate in the cell culture media. One solution was to add pMan-But polymer one day before LPS activation, followed by ELISA on supernatant 24 h after adding LPS, so that polymers had a 48 h period for releasing butyrate. The other solution was to use pMan-PhBut with a faster butyrate release rate. As we expected, through pretreatment of polymers, both pMan-But and pMan-PhBut successfully suppressed the expression of IL12p70 caused by LPS (Figure 3.3.D). For pMan-But, although there was no significant decrease of IL12p70 production at 0.25 mM equivalent of butyrate, the effect of suppression was obvious starting from 0.50 mM, and IL12p70 level was reduced to almost zero at 2.0 mM. Furthermore, pMan-PhBut showed a better suppression effect by starting to reduce IL12p70 production at 0.25 mM, due to the fast release of butyrate. At the meantime, sodium butyrate almost shut down the production of IL12p70 completely from 0.25 mM to 2.0 mM. This study validated that butyrate could induce tolerogenic dendritic cells by suppressing the production of IL12p70 activated by LPS. More importantly, we proved our design of pMan-But and pMan-PhBut polymers could release butyrate and had the same effect in suppressing the activation of dendritic cells.

Given we validated butyrate as a HDAC inhibitor could suppress the activation of dendritic cells, we wondered if hydroxyl analogue of butyrate, including 3-hydroxybutyrate (3-HOBut) and 4-hydroxybutyrate (4-HOBut), could have similar effects. The reason we considered 3-hydroxybutyrate and 4-hydroxybutyrate was they could be synthesized into homopolymers due to the coexistence of hydroxyl group and carboxylic acid group. In fact, poly(4-hydroxybutyrate) had already been used as mesh material for surgery[23,24]. However, in our BMDC activation

assay, neither 3-HOBut nor 4-HOBut showed any significant reduction of IL12p70 production (Figure 3.3.E, F). Thus, we had to proceed with butyrate polymer pMan-But or pMan-PhBut.

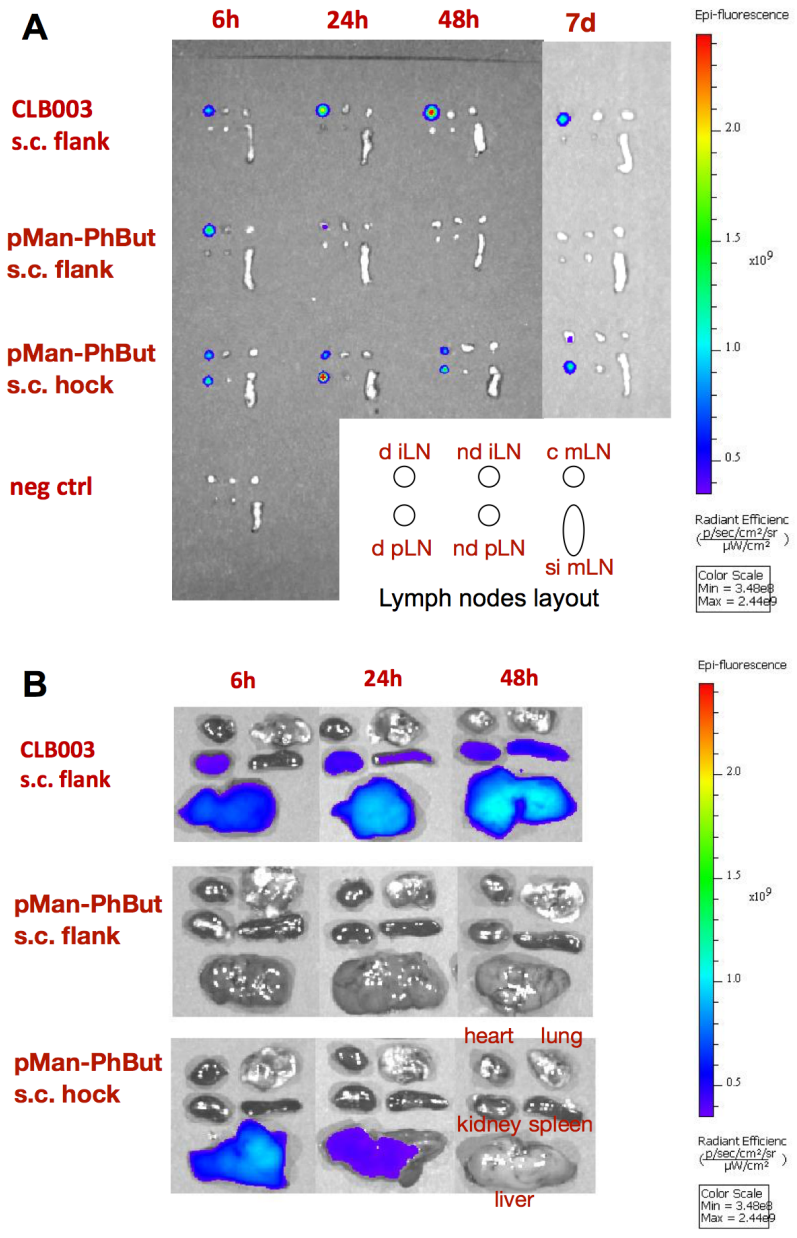

Figure 3.4 Representative IVIS images of biodistribution study of pMan-PhBut. pMan-PhBut was labeled with fluorescent dye IR750 and administered to mouse hock or left flank subcutaneously. Positive control was CLB003 micelle described before. Negative control was PBS. (**A**) pMan-PhBut was drained to both popliteal and inguinal lymph nodes and stayed in popliteal lymph node for up to 7 days if injected subcutaneously to the hock. Such effect was not observed if injected to the flank. The lymph nodes layout illustrated the position of different

(**Figure 3.4, continued**) lymph nodes: d: draining, nd: non-draining, iLN: inguinal lymph node, pLN: popliteal lymph node, c mLN: colon mesenteric lymoh node, si mLN: small intestine mesenteric lymph node. (**B**) Fluorescent signal of pMan-PhBut was also observed in liver but not in other organs.

3.3.4 pMan-PhBut stays in the draining lymph nodes after hock s. c. injection

In order to understand which injection method worked the best for *in vivo* study, we performed biodistribution study to investigate how the polymer drained into the lymph nodes and how long it could stay there. Previously, similar studies focused on polymer-protein conjugate and the fluorescent dye was labeled on the protein[14]. Thus, we would like to see the biodistribution of pMan polymers. Thanks to the azide group on the chain transfer agent, the pMan-PhBut polymer was labeled with IR750-DBCO via azide-octyne cycloaddition. We injected dye labeled polymers subcutaneously to either hock or flank of C57BL/6 mice. Then we obtained lymph nodes and other major organs at different time points to image the fluorescence signal on In Vivo Imaging System (IVIS).

As a positive control, we also had one group of CLB003 micelle labeled with IR750 because previously we demonstrated through flank subcutaneous (s.c.) injection, CLB003 micelles were drained to draining inguinal lymph nodes and stayed there for more than 21 days. This time we repeated the similar results and showed that CLB003 signal showed up in the draining inguinal lymph nodes starting at 6 h and stayed for at least 7 days (Figure 3.4.A). Compared to CLB003, pMan-PhBut also showed fluorescent signal at draining inguinal lymph nodes 6 h after flank s.c. injection (Figure 3.4.A). However, the signal disappeared 24 h after the injection. No fluorescent signal was observed in major organs for this flank s.c. group of pMan-PhBut (Figure 3.4.B). On the contrary, when we did hock s.c. injection, the signal of the polymer showed up in both draining popliteal lymph node and draining inguinal lymph node. The signal

in draining popliteal lymph node stayed for at least 7 days, while the signal in draining inguinal lymph node diminished at day 7 (Figure 3.4.A). We also observed signal of the polymer in the liver at 6 h and 24 h time points when doing hock s.c. injections (Figure 3.4.B). However, no signals were observed in non-draining lymph nodes or mesenteric lymph nodes. Such results met our expectations as when polymer was injection to the hock, popliteal lymph node was the first major draining lymph node and inguinal lymph node was the second. The results also provided strong support to our future animal experiment in that we should use hock s.c. injection instead of flank s.c. injection as administration route. When we sacrifice the mice, we should take popliteal lymph nodes for cell analysis. More importantly, the long dwelling time of pMan-PhBut polymer in the popliteal lymph nodes also provided opportunity for dosing pMan-But. Although pMan-But had slower release rate, the polymer could stay in the lymph node for much longer than the half time of butyrate release. Such long time slow release could be of more interests when studying the induction of regulatory T cells.

3.3.5 Treatments of pMan-PhBut suppress the expression of IL-6 and TNFα from lymph node cells

Given we validated the efficacy of pMan-But and pMan-PhBut on BMDCs and the biodistribution of polymers in draining lymph nodes, we moved forward to investigated if pMan-PhBut could induce tolerogenic DCs *in vivo* on C57BL/6 mice. We choose pMan-PhBut because it had faster release rate and it performed better than pMan-But in *in vitro* BMDCs experiments. We administered mice subcutaneously with sodium butyrate or pMan-PhBut one day or four days before the injection of LPS. The mice were euthanized 24 h after LPS activation and popliteal lymph nodes were collected (Figure 3.5.A). Then, we re-activated cells from popliteal

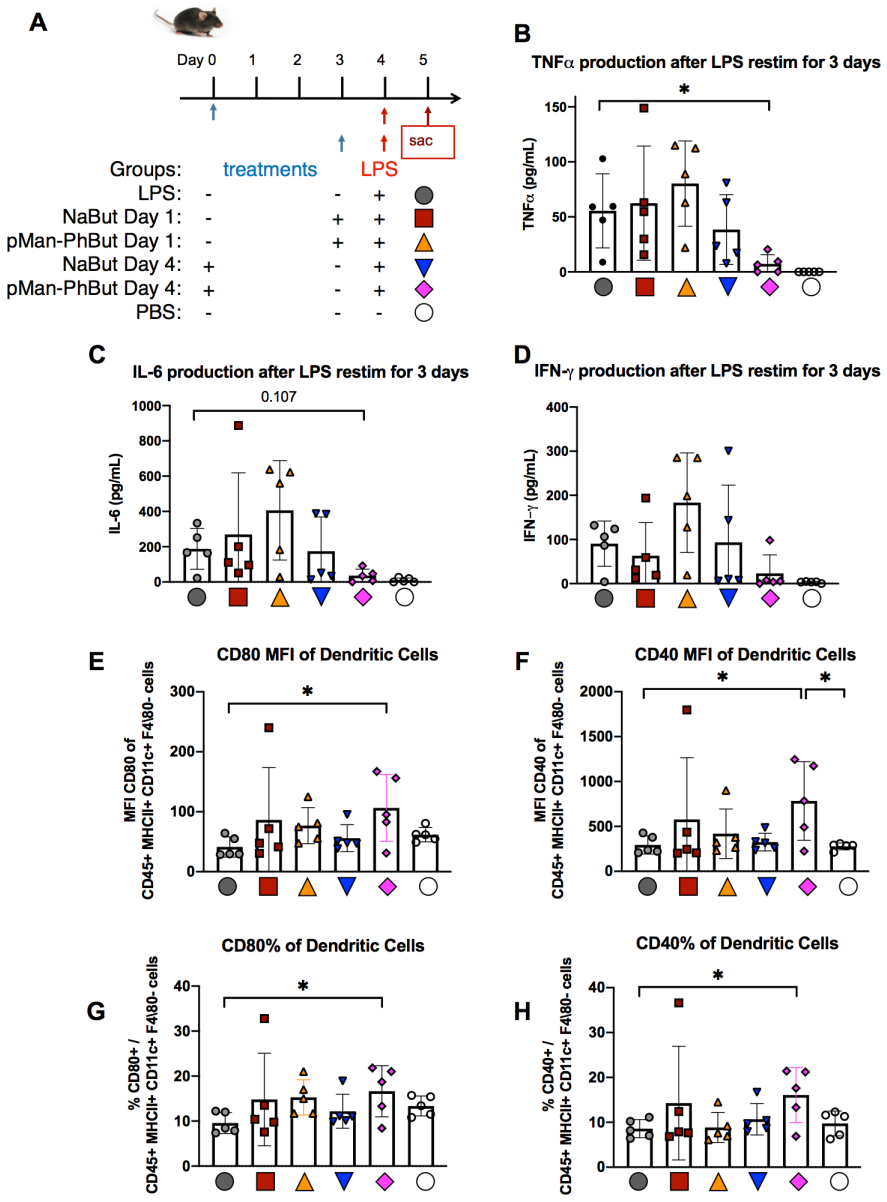

Figure 3.5 pMan-PhBut suppressed the activation of dendritic cells from draining lymph nodes activated by LPS in C57BL/6 mice. (**A**) C57BL/6 mice were treated with NaBut or pMan-PhBut through hock s.c. injection either on day 0 or day 3. On day 4, all mice except PBS group were activated with LPS at 25 μg per hock. On day 5, mice were euthanized and popliteal lymph nodes were examined for activation of DCs. (**B**-**D**) Cells from the popliteal lymph nodes were re-activated with LPS *in vitro* and TNFα (**B**), IL-6 (**C**), and IFN-γ (**D**) were measured by multiplex ELISA. (**E**-**H**) Mean fluorescent intensity of CD80 (**E**) or CD40 (**F**) of dendritic cells and percentage of CD80+ (**G**) or CD40+ (**H**) cells were measured by flow cytometry. All data were presented as mean ± s.e.m. and statistical differences were determined by one-way ANOVA using Turkey's multiple comparisons test. (* $p < 0.05$)

lymph nodes in the cell culture media and measured the cytokines using multiplex ELISA (Figure 3.5.B-D).

From the re-activation assay of lymphatic cells, pMan-PhBut Day 4 group expressed significantly lower concentration of pro-inflammatory cytokines like TNFα (Figure 3.5.B) and IL-6 (Figure 3.5.C). IFN-γ (Figure 3.5.D) of pMan-PhBut Day 4 group also showed a trend of decreasing compared to LPS group although no significant difference was observed. Such results suggested pMan-PhBut had suppression effect on dendritic cells in the draining lymph nodes when activated by LPS *in vitro*. However, NaBut Day 4 group did not show the similar effect, probably due to the small molecule of sodium butyrate could not reach draining lymph node or did not stay there for 4 days. In addition, neither NaBut Day 1 nor pMan-PhBut Day 1 group showed any suppression of cytokine production, suggesting pMan-PhBut needed time to release butyrate and butyrate also needed time to show effects on DCs. Our negative control, PBS group also showed very low expression of IL-6 and TNFα. This suggested the injections of LPS to mice were important to activate dendritic cells in the *in vitro* re-activation assay.

We also stained a portion of cells derived from popliteal lymph nodes for DC makers like CD40 and CD80 for flow cytometry analysis (Figure 3.5.E-H). According to flow cytometry data, no significant difference of CD40 levels or CD80 levels was observed between negative control (PBS) and positive control (LPS). Thus, although pMan-PhBut Day 4 group showed a higher mean fluorescent intensity (MFI) or percentage of CD80 and CD40 compared to LPS group, the results did not mean more activation level of DCs in the pMan-PhBut group. We believed to include an antigen like OVA in the study may raise the positive control level so that we could see the tolerance-inducing effects of pMan-PhBut. Given the promising suppression

effect on dendritic cells in *in vitro* LPS activation study, we also would like to see the downstream effect of pMan-But or pMan-PhBut on T cells in OTI/OTII model.

3.4 Discussion

The design of this projects was based on the effect of short chain fatty acid, especially butyrate, on dendritic cells as an HDAC inhibitor. Such effect could suppress the activation of dendritic cells, thus inducing the tolerogenic effect to immune system. However, either sodium butyrate or butyric acid was so small that could not be applied to animal study through common injection method. In order to formulate butyrate to target dendritic cells in the lymph node, we applied the mannose copolymer system previously developed by Dr. Scott Wilson in the lab[14,15]. The idea was to take advantage of mannose that can target CD206, a mannose receptor, expressed by dendritic cells or macrophages. After the uptake of the polymer, the butyrate ester got hydrolyzed and released butyrate regulated dendritic cells as an HDAC inhibitor.

As a statistical copolymer pMan-But, the ratio of mannose monomer, spacer HEMA, and butyrate monomer should have a balance between butyrate payload and solubility. According to previous results, we believed a ratio of mannose:HEMA:BMA = 30:50:20 was a good trial. Such ratio was also applied to the synthesis of pMan-PhBut, where butyrate monomer was replaced by phenol butyrate. Phenol butyrate had a faster hydrolysis rate than aliphatic butyrate because aromatic hydroxyl group was a better leaving group than aliphatic hydroxyl group. Though phenol group was bulky and more hydrophobic, the product pMan-PhBut could be dissolved in PBS at up to 200 mg/mL when monomer ratio of mannose:HEMA:PhBMA = 30:50:20 was used for polymerization. From *ex vivo* hydrolysis assay in complete cell culture media, we observed typical release curve of butyrate based on first order reaction kinetics. As we expected, pMan-

PhBut had a faster release rate with a seven times higher first order reaction constant than pMan-But. However, polymers did not show butyrate release in pH = 7.4 buffer or pH = 5.3 buffer. The release study analyzed by LC-MS/MS demonstrated the polymer could release pharmacological active butyrate in biological environment. More importantly, we validated two types of mannosylated polymers we synthesized had different release rates of butyrate.

In order to validate the efficacy of pMan-But and pMan-PhBut on dendritic cells, we treated BMDCs with sodium butyrate or butyrate polymers and used ELISA to quantify IL12p70 production. We successfully repeated the suppression of IL12p70 caused by butyrate as reported in the literature[9]. In addition, both pMan-But and pMan-PhBut were able to suppress the cytokine IL12p70 production too. pMan-PhBut showed efficacy at lower concentration than pMan-But, but still higher than free sodium butyrate. The reason was BMDC activation study took only two days and polymers did not have enough time to release all butyrate.

After validating the performance of pMan polymers on BMDCs, we developed biodistribution study to investigate the draining effect of polymers and to choose the best injection method. As we expected, if injected subcutaneously to the hock, polymer was drained to both popliteal and inguinal lymph nodes. To our surprise, the polymer signal stayed in the draining popliteal lymph node for as long as seven days. However, if injected subcutaneously to the flank, the polymer signal did not stay in the draining inguinal lymph node for more than one day. Thus, we chose hock s.c. injection for later animal experiment.

In order to investigate the efficacy of pMan-PhBut in mouse experiment, we studied the DC activation by LPS with the pre-treatment of sodium butyrate or pMan-PhBut for one day or four days. Although there was no difference between LPS and PBS groups in flow data, the *in vitro* re-activation assay showed the group of mice pre-treated with pMan-PhBut for four days

produced significantly lower amount of IL-6 and TNFα. The results suggested the activation of dendritic cells were suppressed by pMan-PhBut. Since the polymer can be conjugated to antigens like OVA through azide-alkyne cycloaddition, we decided to more forward to tolerance T cell experiment. We could do adoptive transfer of OTI/OTII study with the treatment of pMan-PhBut conjugated to OVA to further investigate the tolerance-inducing effect of butyrate polymer. Also, we could use butyrate polymers to investigate the induction of regulatory T cells on C57BL/6 Foxp3^{GFP+} mice. The advantage of slow release of pMan-But could of good use when doing T cell related experiment because the time period was much longer than only four days when inducing tolerogenic dendritic cells.

3.5 Materials and Methods

3.5.1 Animals and cells

Female C57BL/6 mice at age of 8 weeks were obtained from Jackson Laboratory. All animal experiments performed in this study were approved by the Institutional Animal Care and Use Committee of the University of Chicago. Bone marrow derived dendritic cells were prepared according to protocols published before[25]. BMDCs were used on day 9 after obtained from bone marrow of C57BL/6 mice.

3.5.2 Synthesis of pMan-But and pMan-PhBut

3.5.2.1 Materials

All chemicals and solvents were purchased from Sigma Aldrich and used directly without any purification. The mannose monomer, N-[2-(α-D-mannose)ethyl] methacrylamide, was synthesized as described in previous literature[14] by Michal Raczy. The spacer monomer HEMA,

hydroxyethyl methacrylamide, and aliphatic butyrate monomer BMA, N-(2-butanoyloxyethyl) methacrylamide, were synthesized as described in Chapter 2.

3.5.2.2 Synthesis of azide chain transfer agent

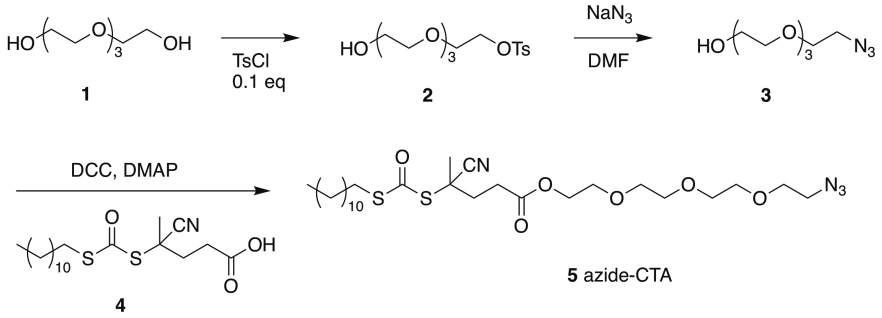

Scheme 3.1 Synthesis route of azide chain transfer agent (**5** azide-CTA)

The synthesis of chain transfer agent, 2-(2-(2-(2-azidoethoxy)ethoxy)ethoxy)ethyl 4-cyano-4(((dodecylthio)carbonthioyl)thio)pentanoate (**5** azide-CTA), was described in the previous literature[14]. Briefly, tetraethylene glycol (**1**, 10 g, 51.5 mmol, 1 eq) and triethylamine (TEA, 1.1 mL, 7.9 mmol, 0.15 eq) was dissolved in 30 mL of anhydrous DCM at 0 ℃. To that solution, p-toluenesulfonyl chloride (TsCl, 1 g, 5.2 mmol, 0.1 eq) in dry DCM was added slowly. The reaction mixture was stirred at 0 °C for 1 hour and allowed to reach room temperature overnight. After that time, the solvent was evaporated by rotary evaporator and the product was purified via silica column eluted by ethyl acetate:hexanes 60:40 v/v. The product 2-(2-(2-(2-hydroxyethoxy)ethoxy)ethoxy)ethyl 4-methylbenzenesulfonate (**2**) was pale yellow oil (1.1 g, yield 60%, calculated based on TsCl). MS (ESI). $C_{15}H_{24}O_7S$, m/z calculated for $[M+H]^+$: 349.13, found: 349.1. ^{1}HNMR (400 MHz, $CDCl_3$) δ 7.80 (d, 2H), 7.34 (d, 2H), 4.17 (m, 2H), 3.60-3.71 (m, 14H), 2.47 (s, 3H)

To synthesize azide substituted compound **3**, compound **2** (1.0 g, 2.87 mmol, 1 eq) was dissolved in dry DMF. NaN_3 (0.60 g, 9.23 mmol, 3.2 eq) was added to the solution. The reaction mixture was raised to 90 °C and allowed for reaction overnight. The reaction was filtered and DMF was removed by rotary evaporator. The product was purified via silica column eluted by ethyl acetate:hexanes 60:40 v/v. The product was yellow oil (0.60 g, yield 95%). MS (ESI). $C_8H_{17}N_3O_4$, m/z calculated for $[M+H]^+$: 242.11, found: 242.1. ^{1}H NMR (400 MHz, $CDCl_3$) δ 3.61-3.73 (m, 14H), 3.41 (t, 2H), 2.53 (br, 1H)

To synthesize compound **5** azide-CTA, 4-Cyano-4-[(dodecylsulfanylthiocarbonyl)sulfanyl]pentanoic acid (**4**, 739 mg, 1.83 mmol, 1.0 eq), compound **3** (600 mg, 2.74 mmol, 1.5 eq), and DCC (377 mg, 1.83 mmol, 1.0 eq) were dissolved in dry DCM. The reaction mixture was stirred at 0 °C for 30 min. After that time, 4-dimethylaminopyridine (11 mg, 0.09 mmol, 0.05 eq) dissolved in dry DCM was added to the reaction mixture dropwise. The reaction was allowed to rise to room temperature overnight. The reaction mixture was filtered and DCM was removed by rotary evaporator. The crude product was purified via silica column eluented by methanol:DCM 2:98 v/v. The product was yellow oil (800 mg, yield 72%). MS (ESI). $C_{27}H_{48}N_4O_5S_3$, m/z calculated for $[M+H]^+$: 604.29, found: 604.2. ^{1}H NMR (400 MHz, $CDCl_3$) δ 4.27 (t, 2H), 3.62-3.72 (m, 12H), 3.40 (t, 2H), 3.33 (t, 2H), 2.66 (dd, 2H), 2.51 (m, 1H), 2.40 (m, 1H), 1.88 (s, 3H), 1.69 (dt, 2H), 1.39 (m, 2H), 1.26 (s, 16H), 0.88 (t, 3H)

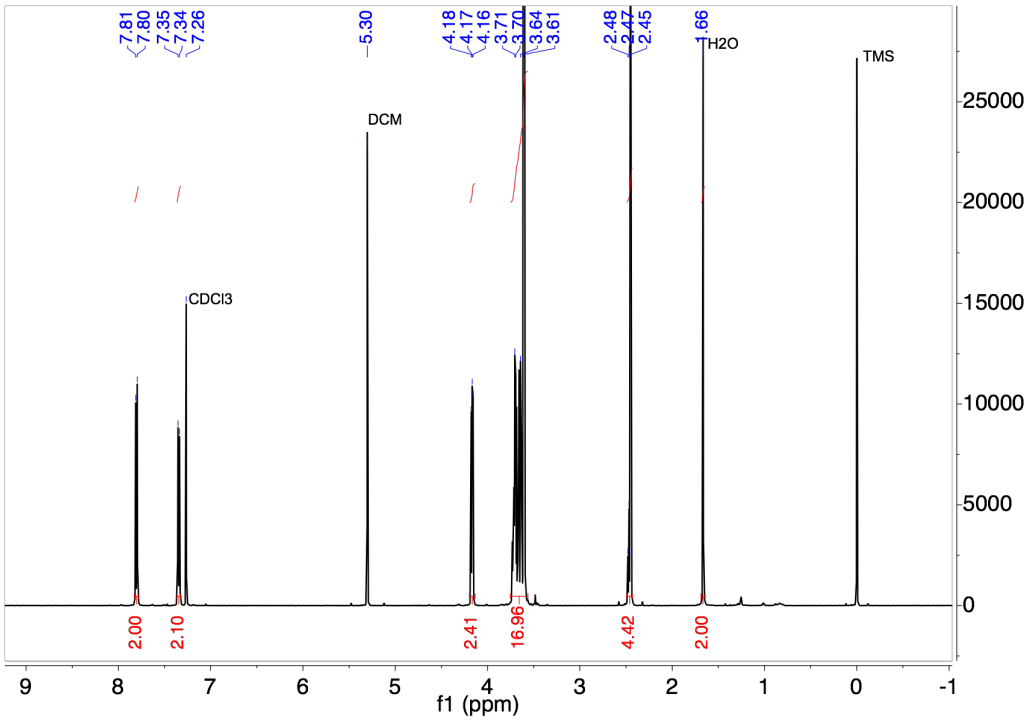

Figure 3.6 ^{1}H NMR (400 MHz, $CDCl_3$) of 2-(2-(2-(2-hydroxyethoxy)ethoxy)ethoxy)ethyl 4-methylbenzenesulfonate (**2**)

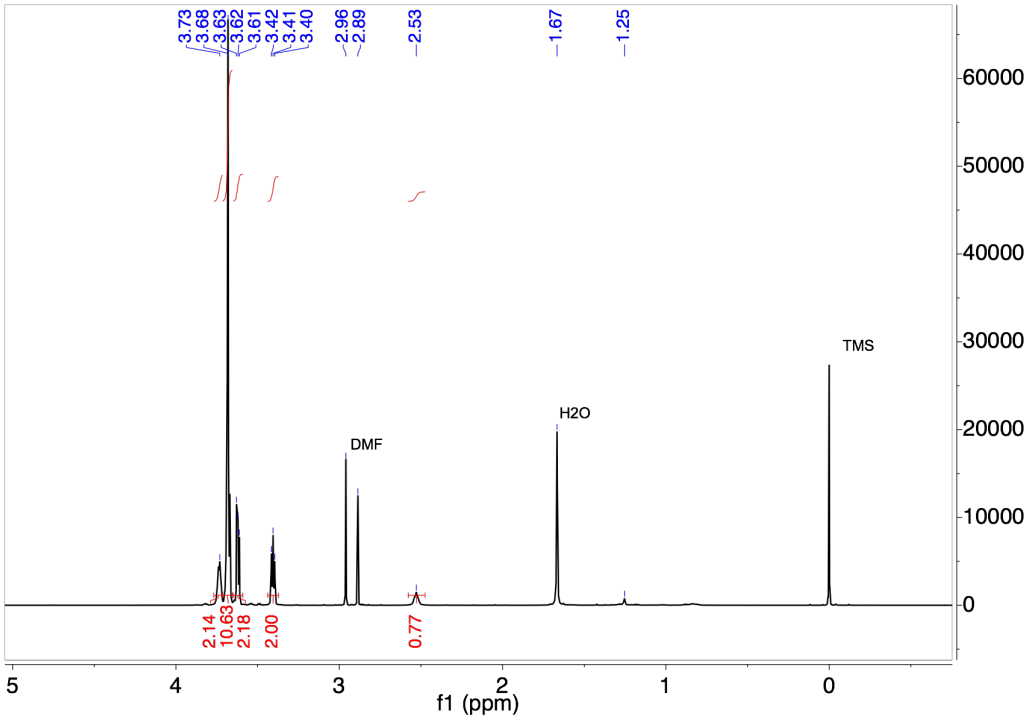

Figure 3.7 ^{1}H NMR (400 MHz, $CDCl_3$) of PEG_4-Azide (**3**)

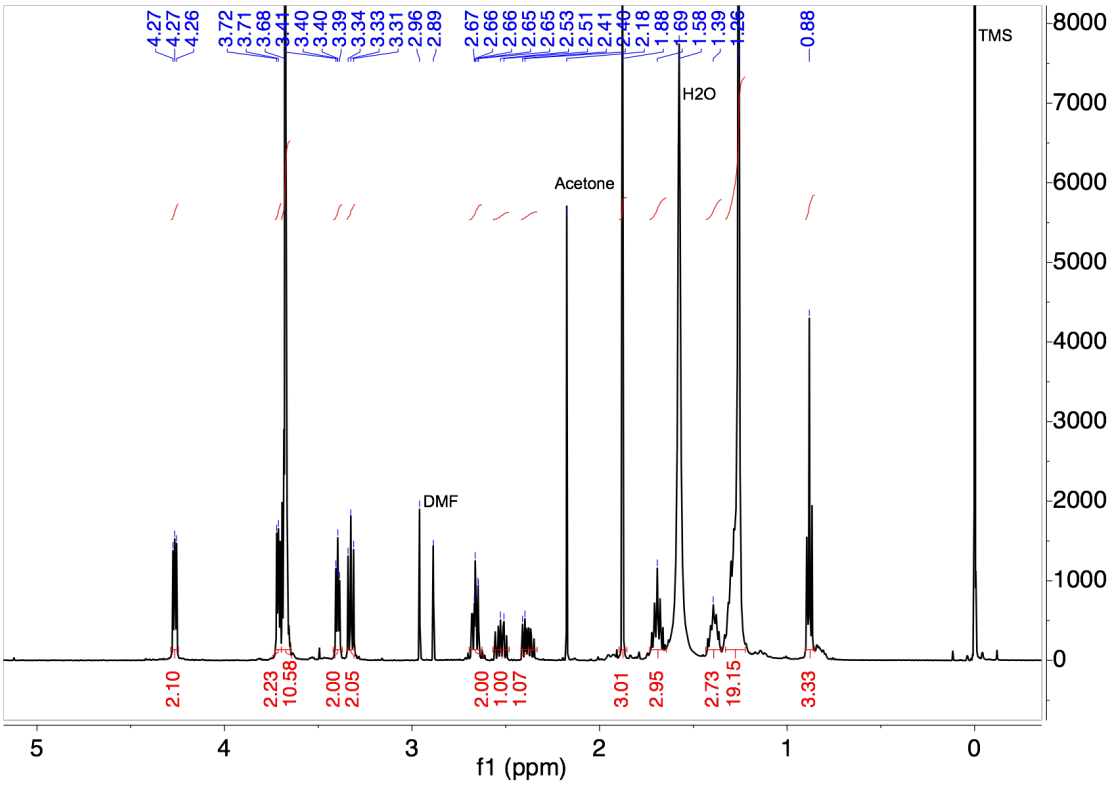

Figure 3.8 ^{1}H NMR (400 MHz, $CDCl_3$) of 2-(2-(2-(2-azidoethoxy)ethoxy)ethoxy)ethyl 4-cyano-4(((dodecylthio)carbonthioyl)thio)pentanoate (azide-CTA **5**)

3.5.2.3 Synthesis of PhBMA monomer

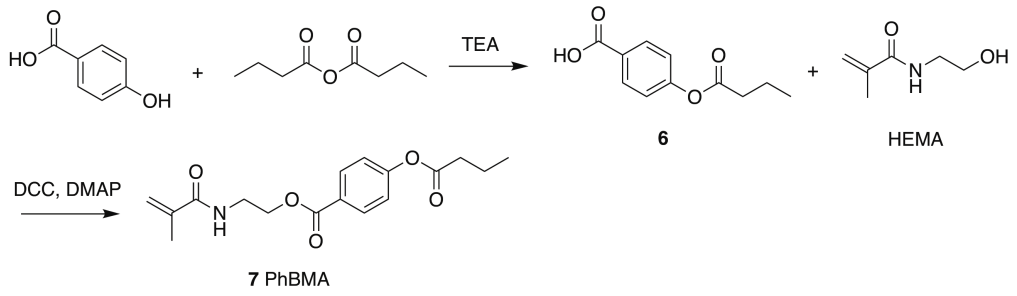

Scheme 3.2 Synthesis route of N-[2-(4-butanoyloxybenzoyloxy)ethyl] methacrylamide (**7** PhBMA monomer)

To synthesize 4-butanoyloxybenzoic acid (**6**), 4-hydroxybenzoic acid (1 g, 7.2 mmol, 1 eq) and triethylamine (4.04 mL, 28.8 mmol, 4 eq) were dissolved in dry DCM. To that solution,

butanoic anhydride (1.42 mL, 8.6 mmol, 1.2 eq) was added. After 8 h, the solvent was removed by rotary evaporator and the crude product was purified by silica column eluted by methanol:DCM 2:98 v/v. The product was white solid (0.92 g, yield 61%). MS (ESI). $C_{11}H_{12}O_4$, m/z calculated for $[M+H]^+$: 208.07, found: 208.0. ^{1}H NMR (400 MHz, $CDCl_3$) δ 8.12 (d, 2H), 7.16 (d, 2H), 2.56 (t, 2H), 1.82 (m, 2H), 1.05 (t, 3H)

To synthesize N-[2-(4-butanoyloxybenzoyloxy)ethyl] methacrylamide (**7**, PhBMA), compound (**6**, 0.67 g, 3.2 mmol, 1.0 eq), N-(2-hydroxyethyl) methacrylamide (HEMA, 0.62 g, 4.8 mmol, 1.5 eq), and DCC (0.99 g, 4.8 mmol, 1.5 eq) were dissolved in dry DCM. The reaction mixture was stirred at 0 °C for 30 min. After that time, 4-dimethylaminopyridine (19 mg, 0.15 mmol, 0.05 eq) dissolved in dry DCM was added to the reaction mixture dropwise. The reaction was allowed to rise to room temperature overnight. The reaction mixture was filtered and solvent DCM was removed by rotary evaporator. The crude product was purified via silica column eluented by ethyl acetate:hexanes 50:50 v/v. The product was white solid (0.98 g, yield 96%). MS (ESI). $C_{17}H_{21}NO_5$, m/z calculated for $[M+H]^+$: 319.14, found: 319.1. ^{1}H NMR (400 MHz, $CDCl_3$) δ 8.07 (d, 2H), 7.18 (d, 2H), 6.24 (br, 1H), 5.71 (s, 1H), 5.35 (s, 1H), 4.48 (m, 2H), 3.72 (m, 2H), 2.57 (t, 2H), 1.97 (s, 3H), 1.79 (m, 2H), 1.05 (t, 3H)

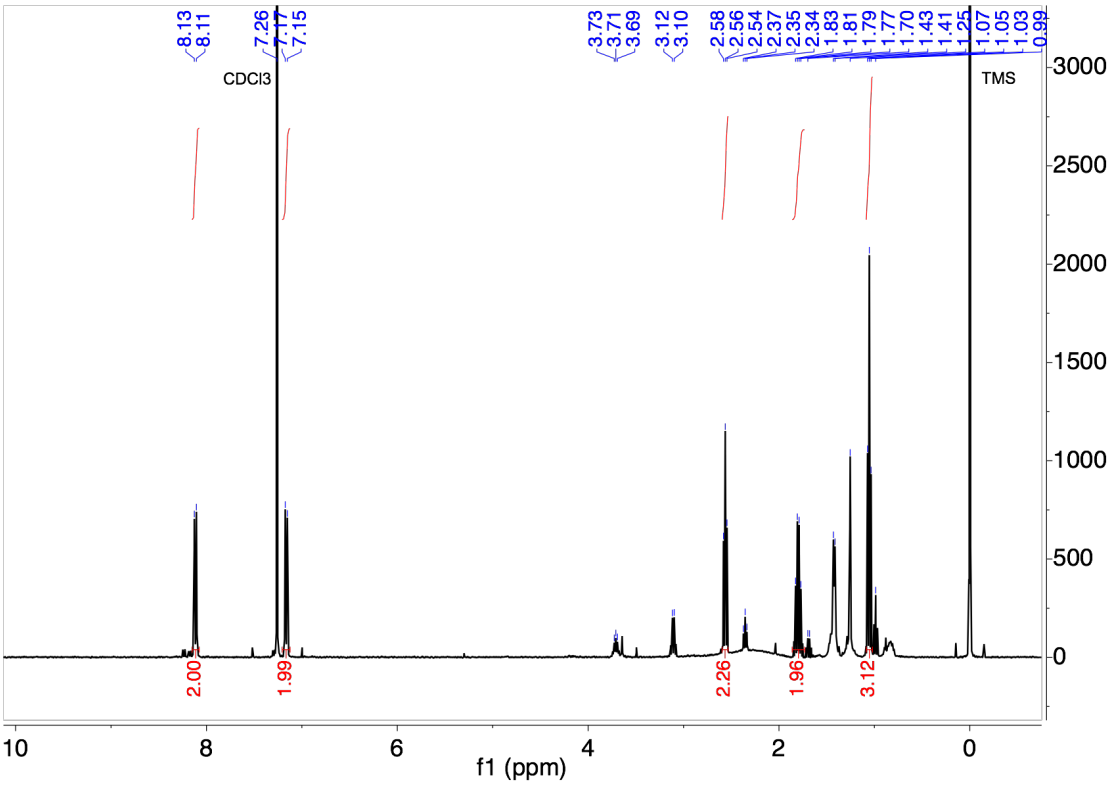

Figure 3.9 ^{1}H NMR (400 MHz, $CDCl_3$) of 4-butanoyloxybenzoic acid (**6**)

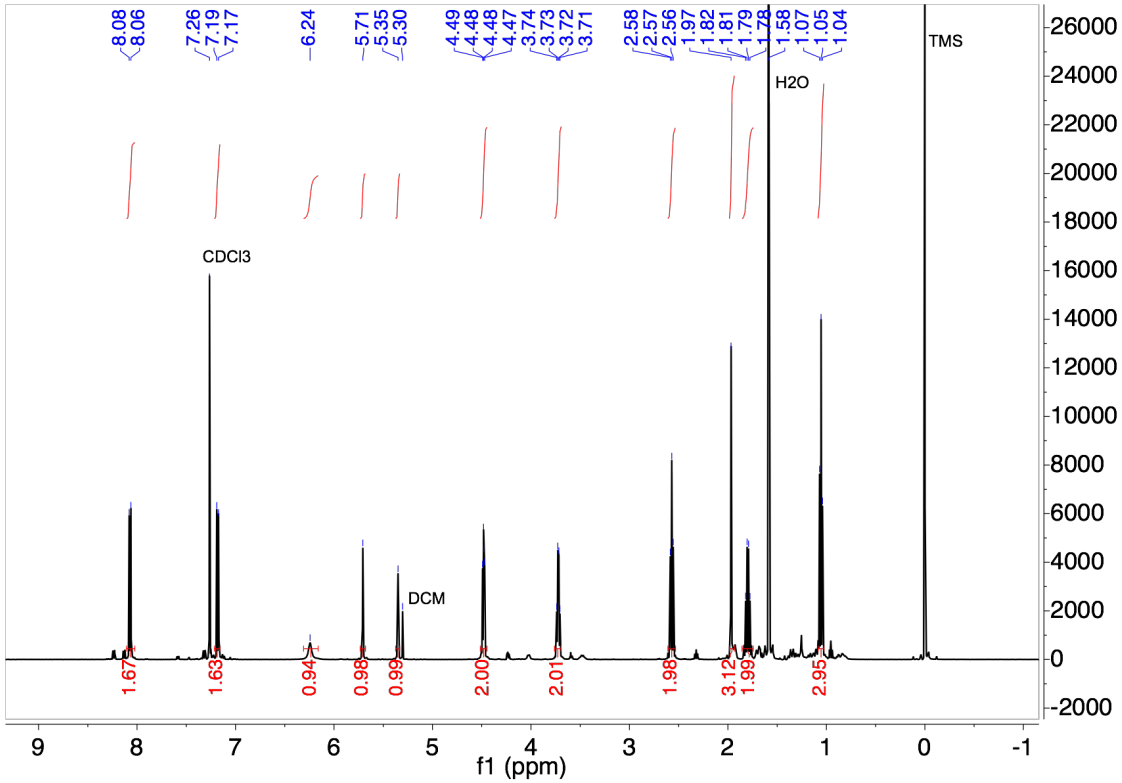

Figure 3.10 ^{1}H NMR (400 MHz, $CDCl_3$) of PhBMA (**7**)

3.5.2.4 Synthesis of pMan-But or pMan-PhBut polymer

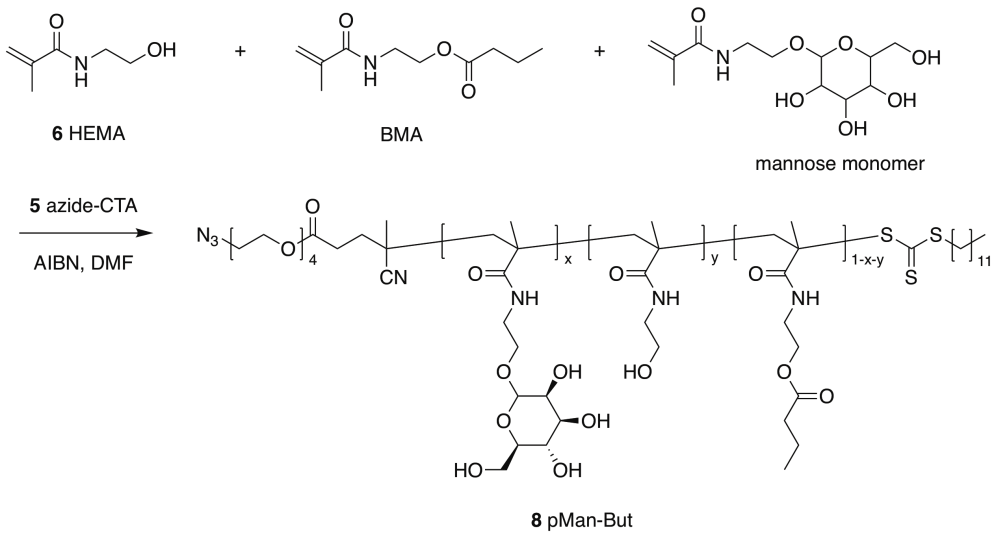

Scheme 3.3 Synthesis route of pMan-But (**8**)

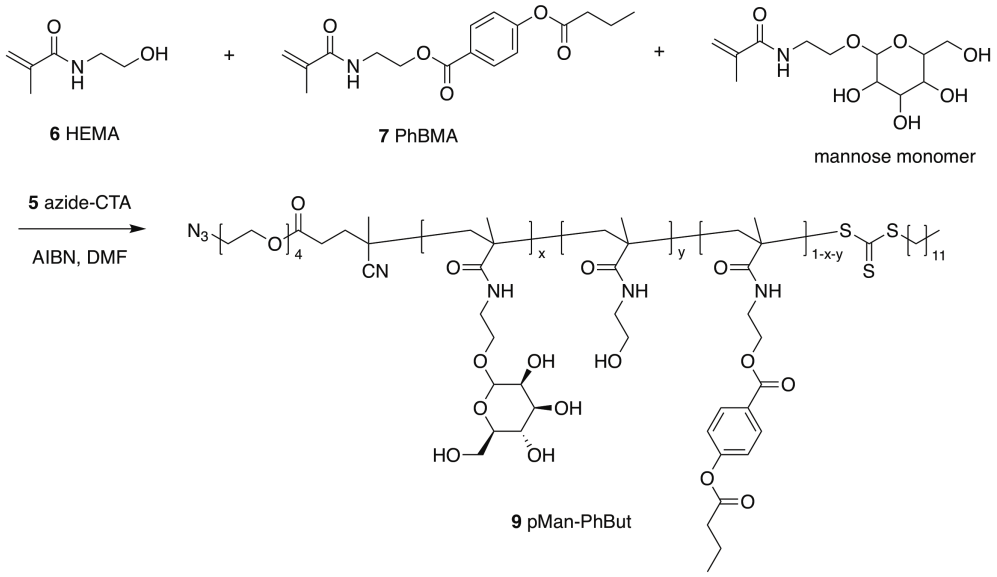

Scheme 3.4 Synthesis route of pMan-PhBut (**9**)

The polymerizations of pMan-But (**8**) or pMan-PhBut (**9**) were similar as described in the previous paper[14]. Briefly, mannose monomer (300 mg, 1.03 mmol), HEMA (500 mg, 3.50 mmol), and butyrate monomer (for pMan-But: BMA, 200 mg, 1.00 mmol; for pMan-PhBut:

compound **7**, PhBMA, 200 mg, 0.63 mmol) were dissolved in dry DMF in a Schlenk tube. To that solution, compound **5** azide chain transfer agent (30 mg, 0.05 mmol) and free radical initiator AIBN (2 mg, 0.01 mmol) were added. The reaction vessel was degassed via four freeze-pump-thaw cycles and then heated to 70 °C to initiate polymerization. The reaction was allowed for 14 h. After that time, the reaction vessel was immersed in liquid nitrogen to stop the reaction. Then the polymer was precipitated in cold acetone. After centrifugation, the supernatant was decanted. The precipitation was repeated for three times. The final product was dried in vacuum oven. The product was white powder (360 mg, yield 72%). The polymer was characterized by ^{1}H NMR and GPC with DMF as eluent. The pMan-But used in the biological studies had a number average molecular weight of 11 kDa, as determined by GPC, using PEO as standard. The pMan-PhBut used in the biological studies also had a number average molecular weight of 11 kDa. The butyrate content of pMan-But or pMan-PhBut was determined by LC-MS/MS after the complete hydrolysis catalyzed by NaOH.

3.5.3 GPC characterization of polymers

GPC characterizations of pMan-But or pMan-PhBut were performed on Tosoh EcoSEC size exclusion chromatography System using Tosoh SuperAW3000 column. Samples were dissolved in eluent DMF with 0.01 M LiBr at 1 mg/mL. The temperature of the column was set to 50 °C. Refreactive index (RI) detector was used to detect polymers. Number averaged molecular weight, weight averaged molecular weight, and polydispersity index were determined via the column calibration using PMMA as standards.

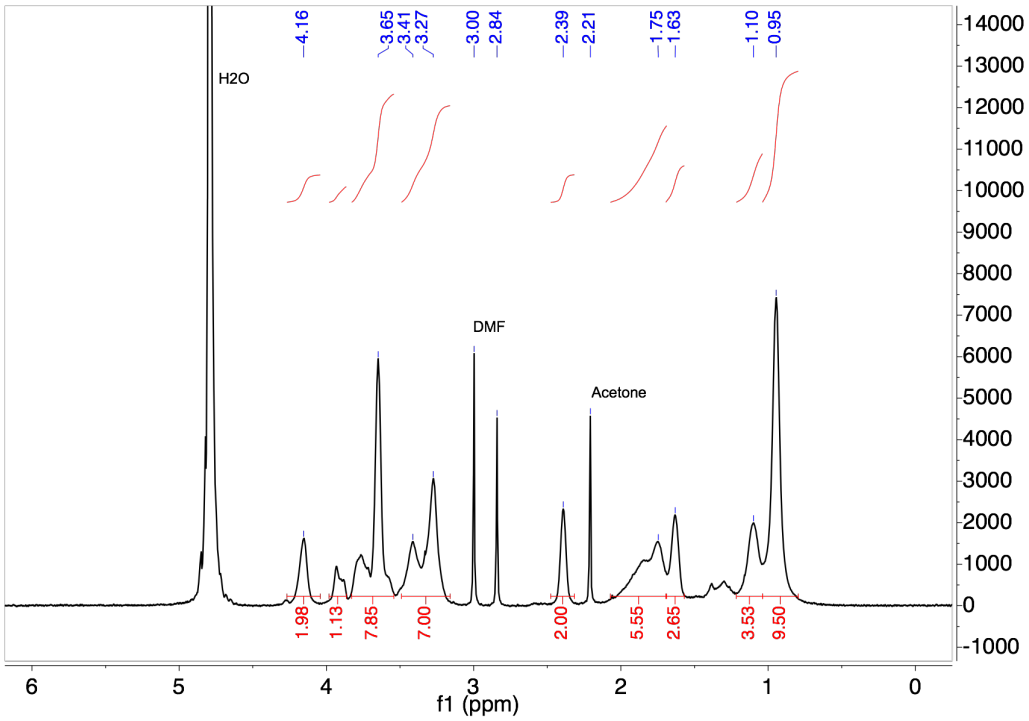

Figure 3.11 ^{1}H NMR (400 MHz, D_2O) of pMan-But (**8**)

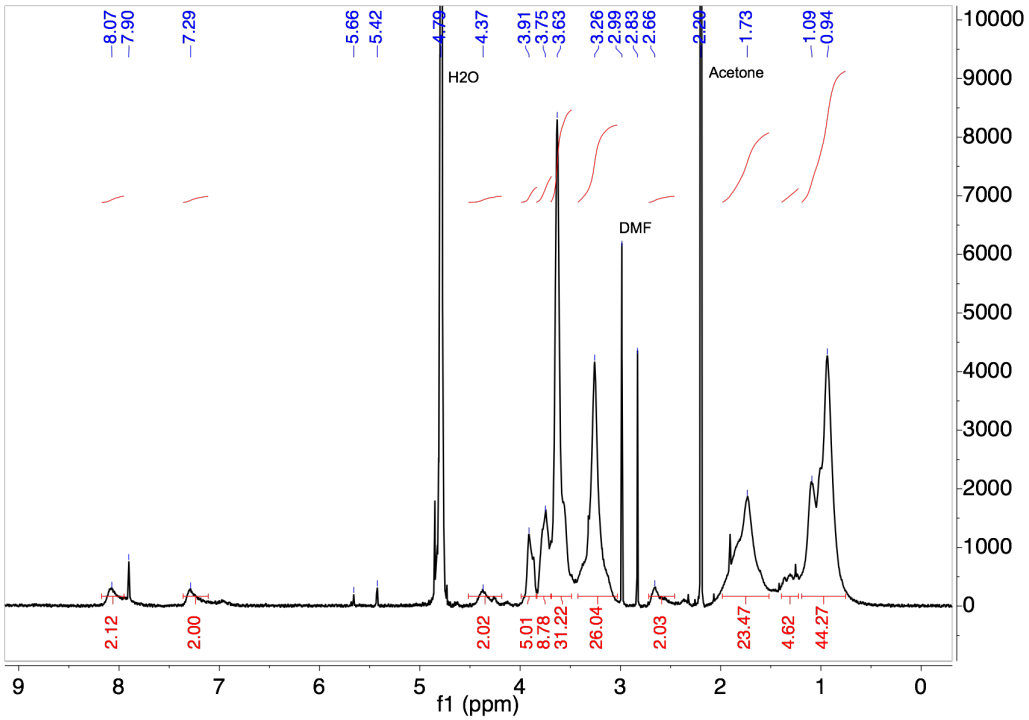

Figure 3.12 ^{1}H NMR (400 MHz, D_2O) of pMan-PhBut (**9**)

A

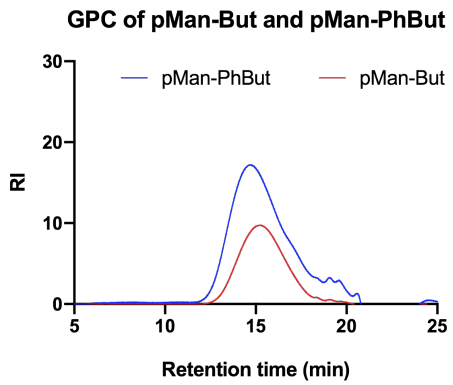

B

	Mn (kDa) by GPC	Mw (kDa) by GPC	PDI
pMan-But	11.77	21.60	1.84
pMan-PhBut	11.25	26.85	2.38

Figure 3.13 GPC characterization of pMan-But and pMan-PhBut polymers. (**A**) Refractive index signal of pMan-But and pMan-PhBut. Samples were run in DMF eluent. (**B**) Number averaged molecular weight, weight averaged molecular weight, and polydispersity index were determined via the column calibration using PMMA as standards.

3.5.4 LC-MS/MS analysis of butyrate release

Sample preparation: Samples were prepared and derivatized as describe in the literature[20]. Briefly, pMan-But or pMan-PhBut was dissolved in RPMI complete cell culture media, pH 7.4 PBS buffer, or pH 5.3 acetate buffer at 10 mg/mL. 20 µL of the solution was transferred into 500 µL of water:acetonitrile 1:1 v/v at 0, 4, 8, 24, 52, 72, 96, 144 h. The sample was centrifuged using Amicon Ultra (Merck, 3 kDa molecular mass cutoff) at 13,000 × g for 15 min, to remove polymers. The filtrate was stored at -80 °C before derivatization.

Sample derivatization: 3-nitrophenylhydrazine (NPH) stock solution was prepared at 0.02 M in water:acetonitrile 1:1 v/v. EDC stock solution was prepared at 0.25 M in water:acetonitrile 1:1 v/v. 4-methylvaleric acid was added as internal standard. Samples were mixed with NPH

stock and EDC stock at 1:1:1 ratio by volume. The mixture was heated by heating block at 60 °C for 30 min. Samples were transferred into HPLC vials and stored at 4 °C before analysis.

LC conditions: The instrument used for quantification of butyrate was Agilent 1290 UHPLC. Column: Thermo Scientific C18 4.6 × 50 mm, 1.8 m particle size, at room temperature. Mobile phase A: water with 0.1% v/v formic acid. Mobile phase B: acetonitrile with 0.1% v/v formic acid. Injection volume: 5.0 μL. Flow rate: 0.5 mL/min. Gradient of solvent: 15% mobile phase B at 0.0 min; 100% mobile phase B at 3.5 min; 100% mobile phase B at 6.0 min; 15% mobile phase B at 6.5 min.

ESI-MS/MS method: The instrument used to detect butyrate was Agilent 6460 Triple Quad MS-MS. Both derivatized butyrate-NPH and 4-methylvaleric-NPH were detected in negative mode. The MS conditions were optimized on pure butyrate-NPH or 4-methylvaleric-NPH at 1 mM. The fragment voltage was 135 V and collision energy was set to 18 V. Multiple reaction monitoring (MRM) of 222 → 137 was assigned to butyrate, and MRM of 250 → 137 was assigned to 4-methylvaleric acid as internal standard. The ratio between MRM of butyrate and 4-methylvaleric acid was used to quantify the concentration of butyrate. For butyrate releasing study, the results were plotted by Prism software and fitted by exponential plateau model to calculate first order reaction constant.

3.5.5 BMDC experiment and ELISA of IL12p70

Mature BMDCs were seated in 96 well plate at 50,000 cells per well in DMEM cell culture media. To each well, sodium butyrate, pMan-But, or pMan-PhBut dissolved in PBS were added at different concentrations. After 24 h of incubation at 37 °C, LPS was added to each well to a final concentration of 100 ng/mL to activate cells. After another 24 h, cells were centrifuged

at 1,500 × g for 2 min and the supernatant was transferred to a new 96 well plate for enzyme-linked immunosorbent assay (ELISA). The ELISA assays of IL12p70, IL-6, or TNFα were performed according to the protocol provided by manufacturer (Thermo Fisher). Briefly, a 96 well plate was coated with capture antibodies overnight at 4 °C, followed by blocking with 2% BSA in PBS with 0.05% Tween 20 (PBS-T) for 1 hour at room temperature. After washing with PBS-T, the plate was incubated with samples for 2 hours at room temperature. After three washes with PBS-T, the plate was incubated with biotinylated detection antibodies. After washes, streptavidin-horse radish peroxidase was added and the level of cytokine was detected with tetramethylbenzidine substrate by measuring the absorbance at 450 nm subtracting the absorbance at 570 nm. The data were plotted and analyzed by Prism software.

3.5.6 IVIS imaging and biodistribution

C57BL/6 mice were used for biodistribution study. pMan-PhBut polymer was labeled with IR 750-DBCO (Thermo Fisher) and purified by Zeta spin desalt column. The polymer was suspended in PBS solution and injected to the mice subcutaneously from hock or flank. After 6 h, 24 h, 48 h, or 7 d, organs and lymph nodes were collected from the mice and whole-organ fluorescence were measured via an IVIS Spectrum in vivo imaging system (Perkin Elmer). Images were processed and analyzed by Living Imaging 4.5.5 (Perkin Elmer).

3.5.7 Animal experiment and flow cytometry

C57BL/6 mice at age 8-10 weeks were used for animal experiment of the induction of tolerogenic dendritic cells. On day 0, mice were injected with sodium butyrate, pMan-PhBut (0.5 mg of butyrate equivalent), or PBS subcutaneously from the back hock. On day 1, mice were

injected with LPS (25 ng per hock). Mice were sacrificed on day 2 and inguinal and popliteal lymph nodes were collected. Lymph nodes were mechanically disrupted and digested at 37 °C for 45 min in collagenase D (Roche) before passing through a 70 μm cell strainer. The lymph node single-cell suspension was washed with PBS and resuspended in DMEM media. The cells were used for LPS re-activation assay and flow cytometry analysis.

For LPS re-activation assay, cells were culture with 100 ng/mL of LPS for three days. The supernatant was collected and analyzed using the inflammation panel of multiplex ELISA (BioLegend's LEGENDplex) according to the manufacture's instruction. The data were obtained via flow cytometer (BD) and analyzed by LEGENDplex data analysis software.

Flow cytometry measurements were performed using a LSRII flow cytometer (BD) and the data were analyzed by FlowJo software. For staining, cells were washed with PBS and stained for 15 min on ice with eFluor 780 fixable live/dead dye (eBioscience). Then, cells were washed with PBS three times, and stained with an antibody cocktail and PBS + 2% FBS for 30 min. The antibody cocktail included antibodies against CD11b, CD11c, F4/80, CD45, CD206, CD40, CD80, and MHCII. Free antibodies were washed from the cells three times with PBS + 2% FBS. Cells were then fixed for 15 min in PBS + 2% paraformaldehyde and washed three times and resuspended in PBS + 2% FBS before analysis via flow cytometry instrument.

3.6 Conclusion

In this study, we used copolymer of mannose and butyrate to target dendritic cells and suppress the activation of DCs. We developed two types of butyrate polymers: pMan-But with aliphatic hydroxyl butyrate ester, and pMan-PhBut with phenol butyrate ester. Both polymers released butyrate in the cell culture media and suppressed the BMDC activation by lowering the

production of cytokine IL12p70. Furthermore, biodistribution study showed the polymer stayed in the draining popliteal and inguinal lymph nodes after hock s.c. injection. More importantly, in the animal study, pMan-PhBut induced tolerogenic DCs in the draining lymph nodes as shown from LPS re-activation assay. Such results motivated us to further investigated T cell response against butyrate polymer as well as conjugate pMan-But or pMan-PhBut with antigen for tolerance study.

3.7 References

1. Lu, R.M.*, et al.* Development of therapeutic antibodies for the treatment of diseases. *J Biomed Sci* **27**, 1 (2020).

2. Baker, M.P., Reynolds, H.M., Lumicisi, B. & Bryson, C.J. Immunogenicity of protein therapeutics: The key causes, consequences and challenges. *Self Nonself* **1**, 314-322 (2010).

3. Fu, K.*, et al.* Immunogenicity of Protein Therapeutics: A Lymph Node Perspective. *Front Immunol* **11**, 791 (2020).

4. Emi Aikawa, N., de Carvalho, J.F., Artur Almeida Silva, C. & Bonfá, E. Immunogenicity of Anti-TNF-alpha agents in autoimmune diseases. *Clin Rev Allergy Immunol* **38**, 82-89 (2010).

5. Arpaia, N.*, et al.* Metabolites produced by commensal bacteria promote peripheral regulatory T-cell generation. *Nature* **504**, 451-455 (2013).

6. Furusawa, Y.*, et al.* Commensal microbe-derived butyrate induces the differentiation of colonic regulatory T cells. *Nature* **504**, 446-450 (2013).

7. Sun, M.*, et al.* Microbiota-derived short-chain fatty acids promote Th1 cell IL-10 production to maintain intestinal homeostasis. *Nat Commun* **9**, 3555 (2018).

8. Koh, A., De Vadder, F., Kovatcheva-Datchary, P. & Bäckhed, F. From Dietary Fiber to Host Physiology: Short-Chain Fatty Acids as Key Bacterial Metabolites. *Cell* **165**, 1332-1345 (2016).

9. Kaisar, M.M.M., Pelgrom, L.R., van der Ham, A.J., Yazdanbakhsh, M. & Everts, B. Butyrate Conditions Human Dendritic Cells to Prime Type 1 Regulatory T Cells. *Front Immunol* **8**, 1429 (2017).

10. Singh, N.*, et al.* Blockade of dendritic cell development by bacterial fermentation products butyrate and propionate through a transporter (Slc5a8)-dependent inhibition of histone deacetylases. *J Biol Chem* **285**, 27601-27608 (2010).

11. Chang, P.V., Hao, L., Offermanns, S. & Medzhitov, R. The microbial metabolite butyrate regulates intestinal macrophage function via histone deacetylase inhibition. *Proc Natl Acad Sci U S A* **111**, 2247-2252 (2014).

12. Macri, C., Dumont, C., Johnston, A.P. & Mintern, J.D. Targeting dendritic cells: a promising strategy to improve vaccine effectiveness. *Clin Transl Immunology* **5**, e66 (2016).

13. Jaynes, J.M.*, et al.* Mannose receptor (CD206) activation in tumor-associated macrophages enhances adaptive and innate antitumor immune responses. *Sci Transl Med* **12**(2020).

14. Wilson, D.S.*, et al.* Antigens reversibly conjugated to a polymeric glyco-adjuvant induce protective humoral and cellular immunity. *Nat Mater* **18**, 175-185 (2019).

15. Wilson, D.S.*, et al.* Synthetically glycosylated antigens induce antigen-specific tolerance and prevent the onset of diabetes. *Nat Biomed Eng* **3**, 817-829 (2019).

16. Krátký, M. & Vinsová, J. Salicylanilide ester prodrugs as potential antimicrobial agents--a review. *Curr Pharm Des* **17**, 3494-3505 (2011).

17. Lee, J.B.*, et al.* Lipophilic activated ester prodrug approach for drug delivery to the intestinal lymphatic system. *J Control Release* **286**, 10-19 (2018).

18. Das, D.*, et al.* RAFT polymerization of ciprofloxacin prodrug monomers for the controlled intracellular delivery of antibiotics. *Polymer Chemistry* **7**, 826-837 (2016).

19. Su, F.Y.*, et al.* Macrophage-targeted drugamers with enzyme-cleavable linkers deliver high intracellular drug dosing and sustained drug pharmacokinetics against alveolar pulmonary infections. *J Control Release* **287**, 1-11 (2018).

20. Tyagi, A.*, et al.* The Microbial Metabolite Butyrate Stimulates Bone Formation via T Regulatory Cell-Mediated Regulation of WNT10B Expression. *Immunity* **49**, 1116-+ (2018).

21. Gee, K., Guzzo, C., Che Mat, N.F., Ma, W. & Kumar, A. The IL-12 family of cytokines in infection, inflammation and autoimmune disorders. *Inflamm Allergy Drug Targets* **8**, 40-52 (2009).

22. Tait Wojno, E.D., Hunter, C.A. & Stumhofer, J.S. The Immunobiology of the Interleukin-12 Family: Room for Discovery. *Immunity* **50**, 851-870 (2019).

23. Wu, Q., Wang, Y. & Chen, G. Medical Application of Microbial Biopolyesters Polyhydroxyalkanoates. *Artificial Cells Blood Substitutes and Biotechnology* **37**, 1-12 (2009).

24. Martin, D. & Williams, S. Medical applications of poly-4-hydroxybutyrate: a strong flexible absorbable biomaterial. *Biochemical Engineering Journal* **16**, 97-105 (2003).

25. Lutz, M.*, et al.* An advanced culture method for generating large quantities of highly pure dendritic cells from mouse bone marrow. *Journal of Immunological Methods* **223**, 77-92 (1999).

Chapter 4

Collagen Binding Protein and Paclitaxel Conjugate Targets Tumor Environment

4.1 Abstract

Serum albumin fused with the A3 collagen-binding domain of von Willebrand factor (A3-MSA) has been developed in our lab for tumor targeting immunotherapy or chemotherapy. To extend the application of A3-MSA in tumor targeting chemotherapy, we developed a protein drug conjugate between paclitaxel (PTX) and A3-MSA to target collagens over-expressed in tumor environment. The conjugates were soluble in water without any aggregation due to the hydrophilic PEG linker. In addition, paclitaxel was chemically conjugated to A3-MSA protein via a pH-sensitive hydrazone linker, which allowed the release of paclitaxel in acidic tumor environment or endosomal pH. Moreover, A3-MSA-PTX conjugate efficiently suppressed the viability of human cancer cell line MDA-MB-231 and human prostate cancer cell line PC3. Finally, although the pilot study of A3-MSA-PTX did not show significant difference from free paclitaxel in PC3 tumor model on nude mice, we believed high dosage could lead to better performance of A3-MSA-PTX conjugates.

4.2 Introduction

Paclitaxel (PTX) is one of the most useful and effective chemotherapeutic drugs[1-3]. Paclitaxel stabilizes the microtubules and blocks the replication of cancer cells[4,5]. Due to its ability of limiting rapid cell proliferation, paclitaxel has been used in the treatment of many malignant tumors, including ovarian cancer, prostate cancer, breast cancer, and pancreatic

cancer. However, paclitaxel has two major challenges limiting its applications: low solubility and strong adverse effects[6-8]. The low solubility of paclitaxel makes it difficult to formulate. Moreover, the anticancer mechanism of paclitaxel on microtubule assembly causes severe hematological, neuromuscular, and gastrointestinal adverse events.

To solve the solubility issue of paclitaxel, one method is to synthesize a prodrug conjugate of paclitaxel and hydrophilic polymer like poly(ethylene glycol) (PEG)[9,10]. However, the molecular weight of PEG polymer has to reach 40 kDa in order to generate a soluble prodrug. Many nanoparticle delivery strategies have been used to formulate paclitaxel including the formulation of micelles, liposomes, or polymersomes[11-14]. One successful formulation is paclitaxel albumin-bound nanoparticles with the trade name of Abraxane[15-17]. Abraxane is composed of paclitaxel absorbed on human serum albumin with a size of 130 nm. The soluble formulation of Abraxane allows intravenous administration at a high paclitaxel dosage. Additionally, researchers have developed peptide-paclitaxel conjugates that formulate into nanoparticles[18-21]. For instance, Chilkoti lab conjugated paclitaxle to recombinant chimeric polypeptides that self-assemble into 60 nm nanoparticles[22,23]. The novel nanoparticles showed better performance than Abraxane or free paclitaxel. Although nanoparticle formulation can increase the payload of paclitaxel, the formulation only accumulate to tumor environment by enhanced permeability and retention (EPR) effect. It would be interesting to design a water-soluble antibody-paclitaxel conjugate that can target tumor cells or tumor environment and release paclitaxel locally[24,25].

To target tumor environment, collagen-binding peptide has been proven to be a competent candidate because of the high expression of collagen in tumor environment and the increased permeability of tumor vasculature[26]. Previously in the lab, Dr. Jun Ishihara and

colleagues have developed a platform of fused protein between extracellular matrix binding peptide and therapeutic proteins to enhance the cancer immunotherapy[27-33]. The combination treatment of immune checkpoint inhibitors and Interleukin-2 conjugated to collagen binding domain (CBD) showed improved efficacy and better safety[29]. In addition, the chemokine CCL4 conjugated to CBD also enhanced the performance of checkpoint blockade therapy by recruiting $CD103^+$ dendritic cells to the tumor[30]. Furthermore, the conjugate between cytokine Interleukin-12 and CBD showed remarkable performance on immunologically cold tumor when combined with checkpoint blockade therapy[33]. More importantly, the conjugate of chemotherapeutic drug doxorubicin and CBD and serum albumin enhanced tumor efficacy and reduced adverse effects compared to free doxorubicin[31]. The conjugate targets tumor through not only active binding to tumor extracellular matrix and also passive accumulation in tumor by enhanced permeability and retention effect.

Here, we present a protein paclitaxel conjugate A3-MSA-PTX that target the tumor environment. The fused protein of collage binding domain A3 and mouse serum albumin (MSA) is linked with paclitaxel through a poly(ethylene glycol) and a pH sensitive hydrazone. The conjugate releases paclitaxel at acidic tumor environment pH and shows efficacy in the cell viability assay. The treatment of A3-MSA-PTX conjugate still needs improvements on human PC3 cancer model on nude mice.

4.3 Results

4.3.1 PTX is conjugated to collagen binding protein A3-MSA through hydrazine linker

The hydrazone formed between ketone and hydrazine is a widely used chemistry for conjugating drug to polymers or proteins[22,31,34,35]. Hydrazone group hydrolyzes at slightly acidic

pH[22]. Thus, drug conjugated through hydrazone will release in either tumor environment or endosome of cells, with acidic pH of 6.5 or 5.3, respectively. In order to conjugate paclitaxel (PTX) to collagen binding protein A3-MSA, we modified the 2'-OH of paclitaxel with levulinic acid to generate PTX-LEV. Then the ketone group of PTX-LEV was used for the next step of reaction with the linker (N-(ε-maleimidocaproic acid) hydrazide (EMCH), which has hydrazide on one end and maleimide on the other end[22,31]. The product PTX-LEV-EMCH was then conjugated to A3-MSA protein via maleimide cysteine coupling. However, from dynamic light scattering (DLS), the conjugate had a hydrodynamic diameter of 100 nm from volume distribution, while A3-MSA itself only had a diameter of 10 nm. On the contrary, previously in the lab, doxorubicin was also conjugated to A3-MSA and only had a diameter of 10 nm in DLS[31]. Thus, we believed A3-MSA-PTX conjugate aggregated in the solution into larger particles due to the hydrophobicity of paclitaxel molecule.

4.3.2 PEG linker increases the solubility of the conjugate and reduces aggregation

Given the aggregation of A3-MSA-PTX caused by the hydrophobicity of paclitaxel, we hypothesized that a hydrophilic PEG-5,000 linker would help increase the solubility of the protein-drug conjugate and prevent the aggregation[9,10] (Figure 4.1.A). To synthesize the linker, we started with the bifunctional PEG linker with maleimide or carboxylate acid on each end and modified the acid end to hydrazide through reaction with BOC-hydrazine[36]. After the deprotection, the linker was reacted with PTX-LEV (Figure 4.1.B). The product PEG-PTX was purified with prep-TLC before conjugating to A3-MSA protein. The conjugate was centrifuged to remove aggregates and then purified through Zeba column to remove unreacted PEG-PTX.

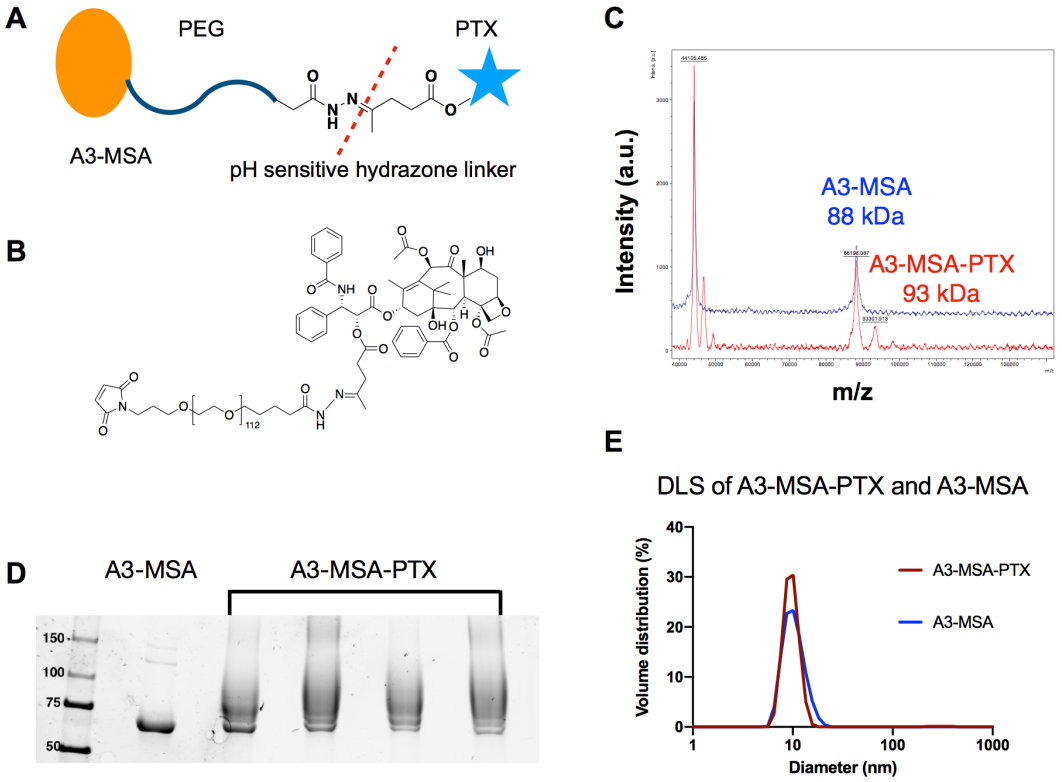

Figure 4.1 Design and characterization of A3-MSA-PTX conjugate. (**A**) Schematic illustration of A3-MSA-PTX design. Collagen binding domain A3 was fused with serum albumin. The protein was linked with paclitaxel through a PEG linker with a pH sensitive hydrazone bond. (**B**) Chemical structure of PTX-LEV-PEG. (**C**) MALDI-TOF showed an increase of molecular weight from A3-MSA at 88 kDa to A3-MSA-PTX at 93 kDa. (**D**) SDS-PAGE image indicated the increase of molecular weight after the conjugation. (**E**) Dynamic light scattering showed the A3-MSA-PTX conjugate did not change size compared to A3-MSA protein by volume distribution.

The conjugation between A3-MSA protein and PEG-PTX was proven successful via MALDI-TOF analysis (Figure 4.1.C). The molecular weight of the conjugate increased from 88 kDa for A3-MSA protein to 93 kDa for A3-MSA-PTX. The increase of molecular weight matched with the molecular weight of PEG-5,000. Then, we did SDS-PAGE on conjugates to figure out the conversion of protein and how many PEG-PTX chains were conjugated to one protein (Figure 4.1.D). From the gel, it was clear that conjugation reaction caused an increase of

molecular weight from 70 kDa to 80 kDa or more. There was a very pale band of unreacted A3-MSA protein. We proceeded to use those A3-MSA-PTX conjugates because the unreacted A3-MSA amount was low and it was difficult to remove from reacted ones through size exclusion column since their molecular weight difference was not significant. Multiple bands were observed on SDS-PAGE, suggesting the protein was linked to multiple copies of PEG-PTX. However, we decided to use LC-MS/MS method to quantify the average copies of PEG-PTX per A3-MSA, or the drug/protein ratio, as LC-MS/MS detection of released paclitaxel was more quantitative than SDS-PAGE[37,38].

Importantly, the A3-MSA-PTX conjugate with PEG-5,000 linker did not have any aggregation from DLS analysis (Figure 4.1.E). In fact, the conjugates had a similar hydrodynamic diameter with A3-MSA protein, with a 10 nm in size from volume distribution. To interpret DLS data, we used volume distribution instead of intensity distribution because the volume distribution is a more applicable method to illustrate DLS data for proteins or protein conjugates.

The starting material equivalence of PEG-PTX was essential to determine not only the drug/protein ratio, but also the amount of aggregations. We observed that there were more aggregates after spinning when we used 10:1 ratio of PEG-PTX/A3-MSA compared to 4:1 ratio. These results suggesting a higher PTX/protein ratio might cause the aggregation of protein-drug conjugate and the decrease of yield. As a result, we decided to use 4:1 ratio of PEG-PTX/A3-MSA for further batches of synthesis to achieve reasonable amount of paclitaxel loading without wasting too much protein-drug conjugate in the aggregates.

4.3.3 A3-MSA-PTX conjugate release PTX at tumor pH and endosomal pH

Given we successfully conjugated paclitaxel to A3-MSA protein through a PEG linker, we further characterized the drug/protein ratio and the drug release at different pH using LC-MS/MS (Figure 4.2.A, B). Previously in the doxorubicin study, we used UV absorbance to quantify the concentration of drug because doxorubicin had characteristic absorbance at 480 nm[31]. However, paclitaxel did not have unique absorbance in high wavelength range that could be used for UV quantification. Thus, we had to use a different detection method to quantify paclitaxel. In the literature, tandem mass spectrometry, or MS/MS, was often used to quantify paclitaxel[22,37,38]. The structure of paclitaxel contained an ester between the hydroxyl group at C13 of the fourteen-member ring and the carboxylic acid of the tail. In the positive mode of tandem MS, this ester bond broke and generated a secondary ion. Such transition was used to quantify the amount of paclitaxel or PTX-LEV released from the conjugate. From LC-MS/MS results, we found the average paclitaxel/protein ratio to be 3.87 ± 0.18 for the batches when we used 4:1 PEG-PTX/A3-MSA molar ratio during conjugation. A higher amount of aggregation was observed when we used higher PEG-PTX/A3-MSA ratio. Thus, we proceeded with the 4:1 ratio because of less aggregation after spinning down the solution after reaction. According to previous study of collagen-binding domain-SA-doxorubicin, the drug/protein ratio of the conjugate was typically close to four[31].

In order to understand the drug release in *ex vivo* environment, we performed drug release study at three different pH: neutral pH = 7.4, tumor environment pH = 6.5, and endosomal pH = 5.3 (Figure 4.2.B). We would like to validate that hydrazone bond could be hydrolyzed at slightly acidic pH while remaining unchanged at neutral physical pH in the blood circulation. The results from LC-MS/MS proved our hypothesis that A3-MSA-PTX did not

release paclitaxel drug at pH = 7.4 for up to 24 hours. At both tumor environment pH and endosomalis pH, we observed almost completed release of paclitaxel drug. However, the release rates were different and the time periods to reach 100% drug release were 2 hours at pH = 5.3, and 8 hours at pH = 6.5, respectively. This confirmed that hydrazone bond had a higher hydrolysis rate at more acidic pH. After reaching the maximum release, the paclitaxel concentrations slightly decreased at 24 hours time point for both tumor pH and endosomal pH groups. The reason might be paclitaxel molecule decomposed at acidic pH for a long time period as reported in the literature[39]. Thus, when we determined the drug/protein ratio, we treated samples at pH of 5.3 for 2 hours to achieve 100% paclitaxel release. Through LC-MS/MS analysis, we not only calculated the drug/protein ratio for our A3-MSA-PTX conjugate, but also confirmed the conjugate could release paclitaxel completely at both tumor environment pH and endosomal pH.

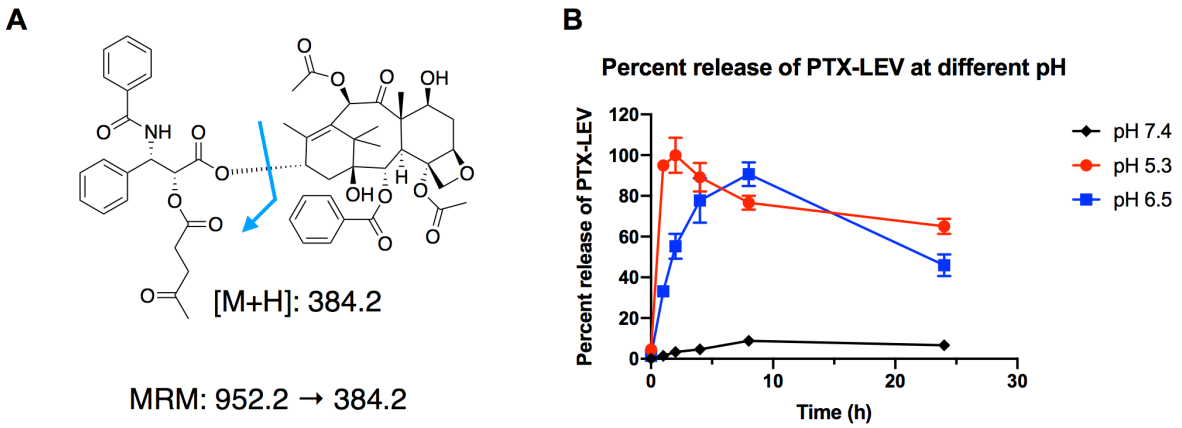

Figure 4.2 Release of PTX-LEV at different pH measured by LC-MS/MS. (**A**) Chemical structure of PTX-LEV and the multiple reaction monitoring of 952.2 → 384.2 used to quantify PTX-LEV in LC-MS/MS analysis. (**B**) The percentage release of PTX-LEV of A3-MSA-PTX at different buffers at pH of 7.4, 5.3, or 6.5 as measured by LC-MS/MS. A3-MSA-PTX showed complete release at tumor environment pH of 6.5 and endosomal pH of 5.3. Data were presented as mean ± s.e.m.

4.3.4 Cell viability assay demonstrates the *in vitro* anticancer efficacy of A3-MSA-PTX

Given the release profile of A3-MSA-PTX *ex vivo* was confirmed by LC-MS/MS, we moved to cell viability assay to study the *in vitro* anticancer efficacy of our conjugates. We chose two cancer cell lines in which paclitaxel were proven to be effective: human breast cancer cell line MDA-MB-231, and human prostate cancer cell line PC3[22,40]. Both cells were used for MTT assay to study the cell viability when treated with either free paclitaxel or A3-MSA-PTX (Figure 4.3.A, B). As shown from the MTT results of both cell lines, we observed a decrease of cell viability as the concentration of drug in equivalent of paclitaxel increased. The data were fitted with inhibitor vs. response - variable slope (four parameters) and half maximal inhibitory concentration (IC50) was reported in the table (Figure 4.3.C). For MDA-MB-231 cells, the IC50 of free paclitaxel and A3-MSA-PTX were 3.6 ± 0.5 nM and 13.5 ± 2.0 nM, respectively. For PC3 cells, the IC50 of free paclitaxel and A3-MSA-PTX were 4.1 ± 0.8 nM and 18.1 ± 4.5 nM, respectively. The IC50s of paclitaxel for both MDA-MB-231 and PC3 cell lines were similar, while the IC50s of A3-MSA-PTX were approximately five times of the value of free paclitaxel. The reason could be A3-MSA-PTX needed more time to release paclitaxel drug compared to free paclitaxel. Additionally, the initial released drug was actually PTX-LEV, which was a less cytotoxic drug than PTX. It was also observed in other research that paclitaxel and protein conjugate had a lower IC50 than free paclitaxel[22]. However, a lower cytotoxicity should not limit the study of A3-MSA-PTX because the current IC50 of A3-MSA-PTX in both cell lines were still in a reasonable range. Moreover, as a protein-drug conjugate, A3-MSA-PTX had more advantages such as long circulation time in blood, accumulation and enrichment in tumor environment due to A3 domain, and high up-taken by tumor cells due to enhanced permeability

and retention (EPR) effect. Thus, we proceeded to study the efficacy of A3-MSA-PTX in *in vivo* mouse tumor model.

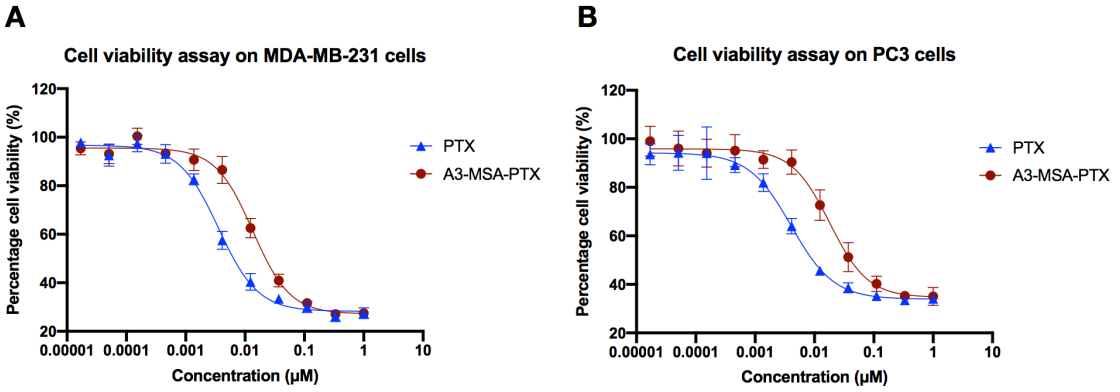

C

IC50	PTX (nM)	CBD-PTX (nM)
MDA-MB-231 cells	3.6 ± 0.5	13.5 ± 2.0
PC3 cells	4.1 ± 0.8	18.1 ± 4.5

Figure 4.3 Cell viability assay showed the efficacy of A3-MSA-PTX on MDA-MB-231 cells and PC3 cells. (**A**) MTT assay showed the efficacy of free PTX and A3-MSA-PTX conjugate on human breast cancer cell line MDA-MB-231. (**B**) MTT assay showed the efficacy of free PTX and A3-MSA-PTX conjugate on human prostate cancer cell line PC3. (**C**) Table of IC50 of free PTX and A3-MSA-PTX for MDA-MB-231 cells or PC3 cells. (**A**, **B**) Data were shown as mean ± s.e.m. and fitted with [inhibitor] vs. response - variable slope (four parameters) model.

4.3.5 Efficacy assay of A3-MSA-PTX on PC3 tumor model

After confirming the *in vitro* efficacy of A3-MSA-PTX in MDA-MB-231 cells and PC3 cells, we further studied the *in vivo* efficacy of A3-MSA-PTX. We used PC3 cells to inoculate tumor on NU/J nude mice. Nude mice were used because the cancer cells were human cancer cell line. At the age of week 8, we inoculated 1.5×10^6 PC3 cells subcutaneously to the left flank of each mouse and monitored the tumor growth (Figure 4.4.A). However, the growth of PC3

tumor on nude mice was slower than what reported in the literature[22,41]. It took four weeks until the tumor grew to about 50 mm^3. Then, we did i.v. injection of either free paclitaxel or A3-MSA-PTX solution twice on day 0 and day 3, with a dose of PTX at 10 mg/kg in total. However, the average tumor volumes of both groups kept growing after the treatment and there was no significant difference between PTX group and A3-MSA-PTX group (Figure 4.4.B-D). All mice were euthanized 13 days after the treatment when the average tumor volumes reached 1,000 mm^3. However, no mouse died or looked very ill on day 13. The body weights of mice in each group did not change much through out the experiment (Figure 4.4.E, F). This was a pilot study and it could be improved by increasing the dosage of paclitaxel to the maximum tolerated dosage or even higher because protein-drug conjugate was less toxic than free paclitaxel.

4.4 Discussion

The hypothesis of this study was that A3-MSA protein could bind to collagens, which were enriched in tumor environment. As paclitaxel was a remarkable chemotherapeutic drug[2,3], the conjugation between A3-MSA and paclitaxel would be a potential tumor-targeting therapeutic drug. Moreover, such idea had been proven successful on the conjugate between A3-MSA and another chemotherapeutic drug doxorubicin[31]. However, paclitaxel had unique hydrophobic structure, making the direct conjugation of A3-MSA and PTX form aggregates in the solution.

Such aggregation was prevented by adding a hydrophilic PEG-5,000 linker. The conjugation between A3-MSA and PEG-PTX appeared to be 10 nm in size by volume distribution in DLS, which was similar to free A3-MSA protein. It was important to review DLS results by volume, instead of by intensity because volume distribution was more appropriate to

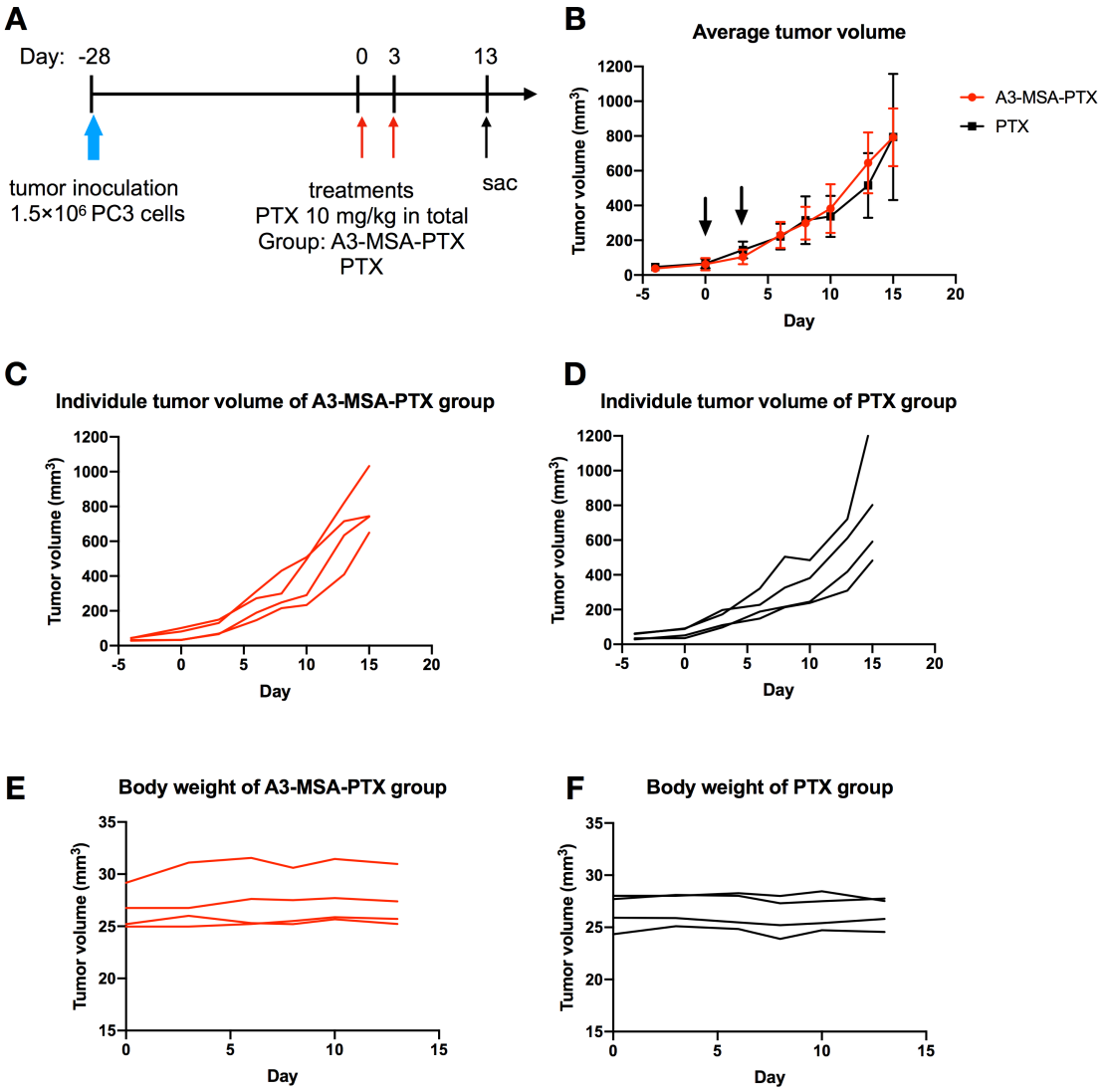

Figure 4.4 Efficacy study of A3-MSA-PTX on PC3 tumor model on nude mice. (**A**) NU/J mice were inoculated with PC3 cancer cells. After 28 days, mice were treated with free PTX or A3-MSA-PTX twice to reach a total dose of 10 mg/kg. Tumor volume and body weight were observed for 13 days. (**B**) The average tumor volume of both PTX and A3-MSA-PTX groups kept increasing after the treatment. (**C**, **D**) Individual tumor plot of each mouse for A3-MSA-PTX group (**C**) or free PTX group (**D**). (**E**, **F**) Individual body weight of each mouse was flat after the treatment and no weight loss was observed for A3-MSA-PTX group (**E**) or free PTX group (**F**).

reveal the size of free protein. In DLS analysis, the intensity of scattered light is in proportion to the sixth power of particle diameter. This means a few large particles in the solution may scatter more light than thousands of small ones. In protein analysis, volume distribution of DLS data is believed to be more representative than intensity distribution[42]. However, when analyzing micelles, liposomes, or polymersomes, intensity distribution is more favorable because nanoparticles are often of more interests than small molecules that are in equilibrium of association and dissociation with larger particles[43].

A3-MSA-PTX conjugated was centrifuged down to remove aggregates and we observed the starting PEG-PTX/A3-MSA ratio was corresponded to the amount of aggregates generated after the conjugation. After several trials, we decided to use 4:1 ratio of PEG-PTX/A3-MSA to achieve products with minimum aggregations. Furthermore, We characterized the conjugate using MALDI-TOF and SDS-PAGE. From the protein gel, we observed multiple copies of PEG-PTX linked to protein. However, the accurate average drug/protein ratio was determined by LC-MS/MS to be around four. The LC-MS/MS analysis was used to quantify paclitaxel released from conjugates at different pH buffers. Due to the hydrazone linkage between PEG linker and PTX-LEV, the conjugates showed complete release of paclitaxel at either tumor environment pH of 6.5 or endosomal pH of 5.3, while no release was observed at neutral pH of 7.4.

After the structural characterization and release study of A3-MSA-PTX conjugate, we investigated the efficacy of conjugates on cancer cell lines. Human cancer cell line MDA-MB-231 and PC3 were used in the study as those two cancer cell lines showed good response to paclitaxel in previous studies[22]. According to MTT assay, A3-MSA-PTX showed cytotoxicity on both cell lines. Although the IC50 of A3-MSA-PTX was higher than free PTX, we hypothesized the conjugate would perform better than free drug due to accumulation of conjugates in tumor

environment caused by A3-MSA. However, in a pilot study of PC3 tumor model on nude mice, the A3-MSA-PTX conjugate did not show better efficacy than free paclitaxel. The tumor kept growing after the injection of PTX or A3-MSA-PTX for 13 days and we had to euthanize the mice. However, the development of tumor took 28 days after the inoculation. Such slow growth might result in no response to not only A3-MSA-PTX but also free PTX. Another possible reason might be the dosage of PTX equivalence at 10 mg/kg of body weight was too low because the maximum tolerated dose of PTX was 25-50 mg/kg. However, the production of materials became difficult when high dosage was required. The PTX/protein ratio could not be too high because the aggregation would increase significantly. Thus, a large amount of A3-MSA protein was still needed even though the conjugation with PEG-PTX gave a relatively high overall yield. Furthermore, although the study on human cancer cell lines could be more relevant to human health, the lack of T-cell immunity in nude mice may also limited the combination treatment of A3-MSA-PTX conjugate and immunotherapy like checkpoint blockade therapy.

Given a better understanding of PC3 tumor model or MDA-MB-231 tumor model, we would like to set up the injection within one week after tumor inoculation as reported in the literature[22,41]. Since we only tested PC3 cell line, MDA-MB-231 tumor model may also be interested to investigate. And a higher dosage of paclitaxel would increase the anti-cancer performance. If enough material production was guaranteed, we can use A3-MSA-PTX at paclitaxel equivalence even higher than the maximum tolerated dosage because the conjugate is less toxic than free paclitaxel. In terms of mice model, if we choose other mouse tumor model instead of human tumor model, we may be able to combine A3-MSA-PTX with immunotherapy like checkpoint blockade, to see if there is synergy effect. Finally, it would also be interesting to compare A3-MSA-PTX with clinic formulation Abraxane.

4.5 Materials and Methods

4.5.1 Mice

NU/J nude mice were obtained from Charles River at age 8 to 10 weeks. The tumor inoculation started after one week of receiving the mice. All the animal experiments performed in this study were approved by the Institutional Animal Care and Use Committee of the University of Chicago.

4.5.2 Cells and proteins

MDA-MB-231 human breast cancer cell line and PC3 human prostate cancer cell line were obtained from American Type Culture Collection (ATCC). MDA-MB-231 cells were cultured in Dulbecco's modified Eagle's medium (DMEM) supplemented with 10% heat inactivated fetal bovine serum and 1% penicillin-streptomycin. PC3 cells were cultured in RPMI 1640 medium supplemented with 10% heat inactivated fetal bovine serum and 1% penicillin-streptomycin. A3-MSA protein was designed, produced, and purified by Dr. Jun Ishihara as described previously[28-31].

4.5.3 Synthesis of PTX-LEV and PEG-PTX

Paclitaxel was purchased from Fisher Scientific (Catalog No. AAJ62734MC) with a purity of 99.5%. Polymer linker maleimide-PEG5,000-NHS was purchased from JenKem Technology (SKU: A5003-1 / MAL-PEG5000-SCM,1g) with a purity of 90%. All other chemicals or solvents were purchased from Sigma Aldrich and were used without further purifications.

4.5.3.1 Synthesis of PTX-LEV (2)

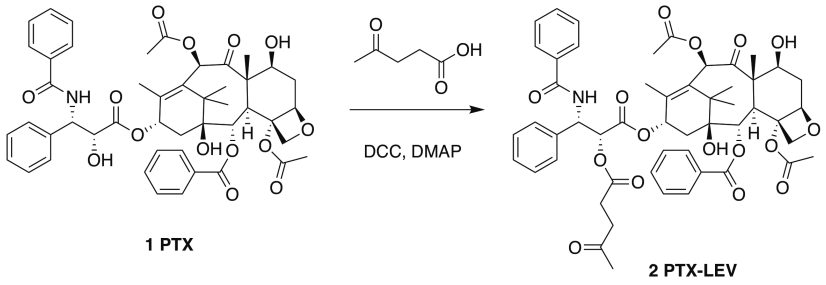

Scheme 4.1 Synthesis of PTX-LEV from PTX

Synthesis of PTX-LEV (**2**) was described previously[22]. Briefly, levulinic acid (LEV, 58.1 mg, 0.50 mmol, 1.4 eq) and N,N'-dicyclohecylcarbodiimide (DCC, 112.5 mg, 0.54 mmol, 1.56 eq) were dissolved in dry DMF and stirred for 20 min at -20 °C. Paclitaxel (PTX **1**, 300 mg, 0.35 mmol, 1.0 eq) and 4-dimethylaminopyridine (DMAP, 42 mg, 0.34 mmol, 0.97 eq) were dissolved in dry DMF and added to the reaction. The reaction was allowed to reach room temperature overnight. Then the reaction mixture was filtered and evaporated on a rotary evaporator. The product was purified by silica column with ethyl acetate and petroleum ether. The final product was obtained as a white solid (200 mg, yield 55%, Rf = 0.48 in EA/PE = 2:1). MS (ESI). $C_{52}H_{57}NO_{16}$, m/z calculated for $[M+Na]^+$: 974.37, found: 974.0.

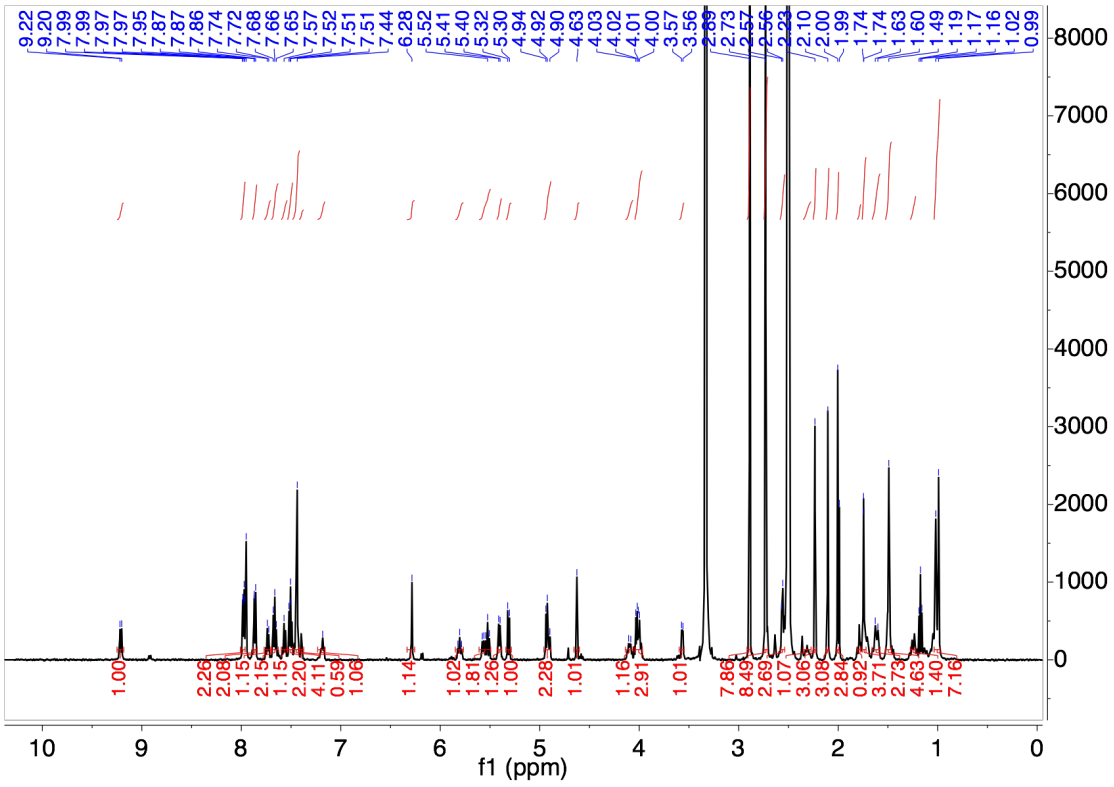

Figure 4.5 ^{1}H NMR (500 MHz, DMSO-6d) of PTX-LEV (**2**)

4.5.3.2 Synthesis of PTX-LEV-EMCH (3)

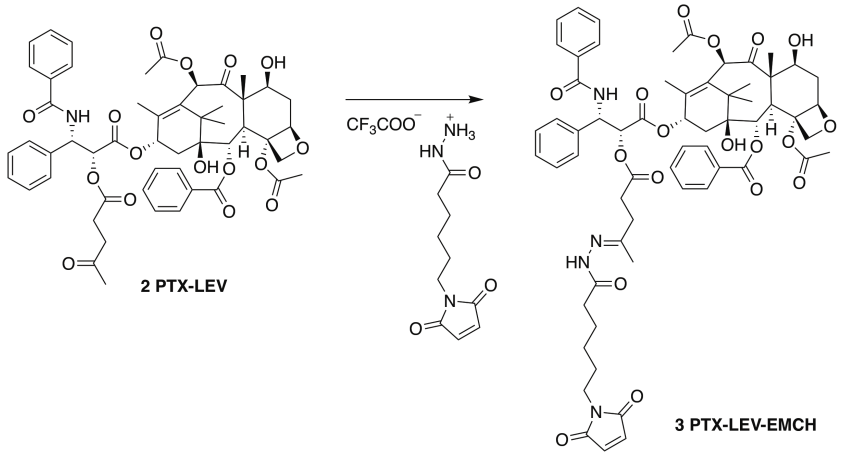

Scheme 4.2 Synthesis of PTX-LEV-EMCH from PTX-LEV

Synthesis of PTX-LEV-EMCH (**3**) was described in the previous paper[22]. Briefly, PTX-LEV (**2**) (200 mg, 0.21 mmol, 1.0 eq) and EMCH (100 mg, 0.29 mmol, 1.4 eq) was dissolved in dry methanol and stirred in dark for 36 h at 45 °C. After the reaction was completed, methanol was removed by rotary evaporator. The product was purified by silica column with 2% methanol in DCM. PTX-LEV-EMCH was immediately used for the conjugation. MS (ESI). $C_{60}H_{70}N4O_{18}$, m/z calculated for $[M+Na]^+$: 1181.47, found: 1181.2.

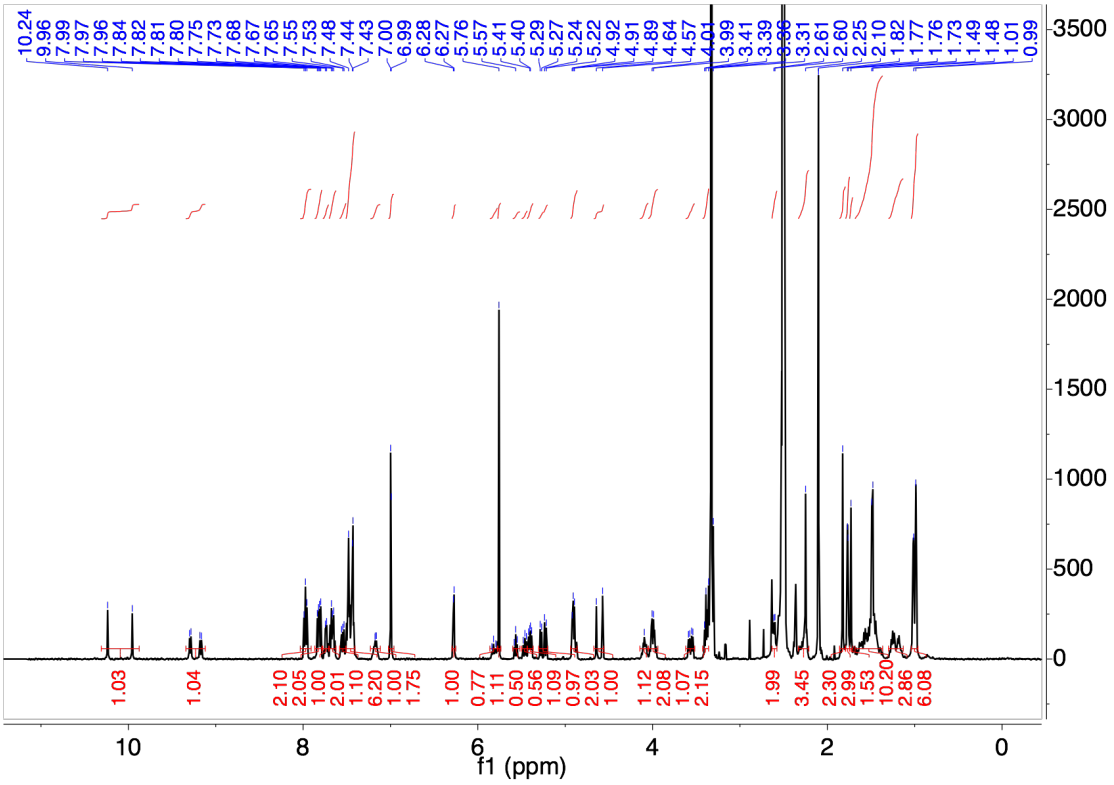

Figure 4.6 ^{1}H NMR (500 MHz, DMSO-6d) of PTX-LEV-EMCH (**3**)

4.5.3.3 Synthesis of Maleimide-PEG-hydrazide (6)

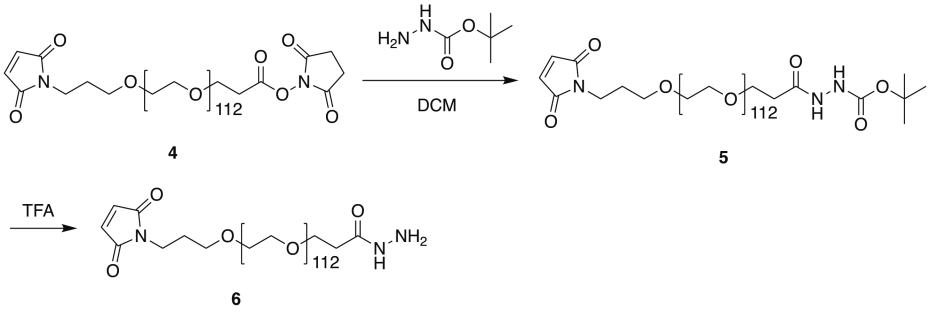

Scheme 4.3 Synthesis of Maleimide-PEG-hydrazide linker from Maleimide-PEG-NHS

Synthesis of maleimide-PEG-hydrazide (**6**) was conducted in two steps. First, maleimide-PEG-NHS (**4**, 100 mg, 0.024 mmol, 1.0 eq) and BOC-hydrazine (24 mg, 0.192 mmol, 8.0 eq) were dissolved in anhydrous DCM and stirred overnight. Then trifluoroacetic acid (TFA) was added to the reaction to de-protect BOC. After 24 h, the reaction was evaporated on rotary evaporator the product was precipitated in hexanes. The product was a white solid (57 mg, 57%).

4.5.3.4 Synthesis of PEG-PTX (7)

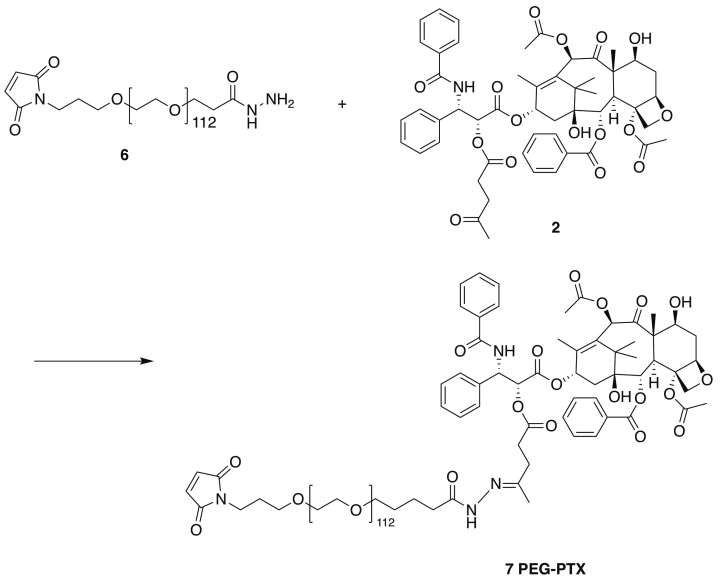

Scheme 4.4 Synthesis of PEG-PTX

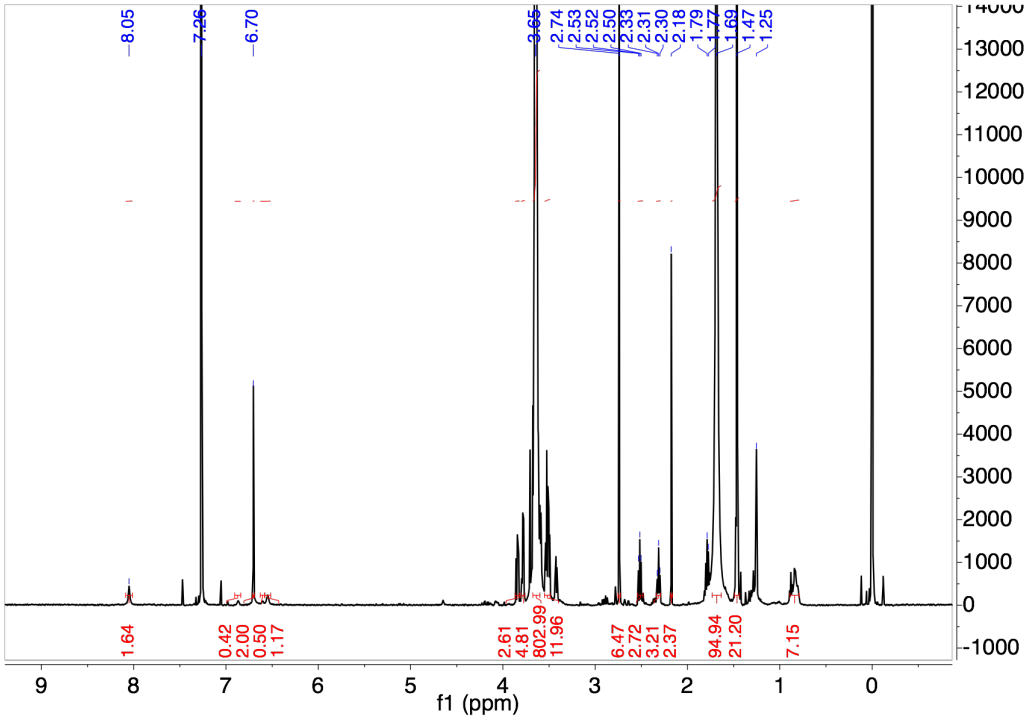

Figure 4.7 [1]H NMR (500 MHz, DMSO-6d) of maleimide-PEG-hydrazide-BOC (**5**)

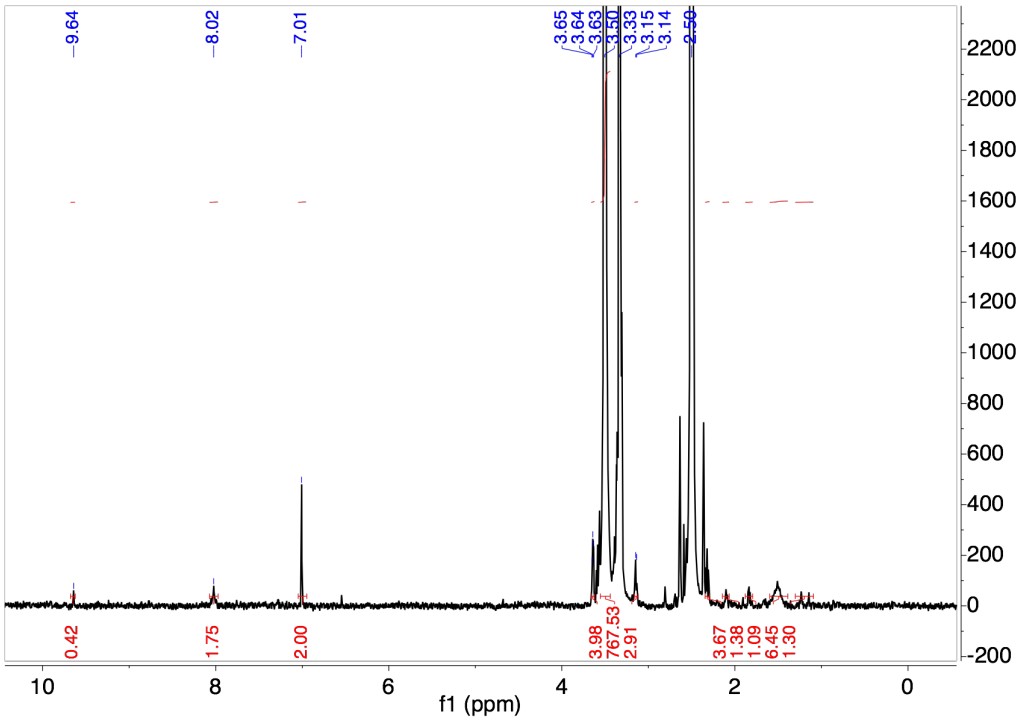

Figure 4.8 [1]H NMR (500 MHz, DMSO-6d) of maleimide-PEG-hydrazide (**6**)

The PEG-PTX (**7**) was synthesized through the conjugation between PTX-LEV (**2**) and maleimide-PEG-hydrazine (**6**). Similar to the synthesis of PEG-LEV-EMCH (**3**), PTX-LEV (**2**, 30 mg, 0.031 mmol, 1.5 eq) and maleimide-PEG-hydrazine (**6**, 100 mg, 0.02 mmol, 1.0 eq) were dissolved in anhydrous DMF. One drop of TFA was added to catalyze the reaction. The mixture was allowed reacting for 2 days in dark. After the reaction was complete, DMF was removed by rotary evaporator. The product was purified by prep-TLC using methanol and DCM as eluent. The product PEG-PTX was white solid (45 mg, yield 38%). The increase of molecular weight was observed in MALDI-TOF. The product was stored at -20 °C as solid and was resuspended right before conjugation. Maleimide was observed to hydrolyze if stored as a stock solution in PBS.

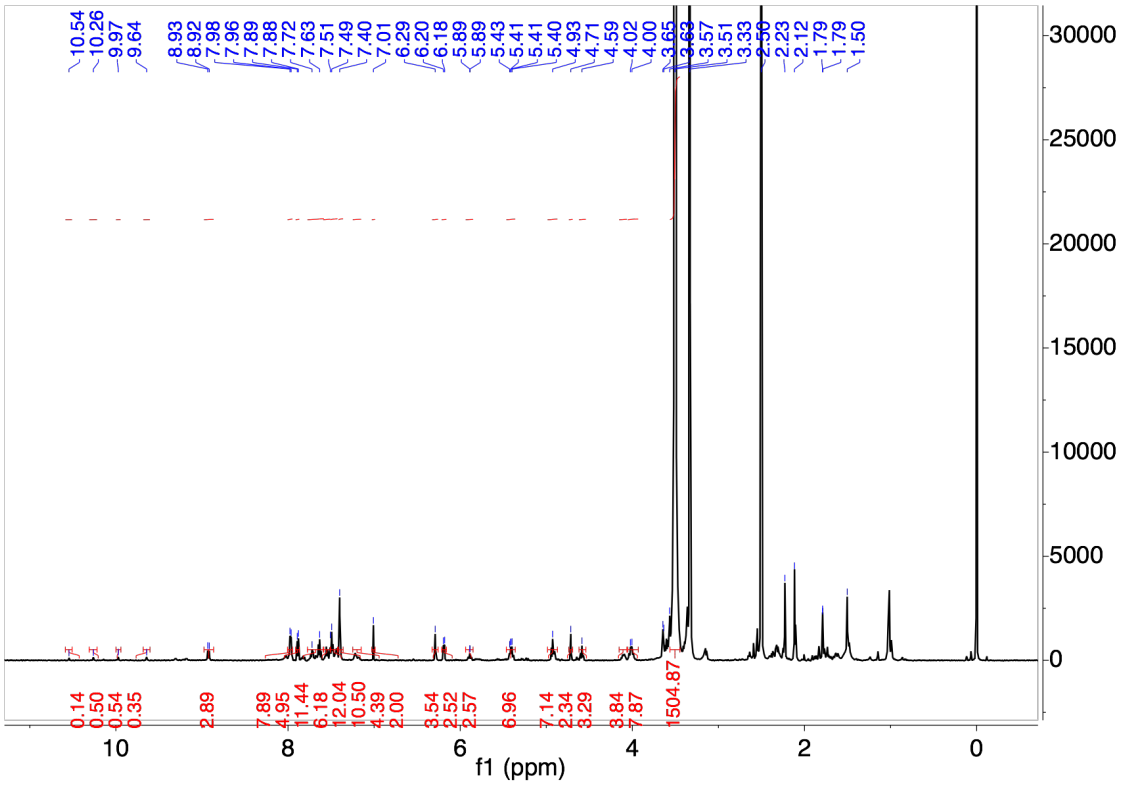

Figure 4.9 ^{1}H NMR (500 MHz, DMSO-6d) of PEG-PTX (**7**)

4.5.4 Conjugation of PTX or PEG-PTX to A3-MSA protein

The conjugation between PTX-LEV-EMCH (**3**) or PEG-PTX (**7**) and A3-MSA was similar as described in previous paper[31]. Briefly, A3-MSA protein was dissolved in PBS containing 2 mM EDTA. Traut's reagents in PBS containing 2 mM EDTA were added to the reaction vial at 4 equivalents. The mixture was incubated for 1 hour at room temperature in the dark. The reaction mixture was passed through a Zeba spin desalting column to remove unreacted Traut's reagent. Then, 4 molar equivalent of PEG-PTX dissolved in PBS was added and incubated for 1 hour at room temperature and overnight at 4 °C in the dark. The reaction was quenched by 20 equivalents of L-cysteine for 5 min. Aggregations were removed by centrifugation (10,000 g, 5 min) and the supernatant was purified by a Zeba spin desalting column. In order to concentrate the product, A3-MSA-PTX was ultracentrifuged using Amicon Ultra (Merck, 10 kDa molecular mass cutoff). The concentration of protein was determined by Nanodrop. The concentration of PTX was quantified by LC-MS/MS. The purity of the product A3-MSA-PTX was determined by SDS-PAGE.

4.5.5 Dynamic light scattering (DLS)

DLS data were obtained from Malvern Nano Zetasizer instrument. Zetasizer software was used to process the data. Samples were diluted 1,000 times in 1×PBS and 300 μL was transferred to DLS cuvette for data acquisition. Samples were scanned for 16 times at 20 °C and pure water was selected as solvent. Results were acquired in intensity, volume, or number distribution. But only volume distribution data were analyzed to show the size distribution of protein or conjugates.

4.5.6 Matrix-assisted laser desorption/ionization-time of fly (MALDI-TOF) mass spectrometry

Purified CBD-SA was analyzed by MALDI-TOF MS (Bruker Ultraflextreme MALDI TOF/TOF) as described previously[31]. Bruker flexControl was used for data acquisition, and Bruker flexAnalysis was used for data processing. Matrix was prepared with a saturated solution of α-cyano-4-hydroxycinnamic acid (Sigma-Aldrich) in 50:50 v/v of acetonitrile and water with 1% trifluoroacetic acid. A3-MSA-PTX in PBS buffer (5 μL, 0.1 mg/mL) and the matrix solution (25 μL) were mixed. 1 μL of that mixture was dropped on the MTP 384 ground steel target plate and was dried by nitrogen gas flow. All samples were analyzed using high mass linear positive mode method with 5,000 laser shots at a laser intensity of 75%.

4.5.7 Sodium dodecyl sulfate-polyacrylamide gel electrophoresis (SDS-PAGE)

SDS-PAGE was performed as described in previous literature[29,31]. Briefly, a 4 to 20% gradient gel (Bio-Rad) was used and 0.5 μg of each A3-MSA-PTX conjugate was loaded without reduction. Free A3-MSA was used as control. After electrophoresis, SimplyBlue SafeStain (Thermo Fisher Scientific) was used for gel staining according to the manufacturer's instruction. ChemiDoc XRS+ system (Bio-Rad) was used for image acquisition.

4.5.8 Liquid chromatography with Triple Quad MS-MS (LC-MS/MS)

To investigate the release of paclitaxel, 20 μL of of A3-MSA-PTX were resuspended in 220 μL of pH 5.3 NaOAc buffer, pH 6.5 Na_2HPO_4 buffer, or pH 7.4 PBS buffer, respectively. 80 μL of acetonitrile was added to each solution to reach a volume fraction of 0.25 in order to dissolve the released PTX-LEV. Samples were incubated at 37 °C for 0, 1, 2, 4, 8, or 24 h and

quenched by diluting in PBS to return to neutral pH. Samples were stored at -80 ℃ before analysis. An aliquot of 20 μL of each sample was transferred to 80 μL of PBS. 20 μL of docetaxel (DTX) at 100 μg/mL was added as internal standard. Samples were extracted with 500 μL of TBME. 450 μL of upper layer was retrieved and dried by nitrogen flow, before resuspended in 100 μL acetonitrile with 0.1% v/v formic acid before LC-MS analysis. In order to determine the drug/protein ratio, samples were prepared in pH 5.3 NaOAc buffer for 2 hours to reach the maximum PTX release without damage the PTX structure. Such hydrolysis condition was better than HCl hydrolysis that caused low PTX detection due to the break of PTX structure.

LC conditions: The instrument used for quantification of PTX or PTX-LEV was Agilent 1290 UHPLC. Column: Thermo Scientific C18, 4.6 × 50 mm, 1.8 m particle size, at room temperature. Mobile phase A: water with 0.1% v/v formic acid. Mobile phase B: acetonitrile with 0.1% v/v formic acid. Injection volume: 5.0 μL. Flow rate: 0.4 mL/min. Gradient of solvent: 20% mobile phase B at 0.0 min; 95% mobile phase B at 2.0 min; 95% mobile phase B at 5.0 min; 20% mobile phase B at 6.0 min; 20% mobile phase B at 6.5 min.

ESI-MS/MS method[22,37,38]: The instrument used to detect PTX or PTX-LEV was Agilent 6460 Triple Quad MS-MS. Conditions for quantifying each compound were optimized using pure compound at 1 mM. All compounds were analyzed in positive model. For PTX-LEV, multiple reaction monitoring (MRM) 952 → 384 was measured with a fragmentor voltage of 125 V and collision energy of 15 V. For PTX, the MRM 854 → 286 was measured with a fragmentor voltage of 125 V and collision energy of 15 V. For internal standard DTX, MRM 808 → 527 was measured with fragmentor voltage of 100 V and collision energy of 10 V. The peak area ratio of PTX-LEV over DTX was used to quantifying the concentration of PTX-LEV.

4.5.9 MTT assay

3-(4,5-dimethylthiazol-2-yl)-2,5-diphenyltetrazolium bromide (MTT) kit was purchased from Fisher Scientific. The cell proliferation assay was performed according to the manufacturer's instructions. Briefly, MDA-MB-231 cells or PC3 cells were seeded in a 96-well tissue culture plate at 5×10^4 cells/well. Serial dilutions of A3-MSA-PTX or PTX were added to wells. Cells were incubated at 37 °C for 24 h. After the incubation, 10 μL of the MTT labeling reagent was added to each well and the plate was incubated for 4 h. 100 μL of solubilization solution was added. After the complete solubilization of the purple formazan crystals, the absorbance was measured at 550 nm subtracting the reference wavelength at 690 nm. Half maximal inhibitory concentration (IC50) was obtained by nonlinear regression analysis in Prism software using inhibitor vs. response - variable slope (four parameters) model.

4.5.10 PC3 tumor inoculation and treatments

The PC3 human tumor model was prepared as described in the literature[22]. A total of 5×10^5 PC3 cells were resuspended in 50 μL of PBS and then injected subcutaneously into the mice right flank. Tumor volume were measured with a digital caliper on indicated days and the volumes were calculated where V = 4/3 × 3.14 × depth/2 × width/2 × height/2. When average tumor volume reached 100 mm^3, mice were treated with either PTX or A3-MSA-PTX (two injections, 5 mg/kg each) with a total dosage of PTX equivalent at 10 mg/kg. Mice were euthanized when tumor volume reached 1,000 mm^3. Body weight of each mouse was also monitored during the experiment.

4.6 Conclusion

In this study, we designed and synthesized a protein drug conjugate for cancer target therapy. The active chemotherapeutic drug was paclitaxel and the protein was collagen-binding protein A3-MSA. To increase the solubility and to prevent aggregation, we included a PEG-5,000 linker between PTX and A3-MSA protein. We characterized the A3-MSA-PTX conjugate with SDS-PAGE, MALDI-TOF, and DLS. In addition, the release of PTX at acidic pH was validated by LC-MS/MS. Furthermore, cell viability assay demonstrated the cytotoxicity of A3-MSA-PTX conjugate on both MDA-MB-231 cell line and PC3 cell line. However, the treatment of A3-MSA-PTX on PC3 tumor model on nude mice did not show better efficacy than free paclitaxel. To improve the performance, we could increase the dosage in paclitaxel equivalent, especially A3-MSA-PTX.

4.7 References

1. GREGORY, R. & DELISA, A. PACLITAXEL - A NEW ANTINEOPLASTIC AGENT FOR REFRACTORY OVARIAN-CANCER. *Clinical Pharmacy* **12**, 401-415 (1993).

2. Bernabeu, E., Cagel, M., Lagomarsino, E., Moretton, M. & Chiappetta, D.A. Paclitaxel: What has been done and the challenges remain ahead. *Int J Pharm* **526**, 474-495 (2017).

3. Zhu, L. & Chen, L. Progress in research on paclitaxel and tumor immunotherapy. *Cell Mol Biol Lett* **24**, 40 (2019).

4. Schiff, P.B. & Horwitz, S.B. Taxol stabilizes microtubules in mouse fibroblast cells. *Proc Natl Acad Sci U S A* **77**, 1561-1565 (1980).

5. Weaver, B.A. How Taxol/paclitaxel kills cancer cells. *Mol Biol Cell* **25**, 2677-2681 (2014).

6. Michaud, L.B., Valero, V. & Hortobagyi, G. Risks and benefits of taxanes in breast and ovarian cancer. *Drug Saf* **23**, 401-428 (2000).

7. Marupudi, N.I.*, et al.* Paclitaxel: a review of adverse toxicities and novel delivery strategies. *Expert Opin Drug Saf* **6**, 609-621 (2007).

8. Frederiks, C.N., Lam, S.W., Guchelaar, H.J. & Boven, E. Genetic polymorphisms and paclitaxel- or docetaxel-induced toxicities: A systematic review. *Cancer Treat Rev* **41**, 935-950 (2015).

9. GREENWALD, R., PENDRI, A. & BOLIKAL, D. HIGHLY WATER-SOLUBLE TAXOL DERIVATIVES - 7-POLYETHYLENE GLYCOL CARBAMATES AND CARBONATES. *Journal of Organic Chemistry* **60**, 331-336 (1995).

10. Greenwald, R.*, et al.* Drug delivery systems: Water soluble taxol 2'-poly(ethylene glycol) ester prodrugs - Design and in vivo effectiveness. *Journal of Medicinal Chemistry* **39**, 424-431 (1996).

11. Meng, Z.*, et al.* Prodrug Strategies for Paclitaxel. *Int J Mol Sci* **17**(2016).

12. Sofias, A.M., Dunne, M., Storm, G. & Allen, C. The battle of "nano" paclitaxel. *Adv Drug Deliv Rev* **122**, 20-30 (2017).

13. Owiti, A., Mitra, A., Joseph, M. & Pal, D. Strategic Pentablock Copolymer Nanomicellar Formulation for Paclitaxel Delivery System. *Aaps Pharmscitech* **19**, 3110-3122 (2018).

14. Jang, E.*, et al.* DHP23002 as a next generation oral paclitaxel formulation for pancreatic cancer therapy. *Plos One* **14**(2019).

15. Hoy, S.M. Albumin-bound paclitaxel: a review of its use for the first-line combination treatment of metastatic pancreatic cancer. *Drugs* **74**, 1757-1768 (2014).

16. Kundranda, M.N. & Niu, J. Albumin-bound paclitaxel in solid tumors: clinical development and future directions. *Drug Des Devel Ther* **9**, 3767-3777 (2015).

17. Zong, Y., Wu, J. & Shen, K. Nanoparticle albumin-bound paclitaxel as neoadjuvant chemotherapy of breast cancer: a systematic review and meta-analysis. *Oncotarget* **8**, 17360-17372 (2017).

18. Liang, L.*, et al.* Novel cathepsin B-sensitive paclitaxel conjugate: Higher water solubility, better efficacy and lower toxicity. *J Control Release* **160**, 618-629 (2012).

19. Huo, M.*, et al.* Somatostatin receptor-mediated specific delivery of paclitaxel prodrugs for efficient cancer therapy. *J Pharm Sci* **104**, 2018-2028 (2015).

20. Yin, T.*, et al.* Well-Defined Redox-Sensitive Polyethene Glycol-Paclitaxel Prodrug Conjugate for Tumor-Specific Delivery of Paclitaxel Using Octreotide for Tumor Targeting. *Mol Pharm* **12**, 3020-3031 (2015).

21. Li, F.*, et al.* A water-soluble nucleolin aptamer-paclitaxel conjugate for tumor-specific targeting in ovarian cancer. *Nature Communications* **8**(2017).

22. Bhattacharyya, J.*, et al.* A paclitaxel-loaded recombinant polypeptide nanoparticle outperforms Abraxane in multiple murine cancer models. *Nat Commun* **6**, 7939 (2015).

23. Luginbuhl, K.M.*, et al.* Recombinant Synthesis of Hybrid Lipid-Peptide Polymer Fusions that Self-Assemble and Encapsulate Hydrophobic Drugs. *Angew Chem Int Ed Engl* **56**, 13979-13984 (2017).

24. Thomas, A., Teicher, B.A. & Hassan, R. Antibody-drug conjugates for cancer therapy. *Lancet Oncol* **17**, e254-e262 (2016).

25. Birrer, M.J., Moore, K.N., Betella, I. & Bates, R.C. Antibody-Drug Conjugate-Based Therapeutics: State of the Science. *J Natl Cancer Inst* **111**, 538-549 (2019).

26. Danhier, F., Feron, O. & Préat, V. To exploit the tumor microenvironment: Passive and active tumor targeting of nanocarriers for anti-cancer drug delivery. *J Control Release* **148**, 135-146 (2010).

27. Ishihara, J.*, et al.* Matrix-binding checkpoint immunotherapies enhance antitumor efficacy and reduce adverse events. *Sci Transl Med* **9**(2017).

28. Ishihara, J.*, et al.* Improving Efficacy and Safety of Agonistic Anti-CD40 Antibody Through Extracellular Matrix Affinity. *Mol Cancer Ther* **17**, 2399-2411 (2018).

29. Ishihara, J.*, et al.* Targeted antibody and cytokine cancer immunotherapies through collagen affinity. *Sci Transl Med* **11**(2019).

30. Williford, J.M.*, et al.* Recruitment of CD103. *Sci Adv* **5**, eaay1357 (2019).

31. Sasaki, K.*, et al.* Engineered collagen-binding serum albumin as a drug conjugate carrier for cancer therapy. *Sci Adv* **5**, eaaw6081 (2019).

32. Katsumata, K.*, et al.* Targeting inflammatory sites through collagen affinity enhances the therapeutic efficacy of anti-inflammatory antibodies. *Sci Adv* **5**, eaay1971 (2019).

33. Mansurov, A.*, et al.* Collagen-binding IL-12 enhances tumour inflammation and drives the complete remission of established immunologically cold mouse tumours. *Nat Biomed Eng* **4**, 531-543 (2020).

34. Jia, X.*, et al.* Fluorescent Copolymer-Based Prodrug for pH-Triggered Intracellular Release of DOX. *Biomacromolecules* **16**, 3624-3631 (2015).

35. Gatti, S.*, et al.* Hydrazone linked doxorubicin-PLA prodrug nanoparticles with high drug loading. *Nanotechnology* **29**, 305602 (2018).

36. Zhang, X.*, et al.* A new procedure for preparation of carboxylic acid hydrazides. *Journal of Organic Chemistry* **67**, 9471-9474 (2002).

37. Fernández-Peralbo, M.A.*, et al.* LC-MS/MS quantitative analysis of paclitaxel and its major metabolites in serum, plasma and tissue from women with ovarian cancer after intraperitoneal chemotherapy. *J Pharm Biomed Anal* **91**, 131-137 (2014).

38. Baati, T.*, et al.* An ultrasensitive LC-MS/MS method with liquid phase extraction to determine paclitaxel in both cell culture medium and lysate promising quantification of drug nanocarriers release in vitro. *J Pharm Biomed Anal* **115**, 300-306 (2015).

39. Tian, J. & Stella, V.J. Degradation of paclitaxel and related compounds in aqueous solutions III: Degradation under acidic pH conditions and overall kinetics. *J Pharm Sci* **99**, 1288-1298 (2010).

40. Yang, M.Y.*, et al.* Luteolin enhances paclitaxel-induced apoptosis in human breast cancer MDA-MB-231 cells by blocking STAT3. *Chem Biol Interact* **213**, 60-68 (2014).

41. Sobue, S.*, et al.* Mechanism of paclitaxel resistance in a human prostate cancer cell line, PC3-PR, and its sensitization by cabazitaxel. *Biochem Biophys Res Commun* **479**, 808-813 (2016).

42. Lorber, B., Fischer, F., Bailly, M., Roy, H. & Kern, D. Protein analysis by dynamic light scattering: methods and techniques for students. *Biochem Mol Biol Educ* **40**, 372-382 (2012).

43. Bhattacharjee, S. DLS and zeta potential - What they are and what they are not? *J Control Release* **235**, 337-351 (2016).

Chapter 5

Summary and Perspectives

5.1 Summary of the thesis

In Chapter 2, we developed novel polymeric micelles that delivered butyrate to the GI tract and enhanced the performance of oral immunotherapy. The micelles were formulated by synthetic block copolymers. The hydrophilic block was made of either HPMA (CLB001) or MAA (CLB003), while the hydrophobic block was made of monomers containing butyrate ester. After testing the block size and ratio between hydrophilic block and hydrophobic block, we achieved CLB001 and CLB003 micelles both with hydrodynamic diameter of 40 nm. The major difference between CLB001 and CLB003 was their surface charge and critical micelle concentration. Interestingly, two micelles had different butyrate release profile in the GI tract. CLB001 raised the butyrate level in the ileum at early time point, while CLB003 raised the butyrate level in the cecum four hours after the gavage. Importantly, the combination of CLB001/003 and oral immunotherapy showed an improved performance compared to oral immunotherapy only. We also investigated the possible interactions between butyrate-containing micelles and the GI tract. RNA-Seq results and intelectin stain showed CLB001 regulated the gene expression of ileal epithelial cells. Flow cytometry showed CLB003 induced $GATA3^{+}$ and $ROR\gamma t^{+}$ regulatory T cells in the ileal mesenteric lymph nodes. Thus, CLB001 and CLB003 provided a potential to be a supplementary treatment to oral immunotherapy.

In Chapter 3, we synthesized a statistical copolymer of mannose and butyrate on the basis of p(Man-TLR7) previously developed in the lab. To increase the hydrolysis rate, we incorporated monomer with phenol butyrate to the polymer (pMan-PhBut) in addition to aliphatic butyrate monomer (pMan-But). As we expected, pMan-PhBut showed a faster butyrate

release *ex vivo* and a better performance *in vitro* by suppressing the IL12p70 production. Thus, we obtained two polymers with "slow" or "fast" butyrate release that were suitable for different situations. Furthermore, in the animal study, pMan-PhBut induced tolerogenic DCs as shown by the re-activation assay. Thus, manosylated butyrate containing polymer could deliver butyrate to dendritic cells and macrophages and induce tolerance response in the draining lymph nodes.

In Chapter 4, we conjugated paclitaxel to collagen binding peptide through a PEG linker and a hydrazone bonding. The conjugate A3-MSA-PTX was soluble in water without forming aggregations. The paclitaxel was released at acidic tumor environment pH or endosomal pH. In cell viability assay, the conjugate showed efficacy in both human breast cancer and human prostate cancer cell lines. However, we still needed more practice on tumor inoculation and dose study to showed the efficacy of A3-MSA-PTX on animal cancer model.

5.2 Future directions

Given the promising results we achieved from CLB001 and CLB003 micelles, I think we can investigate more into the mechanisms on how butyrate-containing micelles interact with the mouse GI tract. We can further validate the Treg induction or the roles $GATA3^+$ or $ROR\gamma t^+$ Treg played. In addition to Treg induction, butyrate is also a G-protein coupled receptor 109 agonist. Thus it would be interesting to investigate if the CLB001 and CLB003 have effect on GPCR109 knock out mice. Given the effect CLB001 can induce the expression of anti-microbial peptides in the ileum, it would be interesting if such effect is related to the protection of the gut or alleviate the allergy response against food allergen. Such effect also provides a potential to treat gut microbiome related disease like Clostridioides difficile colitis. In addition to oral administration, subcutaneous injection of CLB001 or CLB003 micelles also showed promising results in Treg

induction in the draining lymph nodes by Dr. Shijie Cao in the lab. It would be interesting to investigate the materials in inducing systematic tolerance. Finally, back to the structure design, since we have proven the phenol butyrate has faster release rate, we can also incorporate the phenol butyrate (PhBMA) into the core of the micelle if we need to achieve a faster release of butyrate.

As a different formulation of butyrate, the glycopolymer pMan-But or pMan-PhBut also shows promising results in our study. Since we have demonstrated the polymer induced tolerogenic dendritic cells, we can move forward into T cell study including OTI/OTII models and the Treg induction. We can investigate the antigen-specific tolerance by conjugating an antigen to the polymer through azide-alkyne coupling. The readout of T cells will be more standard and informative than dendritic cells. In addition, since mannose receptor CD206 is also expressed on macrophage, we can also investigate macrophage related research like chronic wound healing in db/db mice. Our preliminary results have showed promising trend of pMan-But accelerating wound healing. Moreover, we can also study the liver related tolerance model because the polymer can accumulate in the liver if we use i.v. injection.

Apart from butyrate delivery systems, the collagen binding peptide and paclitaxel conjugate also has potentials to have better performance in cancer therapy. We can evaluate a better tumor model of either MDA-MB-231 or PC3 cells by shortening the tumor developing time. Also, a high dose of paclitaxel equivalent can help to show the advantage of A3-MSA-PTX conjugate.